TITLE

Methods for the Analysis of Boiling Water Reactors Steady State Physics

TR 021
(Rev. 0)

Project No: 5400-40716

R.V. Furia Author

Date January 31, 1986

Approvals:

G.P. Boad 3-14-86
Nuclear Analysis & Fuels - Date
Director

GPU Nuclear
100 Interpace Parkway
Parsippany, New Jersey 07054

Abstract

This report describes the three-dimensional nodal methods used by GPUN for steady state BWR core calculations. The methods employ an integrated neutronic (NODE-B) and thermal-hydraulic (THERM-B) models for detailed core analysis. The methods have been verified against operating data from Oyster Creek and Hatch 1 cycle 1.

Acknowledgment

The author would like to express his appreciation to those who have contributed to this report, especially M.D. Beg, E.R. Bujtas, J.D. Dougher, H. Fu and C.B. Mehta.

TABLE OF CONTENTS

LIST OF TABLES

LIST OF FIGURES

1.0 INTRODUCTION

This report describes the three-dimensional core simulation method in use at GPUN for its Oyster Creek Nuclear Generating Station. The method utilizes a one group neutronic model integrated with a thermal-hydraulic model. The integrated model was developed with the Electric Power Research Institute (EPRI) Power Shape Monitoring System[1] (PSMS) at Oyster Creek. It is derived from the EPRI NODE-B and EPRI-THERM-B computer programs which are part of the EPRI Advanced Recycle Methodology Program[2] (ARMP) code package. A brief description of the Oyster Creek core is provided in Section 2.0 and the code methodology is given in Section 3.0.

The integrated code was extensively tested and verified under the PSMS project while undergoing significant improvements in the process[3]. The NODE-B/THERM-B Code (hereafter referred to as NODE-B) was taken from the on-line PSMS computer and converted for use by GPUN on its IBM computer for off-line core analysis. This enables the off-line analysis to correspond to the on-line PSMS analysis which is used to monitor core thermal limits. It also enables the performance of the off-line code to be continually evaluated through the performance of the on-line code.

The off-line NODE-B code is intended for use in fuel management studies and reload core analysis. The code calculates core exposure and core power distribution based on actual or projected core operating data. NODE-B is used in the development of refueling patterns, target end of cycle exposure and power distribution and target control rod patterns.

The code calculates cold shutdown margin and hot excess reactivity. It is also used to analyze transients which can be simulated with steady state methods such as the fuel bundle mislocation and control rod withdrawal error. These applications are justified by the verification work that has been performed.

The adequacy of NODE-B as a three-dimensional reactor simulator has already been established by the performance of the PSMS[4]. Additional verification work has been performed at GPUN to demonstrate the accuracy of the off-line NODE-B model and GPUN's capability to model reactor cores. The verification includes both cold and hot operating conditions from Oyster Creek Cycles 8 and 9 and hot operating conditions from Hatch 1 Cycle 1. The verifications were performed against cold criticals, TIP measurements and gamma scan data. The results of GPUN's verification work is presented in Section 4.0 and establishes a basis of confidence in using NODE-B for core analysis.

2.0 CORE DESCRIPTION AND MODELING

Oyster Creek is a 560 bundle BWR-2 with a rated thermal power of 1930 MW. The core is controlled by 137 cruciform control rods and has incore instruments at 31 radial locations for monitoring power operation. At each radial location are four detectors at fixed axial locations and a traversing incore probe (TIP) (Figure 2-1). The core is divided into two hydraulic zones by orifices at the inlet of each assembly. The outer zone contains all those assemblies with one or more sides on the core periphery while the inner zone consists of the remainder of the assemblies. The outer zone has a smaller orifice and a reduced core flow relative to the core average flow.

The reactor core is represented in the NODE-B model by a three dimensional mesh of cubic nodes, one node for each bundle in the horizontal plane and 24 axially nodes. The model can handle multiple fuel designs as well as axial variations in the fuel lattice. The control rod pattern is input to the code explicitly, but the code modeling homogenizes each node and treats the nodes as either controlled or uncontrolled. The instrument locations are identified and instrument reading can be predicted.

The Hatch 1 core, which was analyzed for verification purposes, is also a 560 bundle core with 137 control rods. It has a higher power density with a rated thermal power of 2436 MW. There are the same number of power range instruments, but the locations differ from the Oyster Creek layout. The model representation of the core was the same as for Oyster Creek.

Figure 2-1
OYSTER CREEK CORE MAP

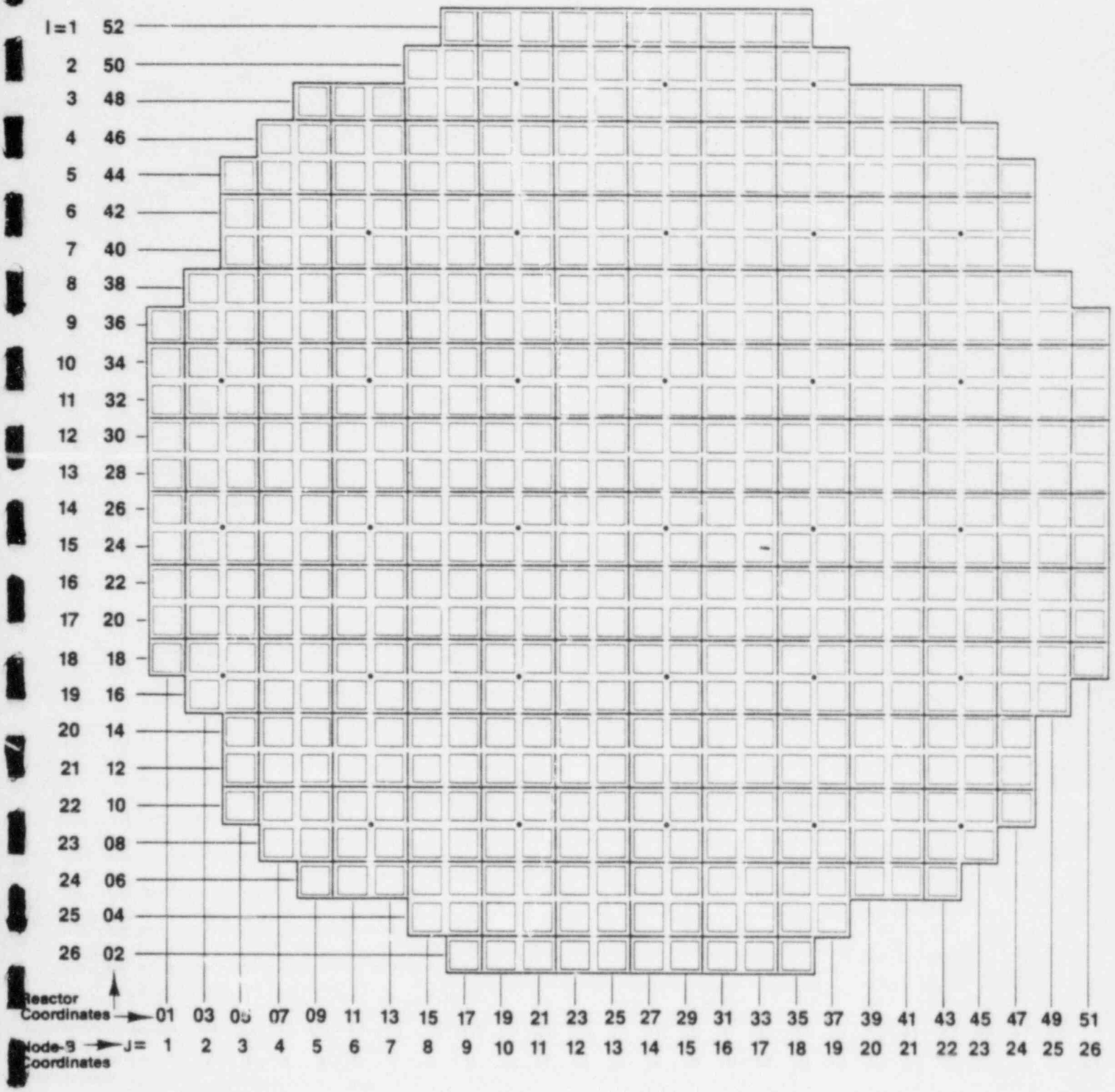

□ - FUEL BUNDLE
+ - CONTROL ROD
● - TIP LOCATION

3.0 TECHNICAL DESCRIPTION

3.1 Overview

The three dimensional simulator code, NODE-B, is a coupled three dimensional neutronic and thermal hydraulic model which is able to predict reactivity, power and coolant-void distribution, and control rod positions throughout the core lifetime. The program uses iterative solution techniques to solve for the interaction between power, coolant flow and voids, fuel temperature and xenon distributions. The complete calculation consists of two levels of iterations, source and coolant voids.

The source iteration in NODE-B treats reflection at the surface of the core with an albedo and employs transport kernels (which track neutrons for a distance of only one node) to represent the coupling between nodes. The neutron source at each node is calculated as a function of the infinite multiplication factor, k^{∞}, and the transport kernel. The latter is a simple function of the migration area, M^2, and the mesh spacing. The migration area is calculated at each node based on a fit to the moderator density. The infinite multiplication factor is calculated at each node including the effects of control rods, local moderator density, fuel exposure, fuel temperature and xenon concentration. The core effective multiplication factor is calculated on the basis of a neutron balance summed over the entire core in each iteration. The void calculation consists of the determination of the average steam quality at each node based on inlet velocity, inlet enthalpy

and power integrated from the bottom of the channel to the node of interest.

The flow of the calculation is to solve the source equation for an initial distribution of coolant voids, xenon, fuel exposure and Doppler reactivity. The power distribution is then calculated and a new coolant void, Doppler and xenon distributions are determined. This sequence is repeated until the power and coolant distributions converge to values within input criteria. In burnup calculations, the fuel exposure distribution is extended from the beginning to the end of the step using the converged power distribution. Figure 3-1 shows a flow chart of the calculational sequence.

The basic inputs to the code are the fuel element data (type, location and dimensions), core flow and power level, control rod position, fuel element nuclear properties, and thermal-hydraulics characteristics. Nuclear properties for each fuel type are input as fits of M^2 vs. relative water density, k^∞ vs. fuel exposure, fuel-temperature, relative water density and xenon, and fits of $\upsilon\bar{\sum}_f$ and $\kappa\sum_f$ vs. exposure weighted voids. Flow characteristics are input as hydraulic constants for each fuel type in terms of dimensions and form loss coefficients. Feedwater flow and temperature are input for the determination of the core inlet subcooling.

Figure 3-1.
NODE-B FLOW CHART

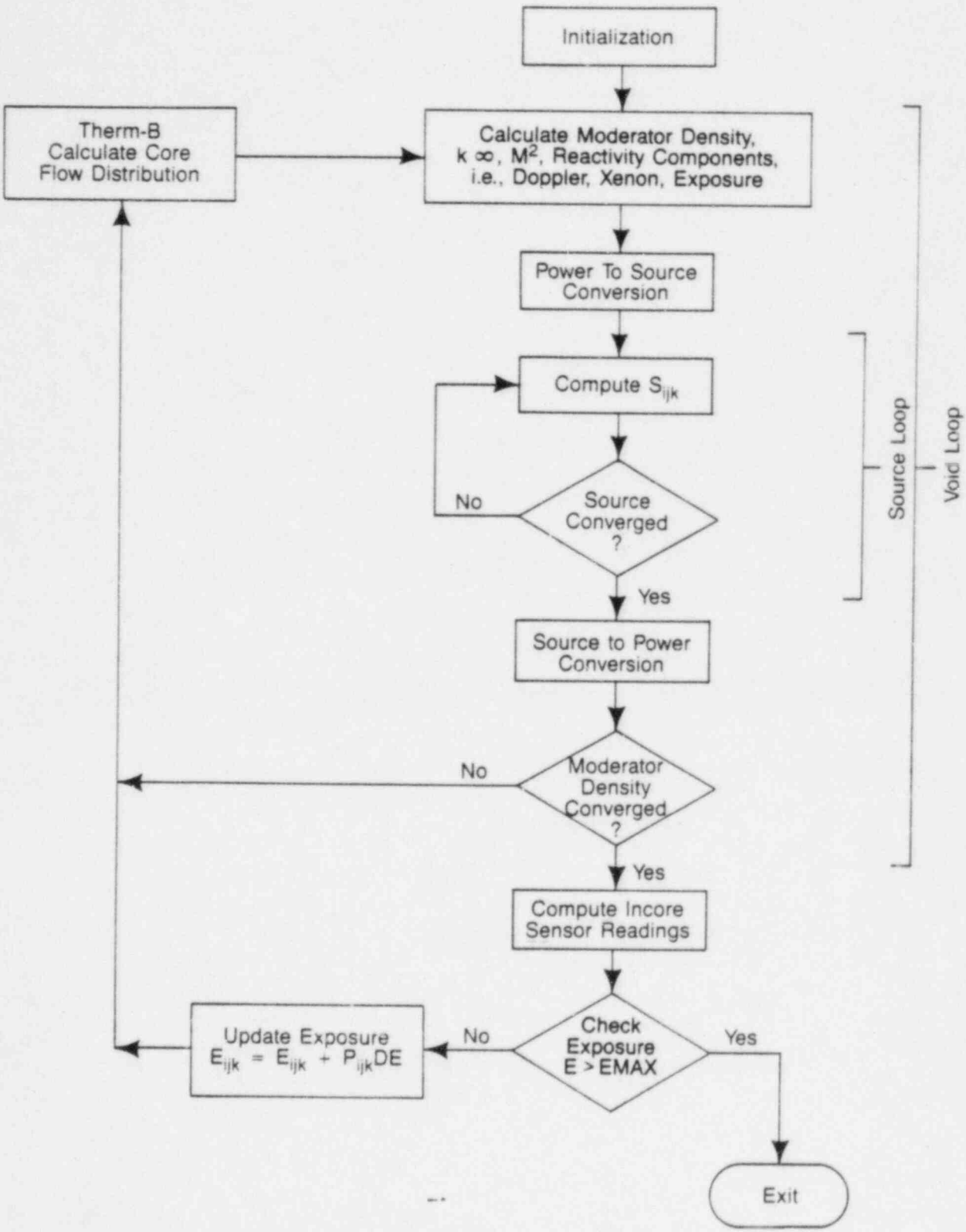

A more detailed discussion of the PSMS NODE-B is provided in Reference 1 including a description of the fits used for k^{∞}. The following discussions are taken, in part, from Reference 1.

3.2 Neutronic Model

The neutronic model of NODE-B uses a modified one group theory. The neutronic source, which is proportional to power, is calculated at each node. The source S at node m is:

$$S_m = \frac{k_m/\lambda \sum S_n W_{nm}}{1 - k_m/\lambda \left[1 - (6 - \alpha_m) W_{mn}\right]}$$

where: n = index of neighboring nodes

λ = eigenvalue

W_{nm} = probability of a neutron born in node n being absorbed in node m

α_m = leakage factor (albedo) for node m

k_m = k-infinity for node m

The leakage factor is zero for internal nodes and a linear function of voids up the height of the bundles on the core edge.

$$\alpha_m^{\ell} = \alpha_m^{\circ} \left[1 + 0.95 \, (v-0.4)\right]$$

where ℓ is 1 or 2 (for the number of faces on the core edge) and v is the local void fraction. Leakage factors are also provided for the top and bottom of the core, α_m^T and α_m^B respectively.

The neutronic kernel, the probability of a neutron leaking from one node to another, is given by:

$$W_{mn} = [(1-g)(\sqrt{M_m^2}/2r_{mn}) + g\ (M_m^2/r^2_{mn})]/\sqrt{k_m}$$

where M^2 is the migration area, and r_{mn} is the distance between the center of nodes. The weighting coefficient or mixing factor, g, takes on the value of g_v in the vertical direction and g_h in the horizontal direction.

The values for α_m, α_m^B, α_m^T, g_v and g_h are referred to as normalization parameters and are determined empirically from plant operating data. The PSMS has an optimization routine to determine these values by minimizing the residuals between measured and predicted TIPs. A fixed set of parameters were obtained for Oyster Creek using cycle 8 data and have been used for cycle 9. A new set of optimized parameters can be generated if model performance warrants it.

The eigenvalue, λ, is re-evaluated after each iteration based on a neutron balance summed over the entire core by

$$\lambda = \frac{\sum_m S_m - \sum_m S_m W_{mn} (n_m - \alpha_m)}{\sum_m \frac{S_m}{k_m}}$$

where n_m represents the number of external nodes adjacent to Node m. The eigenvalue is used for convergence of the source only

the core k-effective in NODE-B is calculated by the more commonly used definition

$$k_{eff} = \frac{\sum_m S_m}{\sum_m \frac{S_m}{k_m} + \sum_m S_m W_{mn} (n_m - \alpha_m)}$$

The value of k_m is determined for each node ijk as follows:

$$k_m = \overset{\circ}{k_m} (1 - \Delta k/\overset{\circ}{k_m})_{DOP} * (1 - \Delta k/\overset{\circ}{k_m})_{Xe} * (1 - \Delta k/\overset{\circ}{k_m})_{BU}$$

A base value of k-infinity, $\overset{\circ}{k_m}$, is determined at average-power Doppler, no Xenon and zero exposure for each fuel type. The base value is determined as a function of relative moderator density, U, for rodded and unrodded conditions. U is defined as the moderator density relative to saturated water at the operating pressure. The base value of k_m also includes the exposure dependence of control rod worth. The base value of k-infinity is then adjusted for Doppler, xenon and burnup.

Doppler Reactivity

The Doppler reactivity effect is calculated at each node ijk by

$$(\Delta k^{\infty})_{ijk} = \frac{\alpha_D}{\sqrt{U_{ijk}}} \left[\sqrt{Pijk * (Pth/Prated) * (T_{fuel} - T_{mod}) + T_{mod}} - \sqrt{T_{fuel}} \right]$$

and

$$\alpha_D = \frac{\Delta k^{\infty}/k^{\infty}}{\sqrt{T_{fuel}} - \sqrt{T_{mod}}}$$

The $\Delta k^{\infty}/k^{\infty}$ term is the relative change in k^{∞} due to fuel heating from the core average coolant temperature (T_{mod}) to the core average fuel temperature (T_{fuel}), and represents the core average Doppler defect. T_{fuel} must be consistent with the core full power level (P_{rated}). The incremental fuel temperature ($T_{fuel} - T_{mod}$) of each node is assumed to be proportional to the power in that node. The core incremental fuel temperature is then multiplied by P_{ijk}, the relative power in the node ijk, to give the node average value of the UO_2 temperature. The P_{th}/P_{rated} ratio accounts for the core power level relative to full power.

Xenon Reactivity

Xenon effects in NODE-B are treated by computing the power in watts per cm^3, the effective thermal neutron flux, the iodine number density, the xenon number density, the xenon absorption cross section, and then computing $(\Delta k/k)_{Xe}$ for each node ijk. The xenon concentration in each node is converted to changes in nodal k^{∞}'s by:

$$(\Delta k/k)ijk = 1 - 1/\left(1 + \frac{N_{Xe}\,\sigma_a^{Xe}}{\nu\Sigma_f}\,k^{\infty}_{no\ xe}\right)_{ijk}$$

and N_{Xe} is calculated internally using the thermal flux and power at each node. The xenon microscope cross section, σ_a^{Xe}, is fitted as a function of U.

Exposure Reactivity

The exposure reactivity effects are determined by computing the $(\Delta k/k)_{SU}$ for each node ijk. The $(\Delta k/k)_{SU}$ from zero exposure is obtained from fit of reactivity versus exposure and exposure weighted voids.

The nodal exposure is computed by

$$E_{ijk}\ (TS) = P_{ijk} * \Delta E(TS) * WT + E_{ijk}\ (TS-1)$$

where $E_{ijk}\ (TS)$ = nodal exposure at end of time step (TS) in GWD/MT

$E_{ijk}\ (TS-1)$ = nodal exposure at the end of the previous time step

P_{ijk} = nodal power at beginning of time step

WT = a constant to account for differences in uranium weight between fuel designs

$\Delta E\ (TS)$ = core average exposure length for the time step in GWD/MT

The exposure weighted voids are computed by

$$V_{ijk}\ (TS) = V_{ijk}\ (TS-1) + P_{ijk}*\Delta E(TS)*WT*[U_{ijk} + CR\ (\delta + 1)]$$

where V_{ijk} (TS) = exposure weighted void at end of time step for node ijk

V_{ijk} (TS-1) = exposure weighted voids at end of previous time step

U_{ijk} = relative moderator density at node ijk

CR = a constant used to introduce control rod history effects

δ = 2f - 1

f = control rod fraction at node ijk

Conversion of Source Distribution to Power Distribution

The nodal burnup dependence of the macroscopic fission cross section, $\nu\Sigma_f$, and the power source macroscopic cross section, $\kappa\Sigma_f$, is accounted for by fuel type. These macroscopic cross sections are input for each fuel type as one-group effective values (Westcott formulation). For two neutron groups:

$$\overline{\kappa\Sigma_f} = \frac{\kappa\Sigma_{f1}\,\phi_1 + \kappa\Sigma_{f2}\,\phi_2}{\phi_2} \text{ , and}$$

$$\overline{\nu\Sigma_f} = \frac{\nu\Sigma_{f1}\,\phi_1 + \nu\Sigma_{f2}\,\phi_2}{\phi_2} \text{ ,}$$

where ϕ_1 is the first energy group flux; and

ϕ_2 is the second energy group flux.

The group cross sections and fluxes are obtained as assembly averaged values from PDQ or CPM calculations. $\overline{\kappa\Sigma_f}$ is used to determine the thermal neutron flux for each node from the nodal

value of watts per cm^3 for calculation of the iodine and xenon number densities. $\overline{\nu\Sigma_f}$ and $\overline{\kappa\Sigma_f}$ are used for the internal conversion of nodal source to nodal power and for the utilization of the nodal power in the moderator density loop where k^n is calculated.

The formulation used in NODE-B for converting source to power (or vice-versa) uses the relationships

$$S \sim \overline{\nu\Sigma_f}, \text{ and}$$

$$P \sim \overline{\kappa\Sigma_f},$$

where:

$\nu\Sigma_f$ and $\kappa\Sigma_f$ are obtained as defined above; and, thus

$$P = \frac{S * \overline{\kappa\Sigma_f}}{\overline{\nu\Sigma_f}}.$$

3.3 Thermal Hydraulic Model

The PSMS thermal hydraulic calculations are based on the THERM-B model, where the inlet flow distribution, void profile, and core inlet subcooling are computed. The core thermal power, feedwater flow, feedwater temperature, core pressure and core flow are the basic inputs to the computations. The core inlet subcooling is derived by a heat balance in the downcomer and the lower plenum region of the vessel. The channel flow distribution is obtained on an iterative basis by changing the coolant velocity to each fuel channel until it yields a pressure drop that corresponds to

the pumphead requirement within a specified tolerance. When a flow distribution is obtained for all of the channels, the individual flow to each channel is summed and compared to the total required flow. If the flow is within a specified tolerance, the problem is converged. If it is not within the specified tolerance, the pumphead is adjusted to reduce the error between the computed total flow and the flow specified by the input, and the entire iterative procedure is repeated.

A newly developed quality-to-void correlation[5] with special treatment of the subcooled region has been implemented in the PSMS. This mechanistic model has been reduced to an approximate formulation that in steady-state cases has been shown to be in good agreement with the original model.

Flow Distribution and Pressure Drop

For a specified total core flow rate, the flow rate distribution is determined by equalizing the pressure drop across each channel. The equation used to calculate the fuel assembly pressure drop in a BWR is

$$\Delta P = \frac{V_{in}^2}{2g_c} * \left[\frac{f_o L_o}{De} + \frac{R f_o L_B}{De} + 2r + K\right],$$

where

V_{in} = liquid coolant velocity in, ft/sec

g_c = gravitational constant

f_o = friction factor

L_o = non-boiling length, ft

L_s = boiling length, ft

De = equivalent diameter, ft

R = ratio of the two phase friction loss to the single phase friction loss

r = the acceleration multiplier

K = form loss coefficient for fuel assembly entrance, exit, and intermediate spacers

Total flow through the individual channels is calculated as a part of the NODE-B program. The input required for this calculation is the fuel assembly length, flow area, equivalent diameter, orifice loss coefficient, and intermediate spacer loss coefficient. A single velocity head loss is used for the fuel assembly loss coefficient to the upper plenum. The form loss coefficients are based on single-phase flow and are adjusted within the code for two-phase flow effects. The above equation treats friction loss for boiling and non-boiling regions. It also considers the losses resulting from the acceleration of the coolant due to two-phase flow.

The velocity used in the above equation is the inlet velocity to the fuel assembly based upon the flow area within the fuel assembly.

The friction factor for single-phase flow is determined from the following correlation,

$$f_o = 0.19\ (N_{Re})^{-0.188}, \text{ where}$$

N_{Re} = Reynolds Number.

This formula is a curve fit to the Fanning friction factor curve given in Reference 5.

The Reynolds number in the above correlation is a dimensionless parameter which is a measure of flow and turbulence in a flow channel. The definition of the Reynold's number is

$$N_{Re} = \frac{D_e\ V\ \rho}{\mu},$$

where:

De = equivalent diameter, ft;

V = liquid coolant velocity, ft/sec;

ρ = liquid coolant density, lbs/ft^3; and

μ = liquid viscosity, lb/(sec-ft).

Subcooling Equations

The subcooling is calculated in NODE-B by performing a heat balance in the downcomer and lower plenum regions of the BWR vessel. The subcooling is defined as $H_{sc} = (H_{sat,\ Pcore}) - (H_{in})$,

where:

H_{sc} = subcooling, BTU/lb;

$H_{sat.\ Pcore}$ = saturated liquid enthalpy at core average pressure, BTU/lb; and

H_{in} = core inlet coolant enthalpy, BTU/lb.

The following heat balance is made to determine the core inlet coolant enthalpy.

$$H_{in} = \frac{1}{WT}\left[(WT - WST - WCU)HF + WCU*HG + WFW*HFW + HRD*WRD + QPUMP - QLOSS - QCL\right]$$

where:

H_{in} = Core inlet coolant enthalpy, BTU/lb;

WT = Total core flow, lbs/hr;

WST = Steam flow leaving reactor vessel, lbs/hr;

WCU = Steam carryunder in recirculation flow entering, downcomer, lbs/hr;

WFW = Feedwater flow, lbs/hr;

QPUMP = Energy from recirculation pumps, BTU/hr;

QLOSS = Heat loss from reactor vessel, BTU/hr;

HF = Enthalpy of saturated liquid entering downcomer (evaluate at dome pressure), BTU/lb;

HG = Saturated steam enthalpy of carryunder, BTU/lb;

HFW = Feedwater flow enthalpy, BTU/lb;

HRD = Control rod drive flow enthalpy, BTU/lb;

WRD = Control rod drive flow, lbs/hr; and

QCL = Energy loss to the cleanup system, BTU/hr.

The flows (WT,WFW, and WRD) and QLOSS are input to NODE-B. The steam flow is assumed to be equal to (WFW + WRD). The saturated liquid and steam enthalpies are evaluated based on the dome and core pressure which are input to the code. The enthalpies for the feedwater flow and control rod drive flow are evaluated based on the inlet coolant temperatures. The energy from the recirculation pumps is determined from the power drawn by each motor and the efficiency of the pumps; these values are input to the code. The steam carryunder flow is defined as a fraction of the total core flow.

Boiling Effect on Pressure Drop

The equation solved to determine the non-boiling length in the fuel channel is

$$A_{in} * 3600 * V_{in} * \rho_{in} (H_{sat} - H_{in}) = \int_{o}^{L_o} q(x)*p*dx,$$

where:

H_{sat} = Saturated liquid enthalpy, BTU/lb;

H_{in} = Inlet coolant enthalpy, BTU/lb;

ρ_{in} = Inlet coolant density, lb/ft^3;

V_{in} = Inlet coolant velocity, ft/sec;

$q(x)$ = Heat flux as a function of axial location, x, within the fuel assembly, $BTU/hr-ft^2$;

P = Perimeter of the heated surface, ft;

L_o = Non-boiling length; and

A_{in} = Fuel bundle flow area, ft^2.

The boiling length L_B is determined from the total length L and the non-boiling length by

$$L_B = L - L_o.$$

The ratio of the two-phase friction loss to single phase friction loss, R, is obtained from the Lottes-Flinn[7] correlation

$$R = \frac{f \text{ two-phase}}{f_o} = \frac{1}{2}*\left(1 + \frac{1}{1-\alpha_e}\right)^2,$$

where:

α_e = the void fraction at the end of the fuel channel.

The acceleration multiplier, r, used is the Martinelli-Nelson relationship derived for two-phase flow assuming complete separation of the phases[8]. This relationship is given as

$$r = (1 - x_e)^2/(1 - \alpha_e) + \frac{x_e^2}{\alpha_e}\frac{\rho_l}{\rho_s} - 1,$$

where:

x_e = Channel exit quality;

α_e = Channel exit void friction;

ρ_l = Liquid phase density, lbs/ft^3; and

ρ_s = Steam phase density, lbs/ft^3.

The loss coefficient K is the summation of all of the form losses along the fuel assembly. The loss coefficient includes the following:

- Orifice loss to each fuel channel;
- Each intermediate spacer loss; and
- Exit loss from fuel channel to upper plenum (this loss is assumed to be one velocity head).

The single-phase loss coefficients are input to NODE-B. In the bulk boiling region they are corrected for the local quality and void condition within the fuel channel. The correction is

$$K = K_{single\text{-}phase} * \left(\frac{1 - x}{1 - \alpha} \right)^2,$$

where:

x = local equilibrium coolant quality evaluated in NODE-B as Q_{ijk}; and

α = local coolant void fraction.

This correction assumes that the pressure loss along the fuel channel can be based upon the liquid phase velocity. This correction accounts for the decrease in the liquid phase mass flow due to steam formation and the increase in the liquid phase velocity due to the local steam void fraction. The value of the single phase loss coefficient is usually obtained experimentally. However, if experimental data are not available, the coefficient can

be estimated by calculating the loss coefficient based upon standard coefficients for entrance and exit effects.

In the boiling water reactor the water in the downcomer is either saturated or slightly subcooled, depending on where the feedwater is introduced. If the feedwater is added at the top of the downcomer and good mixing with recirculating water is achieved, the density in the downcomer is equal to the density of the coolant at the fuel channel inlet. Due to the density difference between the downcomer and fuel channel, a driving pressure or buoyant head is established.

If the feedwater enters the top of the downcomer, the downcomer density is an average based upon the two principal flow streams to the downcomer. The buoyant head associated with a particular channel can be written as

$$\text{Buoyant Head} = \left(1 - \frac{\bar{\rho}_1}{\rho_1}\right) L_o + \left(1 - \frac{\bar{\rho}_s}{\rho_1}\right) L_B ,$$

where:

Buoyant head = feet of fluid at inlet density;

ρ_1 = Average density of liquid phase in the channel over the non-boiling length L_o;

ρ_1 = Inlet liquid density, also downcomer liquid density; and

$\bar{\rho}_s$ = Average density of two-phase mixture over the boiling length, L_B.

As the coolant flows through the various fuel channels, it encounters resistances which are described in terms of pressure losses. The sum of these losses for a fuel channel less any buoyant head contribution then has to be recovered by the pumps in the recirculation loop.

For the NODE-B code, the term pumphead is used to denote the difference between the flow head losses and buoyant head.

Moderator Density Determination

The nuclear characteristics of the fuel are represented, in part, as a function of the relative moderator density, U_{ijk}. The program determines U_{ijk} by first calculating the nodal quality from the power and channel flow rates, then determining the steam volume fraction and finally converting this volume fraction to the relative moderator density. Details of this calculation are described as follows.

Node Quality Calculation

The equilibrium quality at each node, Q_{ijk}, is calculated from the expression

$$Q_{ijk} = \frac{P}{P_r} * \frac{W_r}{W} * \frac{1}{(F_{ij})*KMAX} * \left[\sum_{\ell=1}^{\kappa} Pij\ell - \frac{Pijk}{2} \right] * (Q_{ex}-Q_o) + Q_o$$

where the summation is up channel ij and:

$\frac{W_r}{W}$ = ratio of rated to actual flow;

$\frac{P}{P_r}$ = ratio of actual to rated power;

KMAX = the number of axial nodes in the problem; and

F_{ij} = the ratio of flow in channel ij at power P_{ij} to average channel flow.

The inlet and exit qualities, Q_o and Q_{ex}, are obtained as follows.

$$Q_o = \frac{H_{in} - H_{sat}}{H_{fg}} ,$$

and

$$Q_{ex} = \frac{H_{ex} - H_{sat}}{H_{fg}} = \frac{H_{ex} - H_{in}}{H_{fg}} + Q_o ,$$

where H_{fg} is the heat of vaporization of water at the system pressure. Note that $H_{in} - H_{sat}$ is the inlet subcooling which is an input quantity and that $H_{ex} - H_{in}$ is just the total enthalpy rise in all channels:

$$H_{ex} - H_{in} = (3.4129 \times 10^6) * P/W.$$

Void-Quality Relationship

The relationship between local equilibrium quality and local void is provided by the Zolotar-Lellouche Profile Fit Model (Reference 3). The relationship is in the form

$$\alpha = \frac{x}{C_o \left[x + \frac{P_g}{P_l}(1-x)\right] + \frac{P_g V_{gi}}{G}}$$

where:

α = void fraction

x = flow quality;

C_o = concentration parameter;

V_{gi} = drift velocity of the vapor, relative to the liquid;

G = mass flux;

P_g, P_l = the mass densities of vapor and liquid.

The void model includes equations which specify the flow quality drift velocity and C_o in terms of the thermal hydraulic valuables.

Relative Moderator Density

The relative moderator density, U, which is the ratio of the two phase density to the saturated water density, is then determined from

$$U_{ijk} = 1.0 - \alpha_{ijk} * (1 - \rho_s/\rho_w) ,$$

where ρ_s and ρ_w are the saturated steam and water densities at system pressure and α_{ijk} is the void fraction for node ijk.

3.4 Instrumentation Model

The in-core instrument readings are predicted by NODE-B. The prediction of an instrument reading at a given location is based on the nodal power of the four fuel nodes adjacent to the instrument. The four nodal powers are multiplied by a conversion factor and summed to get the relative instrument reading, IR, as follows:

$$IR_{ijk} = \sum_{ij} P_{ijk} * RF_{ijk}$$

where P_{ijk} is the nodal power and RF_{ijk} is the conversion factor. The conversion factor is a function of voids, exposure, fuel type and control rod presence. The conversion factor is obtained from CPM calculations. The values of RF are fitted to the equation:

$$RF = C1 + C2*E + C3*E^2 + C7*E^3 + (C5 + C8*E) * (1 - (U/UBASE)$$

where the C constants are input for each fuel type and E and U are the nodal exposure and relative moderator density, respectively. A second set of C constants are used for controlled nodes.

The relative instrument reading is multiplied by input factors XMONO and PTH to convert the reading to absolute readings in watts/cm^2.

3.5 Haling Option

The Haling option[9] allows the user to determine the optimum power shape for an operating cycle. The optimum power shape is the power shape that will maintain a minimum power peaking factor throughout the cycle. The Haling principle states that for any given set of end-of-cycle conditions, the power peaking factor is maintained at the minimum value when the power shape does not change during the operating cycle.

The power, void and exposure distribution are iterated until these three distributions converge. Convergence is reached when the BOC power distribution is the same as the EOC power distribution (within a specified convergence criteria) after the core is burned with the BOC power distribution.

The Haling option is used to estimate cycle energy and to evaluate core loading patterns. It is used to generate the end of cycle exposure and void array and target power shape for the reload analysis.

4.0 VERIFICATION

The verification work that has been performed was to establish confidence in the methods described here. Confidence is established by the ability of the methods to reproduce criticality and power distribution data measured in operating plants over a period of time and conditions. The verification work, therefore, encompasses comparisions of NODE-B calculations to measured data over several operating cycles. Since Oyster Creek is the primary focus for the applications of these methods, the majority of the verification is with Oyster Creek data. The addition of the Hatch 1, cycle 1 data was to also include gamma scan measurements that were made at end of cycle 1 in this verification. It also demonstrates the application of methods over a wider range of conditions and fuel designs.

4.1 Comparison with Data Measured at Oyster Creek.

4.1.1 Cold Criticals

The NODE-B cold model was evaluated against cold criticals performed at Oyster Creek during startup tests at the beginning of cycles 8, 9 and 10. The criticals were performed at the beginning of each cycle with the head off the vessel and moderator temperature around 90°F. The criticals performed are local criticals with a series of positive and negative periods to notch calibrate a control rod and measure shutdown margin. These criticals are particularly good to demonstrate the capability of the model to calculate shutdown margin.

The criticals performed for each cycle are shown in Table 4.1 to 4.3 along with the calculated k-effectives corrected for temperature. The critical k-effective is corrected for period and temperature. The combined average k-effective for the 3 cycles is 1.00193 with a standard deviation of 0.00293. Part of the variation in the k-effective from cycle to cycle is due to the different number of control rods used in and location of, the critical configurations. The critical k-effective with a minus one sigma uncertainty is used to predict shutdown margin.

4.1.2 Hot Reactivity Calculation

NODE-B core follow calculations were performed for Oyster Creek cycles 8 and 9. Twelve statepoints were analyzed for each cycle. Key information for each statepoint is provided in Tables 4.4 and 4.5. The core average k-effective is calculated for each statepoint and the mean k-effective for the cycle is provided in Tables 4.6 and 4.7. The mean k-effective for both cycles 8 and 9 is 0.986245 with a standard deviation of 0.00177. The consistency of the k-effective is very good both within cycle 8 and 9 and from cycle 8 to cycle 9.

4.1.3 Power Distribution Comparison

The accuracy of the NODE-B power distribution was determined by comparing measured TIPs to TIPs predicted by NODE-B.

These comparisons were performed for the cycle 8 and 9 statepoints with the results shown in Tables 4.6 and 4.7.

The TIP nodal uncertainty is given in percent RMS which is calculated as follows

Residual for node ijk

$$R_{ijk} = (M - C)/\bar{M}$$

Overall Nodal RMS error

$$RMS = \left[\sum_{\ell,k} R^2(\ell, k)/\ell * k \right]^{\frac{1}{2}}$$

where:

M = measured TIP for node ijk

C = calculated TIP for node ijk

$\bar{M}$ = average measurement

ℓ = number of TIP strings

k = number of axial nodes.

The mean nodal RMS is 7.65% $\pm$ 1.41% for cycles 8 and 9. Figures 4.1 to 4.24 contain the comparison of the core average axial TIP between NODE-B and measurements. The nodal uncertainty of 7.65% is very good. Part of the uncertainty is in the TIP measurements themselves. The TIP asymmetry (unexplained differences between readings of symmetrically located TIPs) was 2.97% and 2.90% for cycles 8 and 9 respectively.

TABLE 4.1

SHUTDOWN MARGIN CRITICALS FOR CYCLE 8

Critical*	Calculated k	Measured k	Bias
1 Pos	1.00504	1.00122	0.00382
1 Neg	1.00469	0.99961	0.00508
2 Pos	1.00665	1.00121	0.00544
2 Neg	1.00591	0.99925	0.00666
3 Pos	1.00655	1.00122	0.00534
3 Neg	1.00507	0.99930	0.00577
4 Pos	1.00703	1.00089	0.00615
5 Pos	1.00586	1.00032	0.00554

Temperature = 97°F

Critical k_{eff} = 1.00548
1σ = 0.00083

*
Pos - positive period
Neg - negative period

TABLE 4.2

SHUTDOWN MARGIN CRITICALS FOR CYCLE 9

Critical	Calculated k	Measured k	Bias
1 Pos	0.99688	1.00082	-0.00394
1 Neg	0.99646	0.99961	-0.00315
2 Pos	1.00043	1.00077	-0.00035
2 Neg	0.99979	0.99943	0.00036
3 Pos	1.00084	1.00076	0.00009
3 Neg	0.99931	0.99891	0.00040
4 Pos	1.00106	1.00083	0.00023
4 Neg	0.99863	0.99968	-0.00105

Temperature = 90°F

Critical k_{eff} = 0.99907
1σ = 0.00170

TABLE 4.3

SHUTDOWN MARGIN CRITICALS FOR CYCLE 10

Critical	Calculated k	Measured k	Bias
1 Pos	1.00075	1.00075	0.00000
1 Neg	0.99999	0.99934	0.00065
2 Pos	1.00230	1.00094	0.00136
2 Neg	1.00144	0.99977	0.00167
3 Pos	1.00207	1.00068	0.00139
3 Neg	1.00085	0.99966	0.00119
4 Pos	1.00242	1.00070	0.00172
4 Neg	1.00194	0.99994	0.00200

Temperature = 93°F

Critical k_{eff} = 1.00125
1σ = 0.00065

TABLE 4.4

KEY INFORMATION FOR OYSTER CREEK CYCLE 8 STATEPOINTS

Date	Power (MWth)	Recirc. Flow (Mlbs/hr)	Core Avg. Exp. (GWD/MTU)	Rod Sequence	% Rod Density
01-26-79	1917.4	58.69	11.02	A	14.89
02-22-79	1914.3	59.50	11.52	A	17.03
03-01-79	1916.8	58.08	11.64	A	17.03
03-20-79	1912.5	57.59	12.02	A	18.19
04-19-79	1912.3	59.95	12.30	B	18.49
06-08-79	1805.6	53.37	12.66	B	18.31
07-03-79	1910.3	59.41	13.15	B	16.85
07-26-79	1914.2	58.35	13.57	A	16.33
08-30-79	1892.3	56.79	14.25	A	12.68
09-06-79	1905.9	59.31	14.37	A	12.68
10-25-79	1907.3	57.46	15.27	A	7.18
12-05-79	1777.4	59.50	15.95	A	3.65

TABLE 4.5

KEY INFORMATION FOR OYSTER CREEK CYCLE 9 STATEPOINTS

Date	Power (MWth)	Recir. Flow (Mlbs/hr)	Core Avg. Exp. (GWD/MTU)	Rod Sequence	% Rod Density
07-30-80	1635.7	49.36	9.93	A	17.15
08-29-80	1677.4	50.06	10.35	A	17.64
09-29-80	1928.7	60.23	10.81	A	18.30
11-11-80	1840.6	58.44	11.58	B	21.35
12-16-80	1833.1	57.24	12.07	B	20.38
02-27-81	1685.2	53.04	13.35	B	16.24
03-24-81	1907.7	56.76	13.71	B	14.48
06-16-81	1923.1	60.50	14.32	A	11.53
07-09-81	1247.6	39.58	14.59	A	11.92
08-11-81	1274.8	49.69	15.02	A	10.71
11-25-81	1860.8	57.97	15.66	A	4.26
12-09-81	1840.4	60.89	15.92	A	4.01

TABLE 4.6

CORE REACTIVITY AND POWER DISTRIBUTION COMPARISON
FOR OYSTER CREEK CYCLE 8

Statepoint	Calculated k_{eff}	TIP Nodal Uncertainty in % RMS
01-26-79	0.98666	10.16
02-22-79	0.98512	8.19
03-01-79	0.98394	7.77
03-20-79	0.98517	6.74
04-19-79	0.98476	6.92
06-08-79	0.98582	7.39
07-03-79	0.98810	7.28
07-26-79	0.98637	9.43
08-30-79	0.98624	8.24
09-06-79	0.98669	7.47
10-25-79	0.98906	7.17
12-05-79	0.98914	11.04
Mean	0.98[illegible]2	8.15
1σ	0.00[illegible]5	1.36

TABLE 4.7

CORE REACTIVITY AND POWER DISTRIBUTION COMPARISON
FOR OYSTER CREEK CYCLE 9

Statepoint		Calculated k_{eff}	TIP Nodal Uncertainty in % RMS
07-30-80		0.98517	7.60
08-29-80		0.98523	7.56
09-29-80		0.98527	6.63
11-11-80		0.98385	6.14
12-16-80		0.98534	6.26
02-27-81		0.98747	6.15
03-24-81		0.98578	6.30
06-16-81		0.98707	6.30
07-09-81		0.98562	7.89
08-11-81		0.98317	10.83
11-25-81		0.98953	7.31
12-09-81		0.98931	6.85
	Mean	0.98607	7.15
	1σ	0.00195	1.32

Figure 4.1
COMPARISON OF CORE AVERAGE AXIAL TIP READING FOR THE
OC CYCLE 8 STATEPOINT 01-26-79

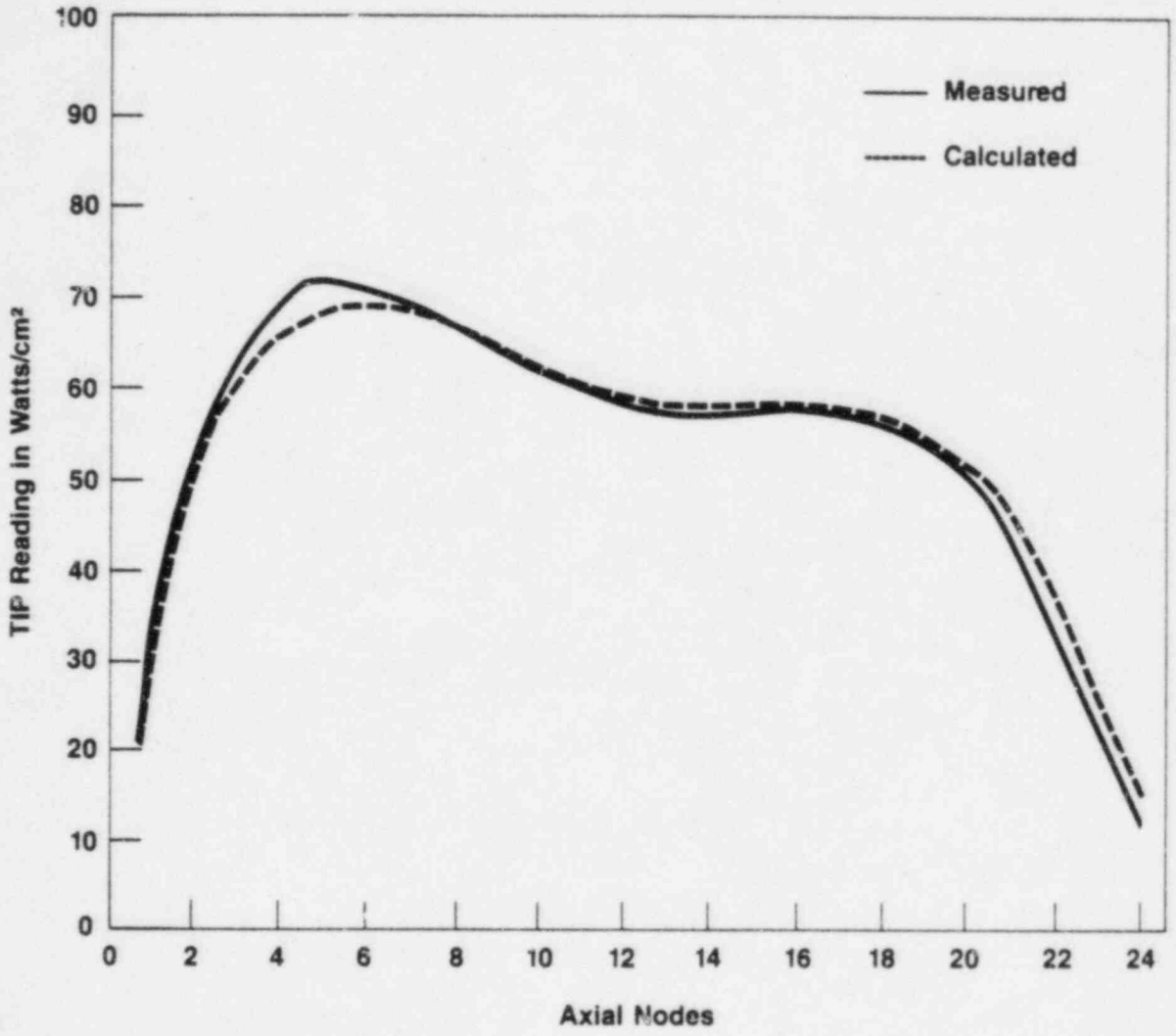

Figure 4.2
COMPARISON OF CORE AVERAGE AXIAL TIP READING FOR THE
OC CYCLE 8 STATEPOINT 02-22-79

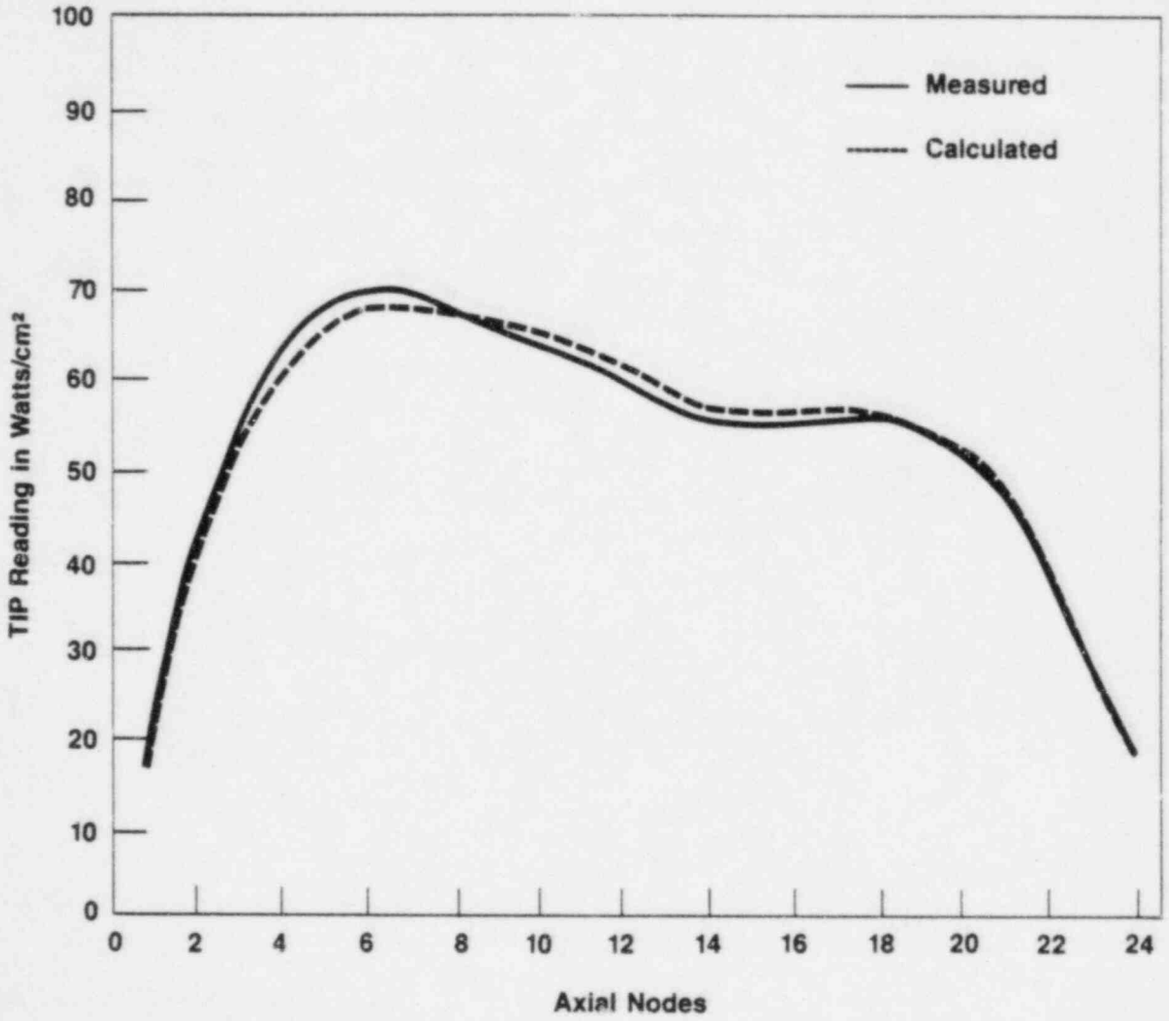

Figure 4.3
COMPARISON OF CORE AVERAGE AXIAL TIP READING FOR THE
OC CYCLE 8 STATEPOINT 03-01-79

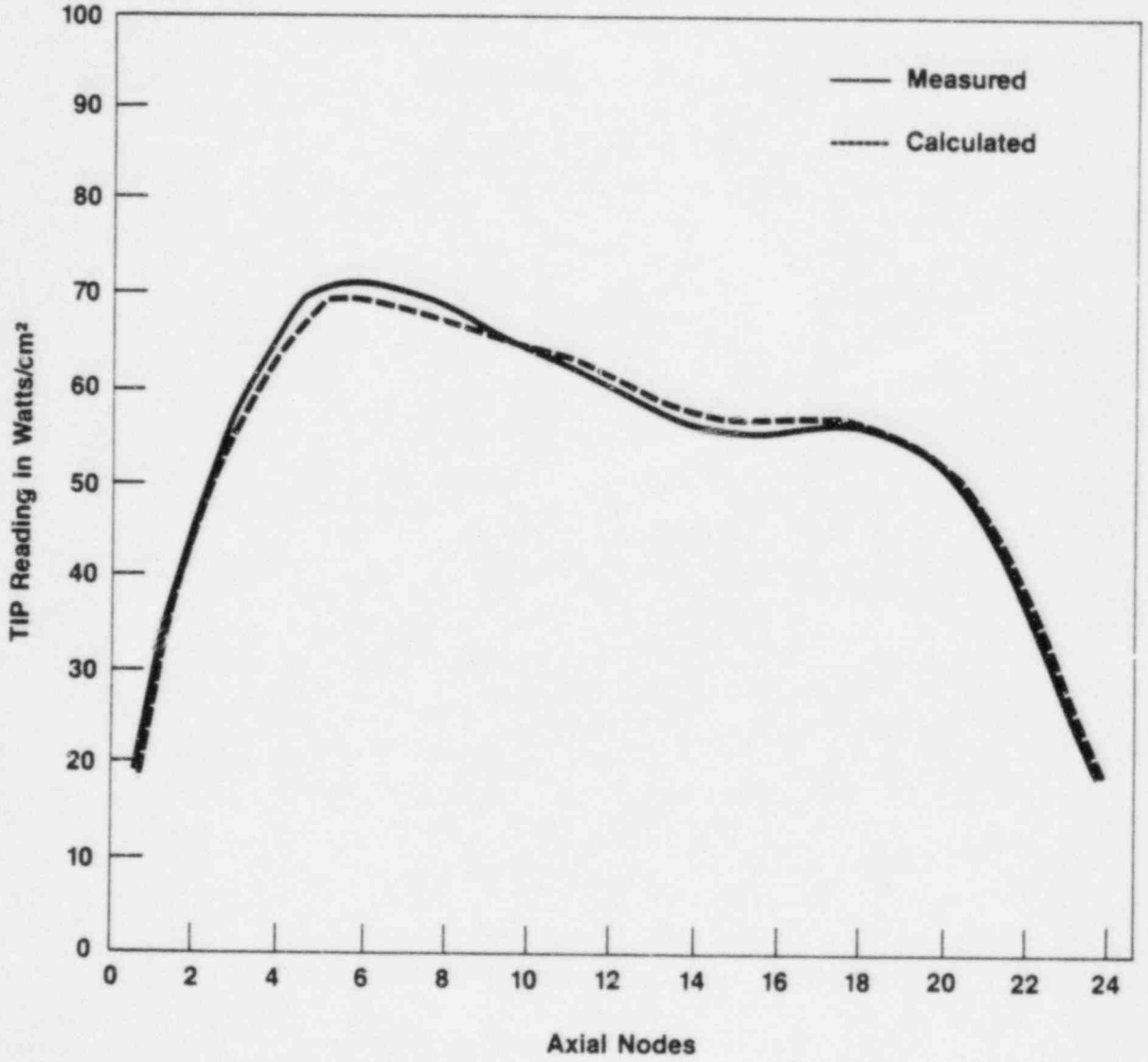

Figure 4.4
COMPARISON OF CORE AVERAGE AXIAL TIP READING FOR THE
OC CYCLE 8 STATEPOINT 03-20-79

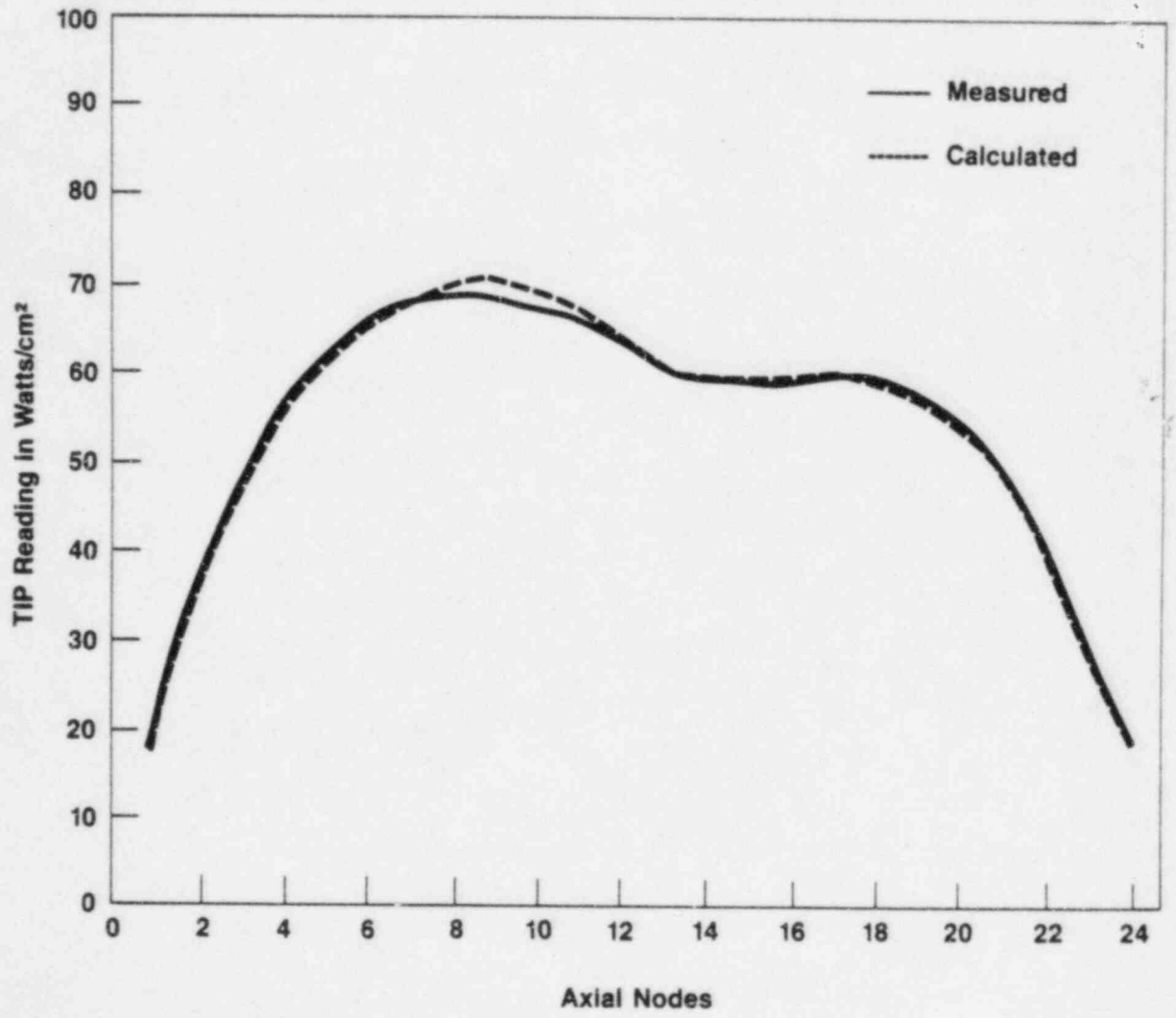

Figure 4.5
COMPARISON OF CORE AVERAGE AXIAL TIP READING FOR THE
OC CYCLE 8 STATEPOINT 04-19-79

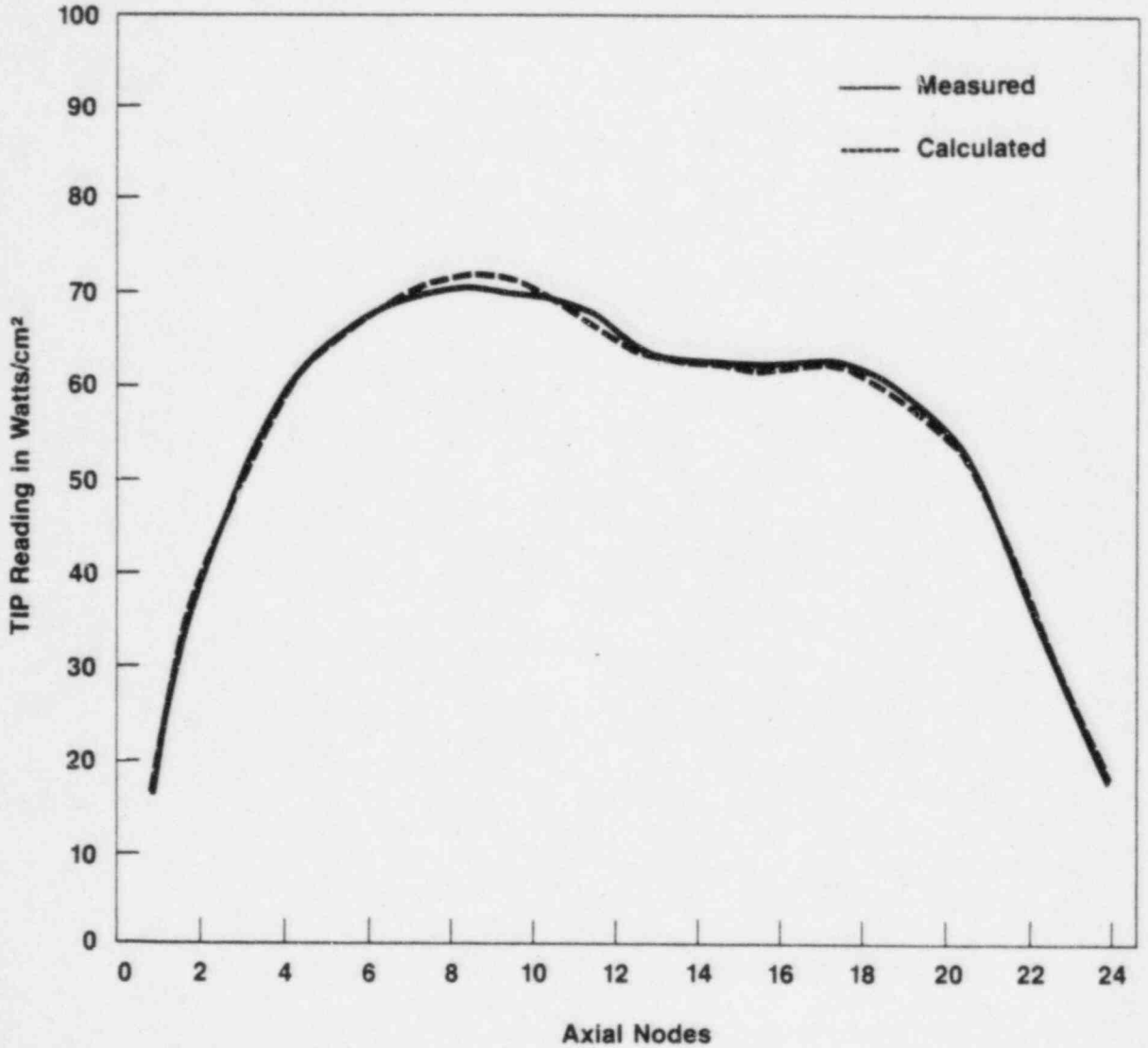

Figure 4.6
COMPARISON OF CORE AVERAGE AXIAL TIP READING FOR THE
OC CYCLE 8 STATEPOINT 06-08-79

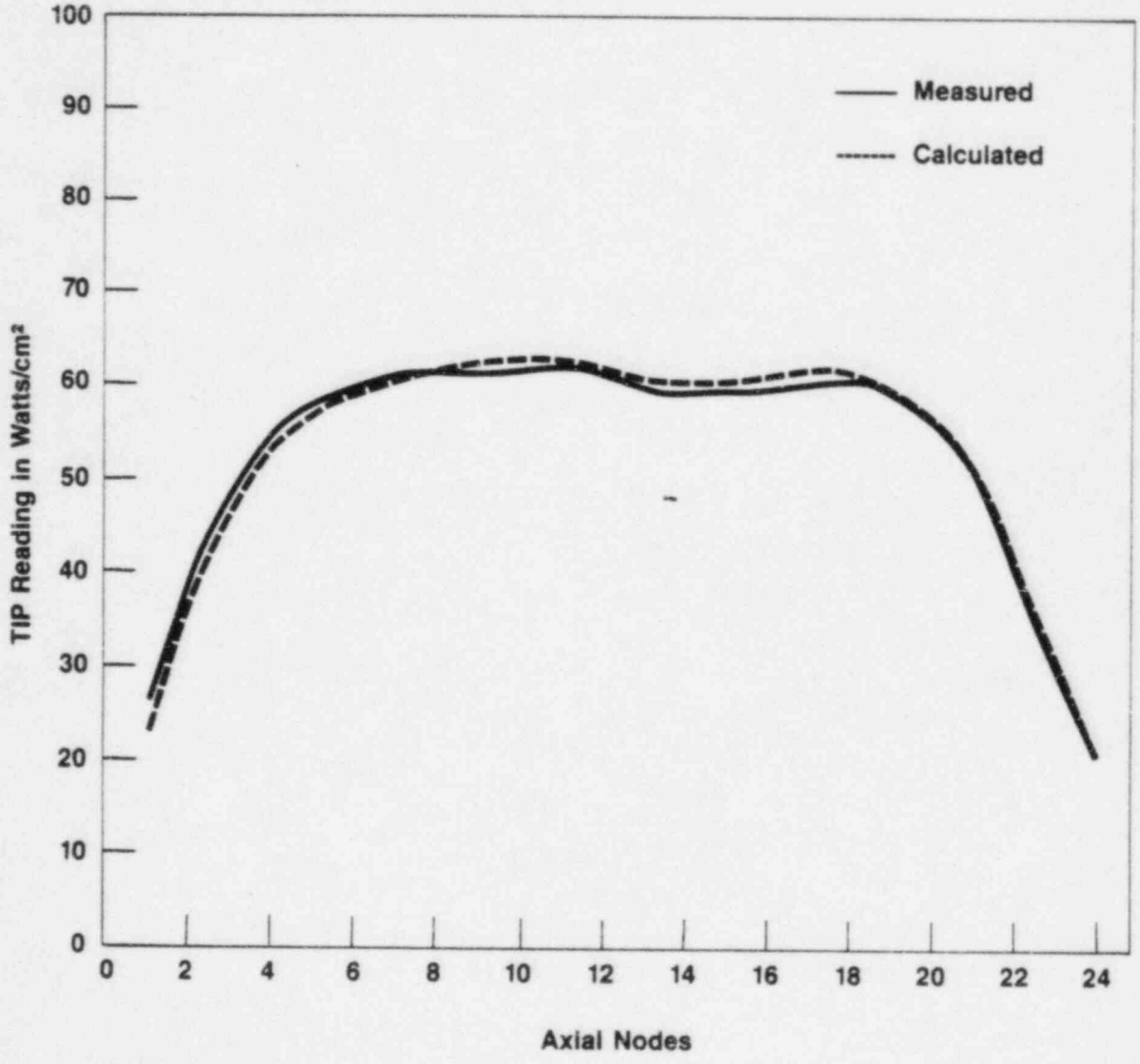

Figure 4.7
COMPARISON OF CORE AVERAGE AXIAL TIP READING FOR THE
OC CYCLE 8 STATEPOINT 07-03-79

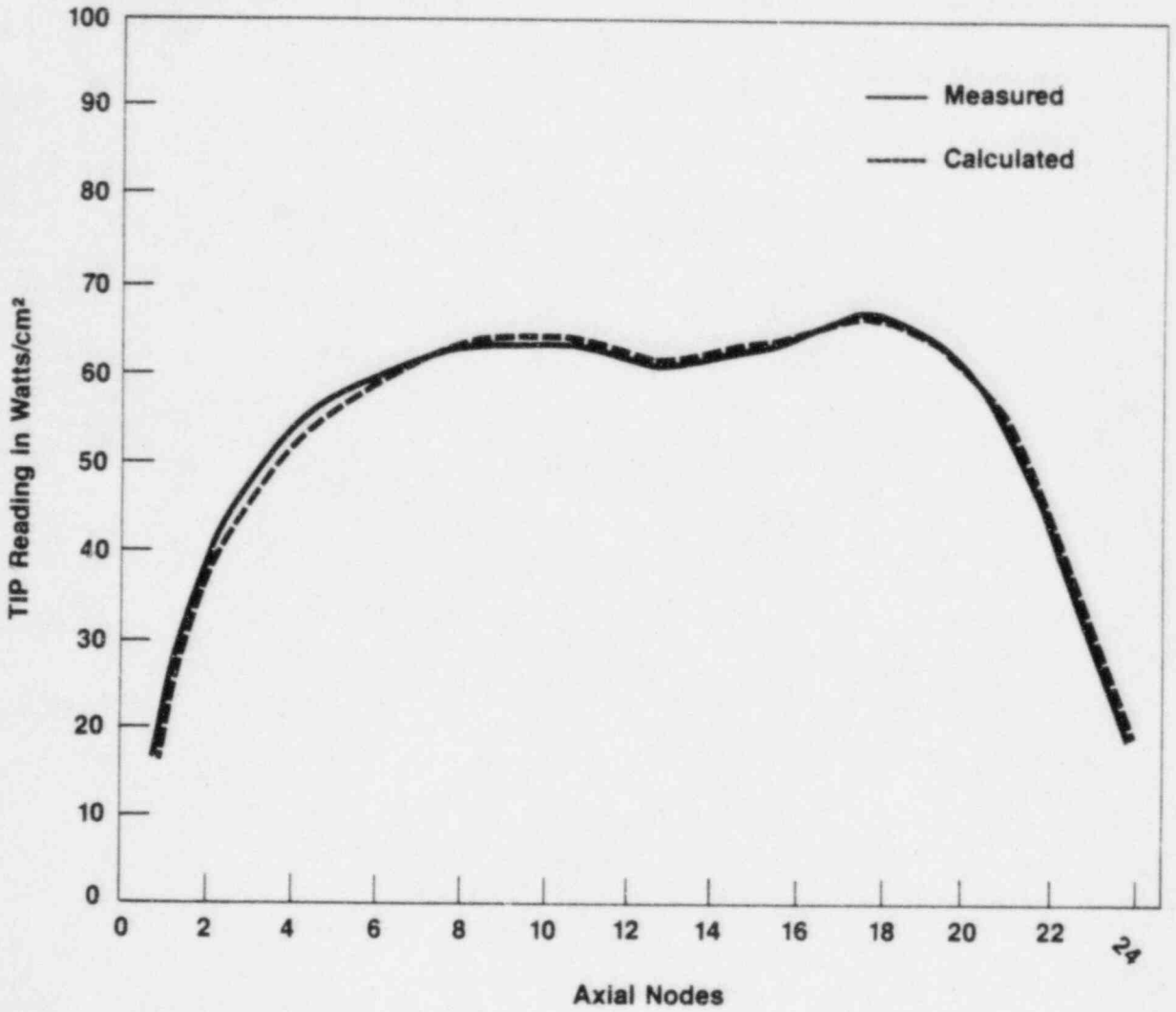

Figure 4.8
COMPARISON OF CORE AVERAGE AXIAL TIP READING FOR THE
OC CYCLE 8 STATEPOINT 07-26-79

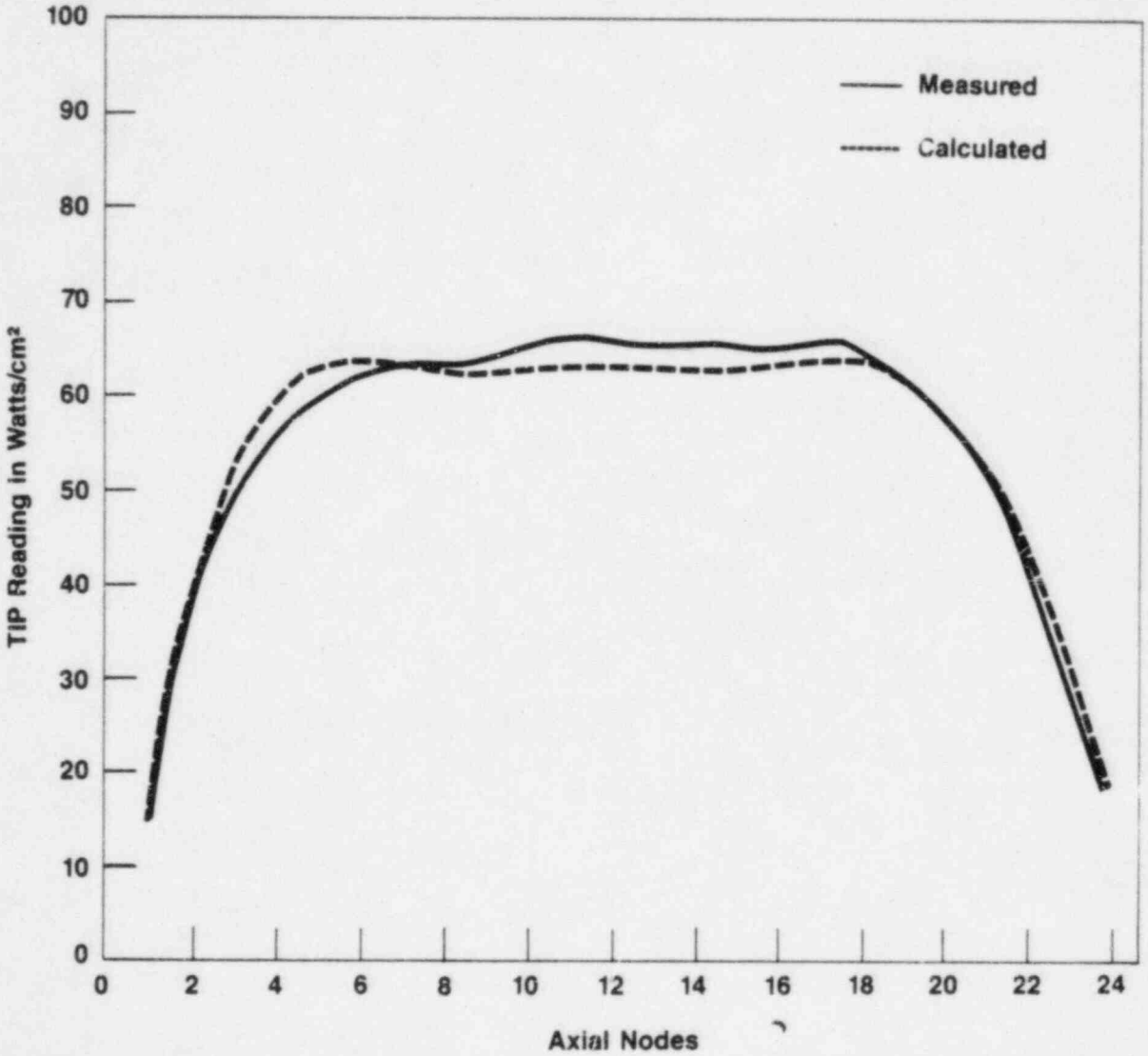

Figure 4.9
COMPARISON OF CORE AVERAGE AXIAL TIP READING FOR THE
OC CYCLE 8 STATEPOINT 08-30-79

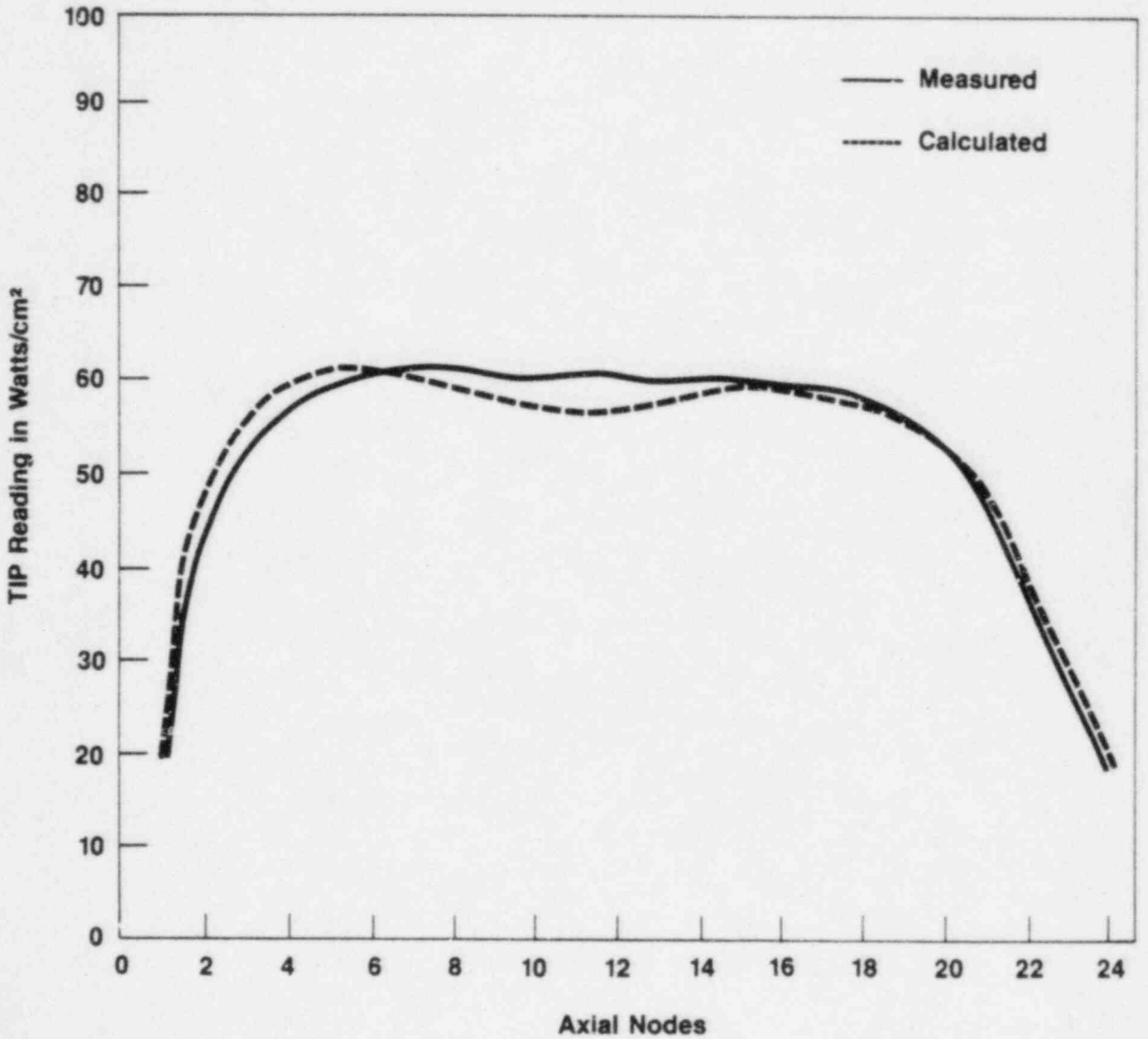

Figure 4.10
COMPARISON OF CORE AVERAGE-AXIAL TIP READING FOR THE
OC CYCLE 8 STATEPOINT 09-06-79

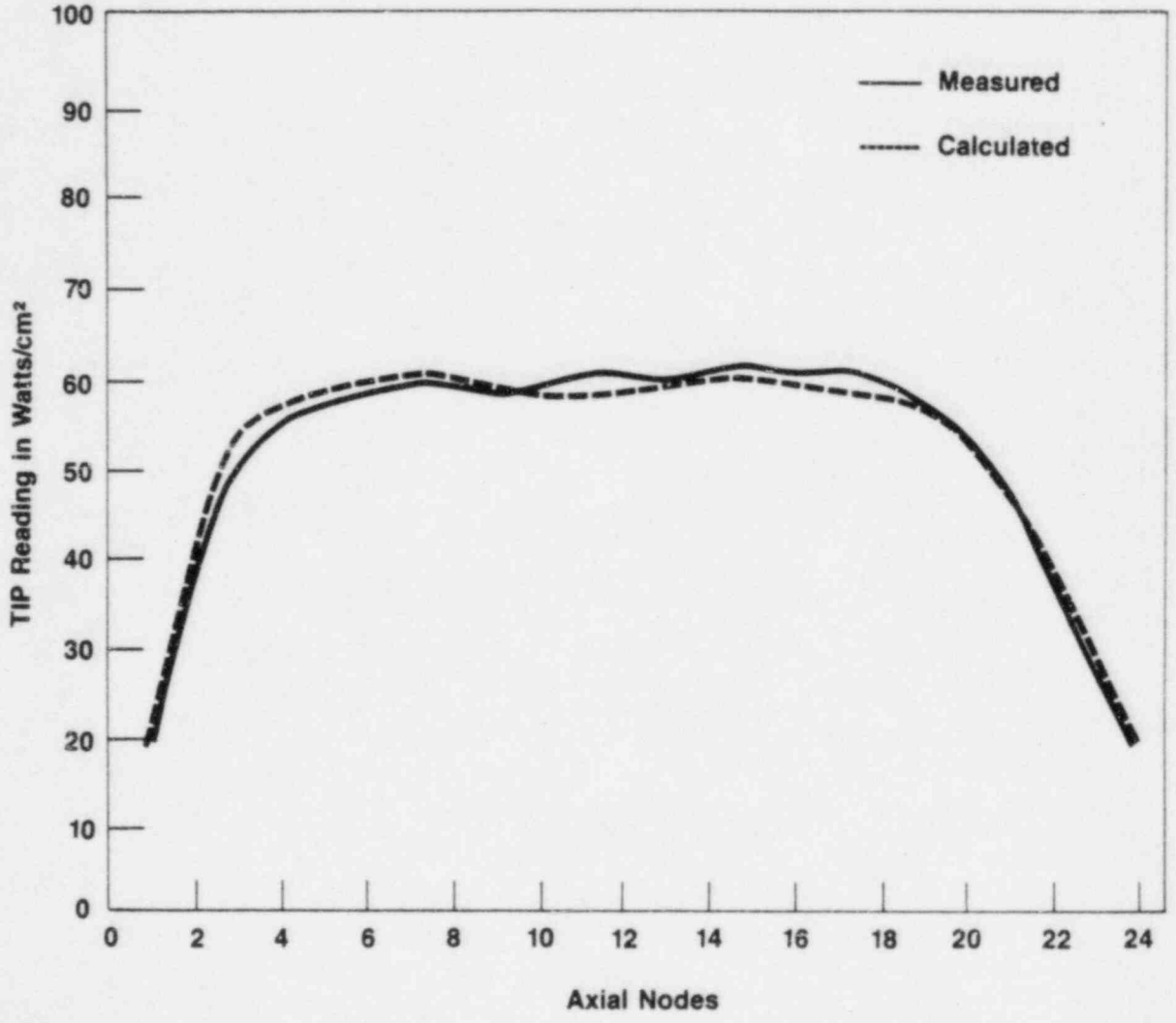

Figure 4.11
COMPARISON OF CORE AVERAGE AXIAL TIP READING FOR THE
OC CYCLE 8 STATEPOINT 10-25-79

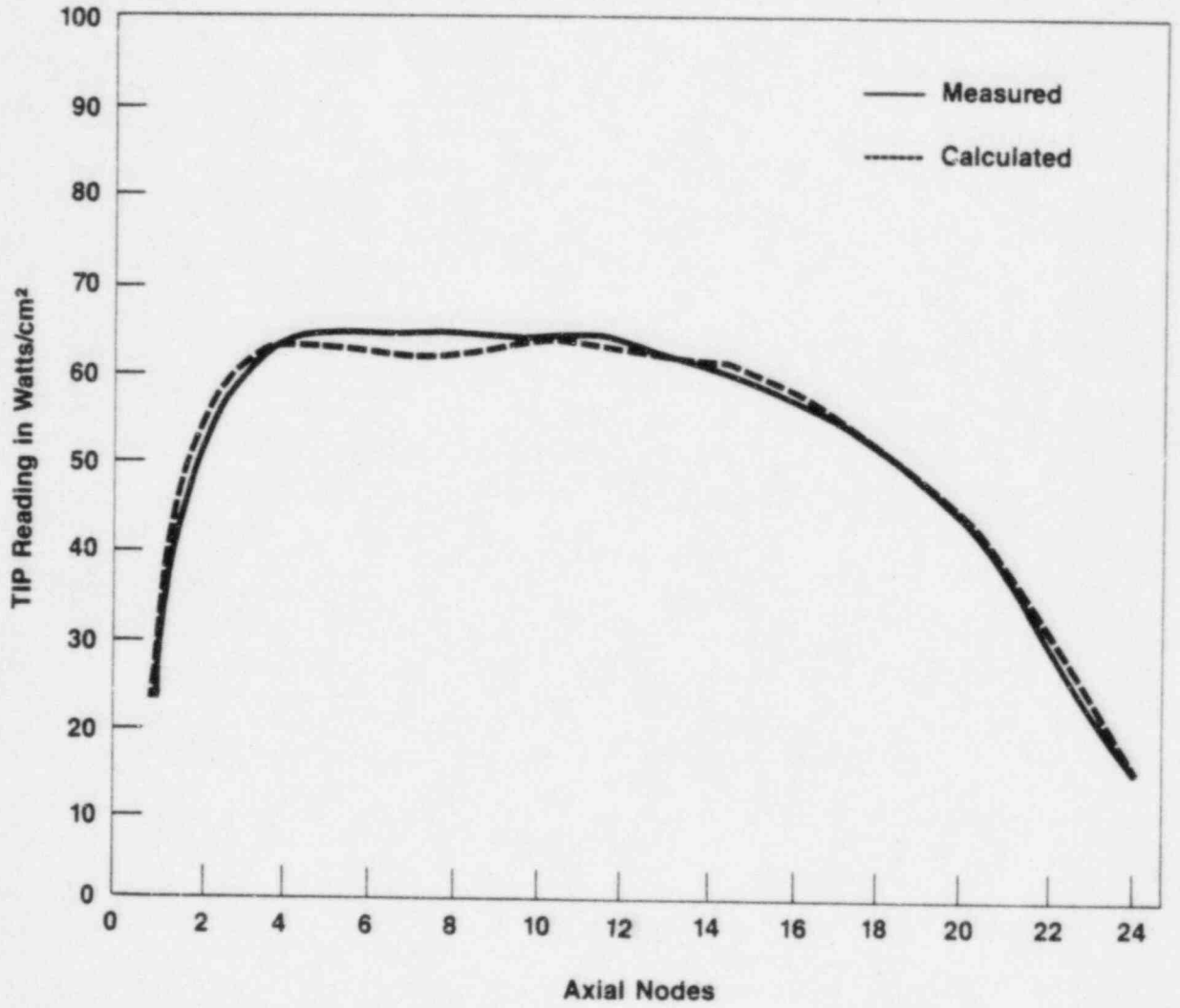

Figure 4.12
COMPARISON OF CORE AVERAGE AXIAL TIP READING FOR THE
OC CYCLE 8 STATEPOINT 12-05-79

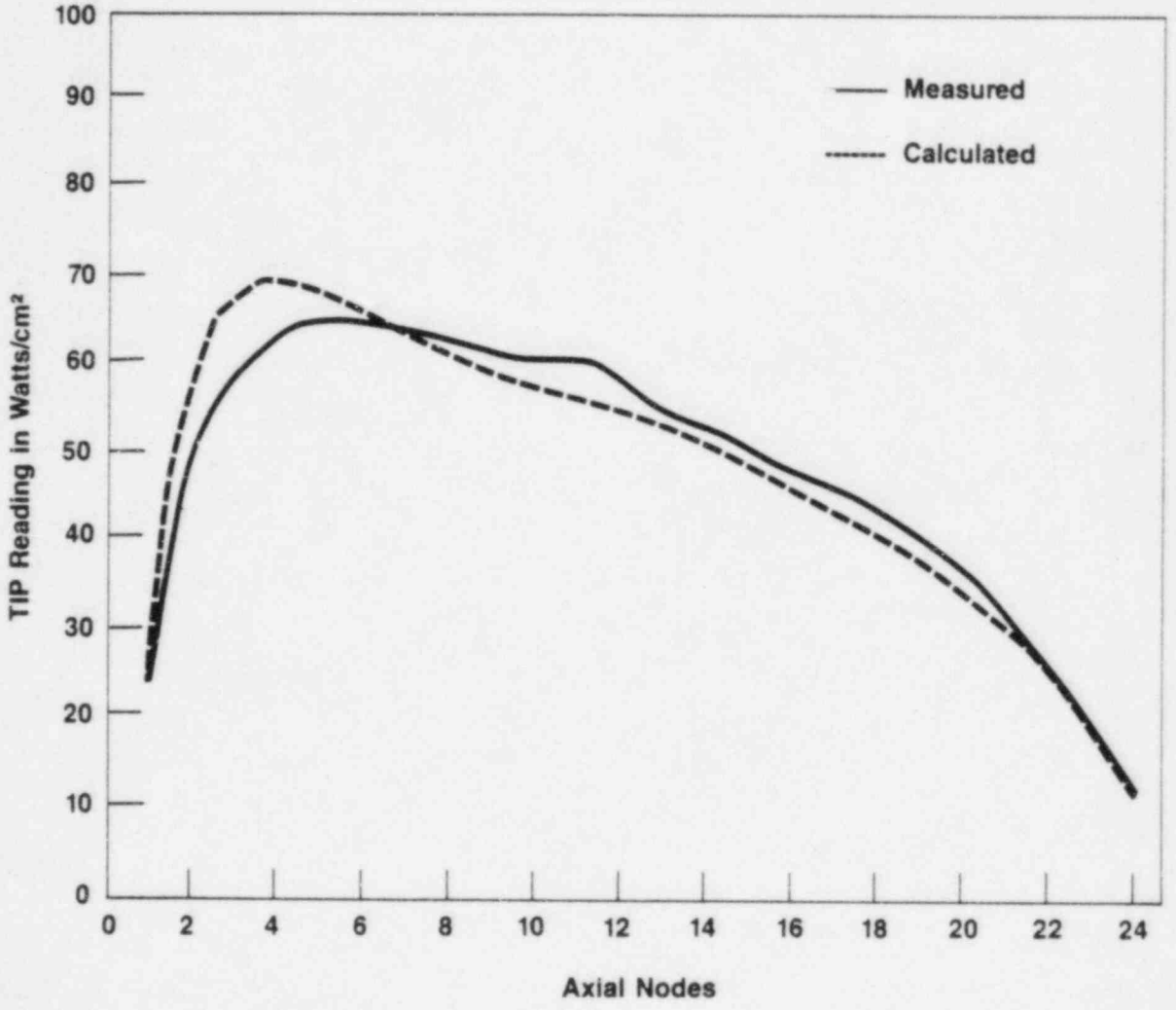

Figure 4.13
COMPARISON OF CORE AVERAGE AXIAL TIP READING FOR THE
OC CYCLE 9 STATEPOINT 07-30-80

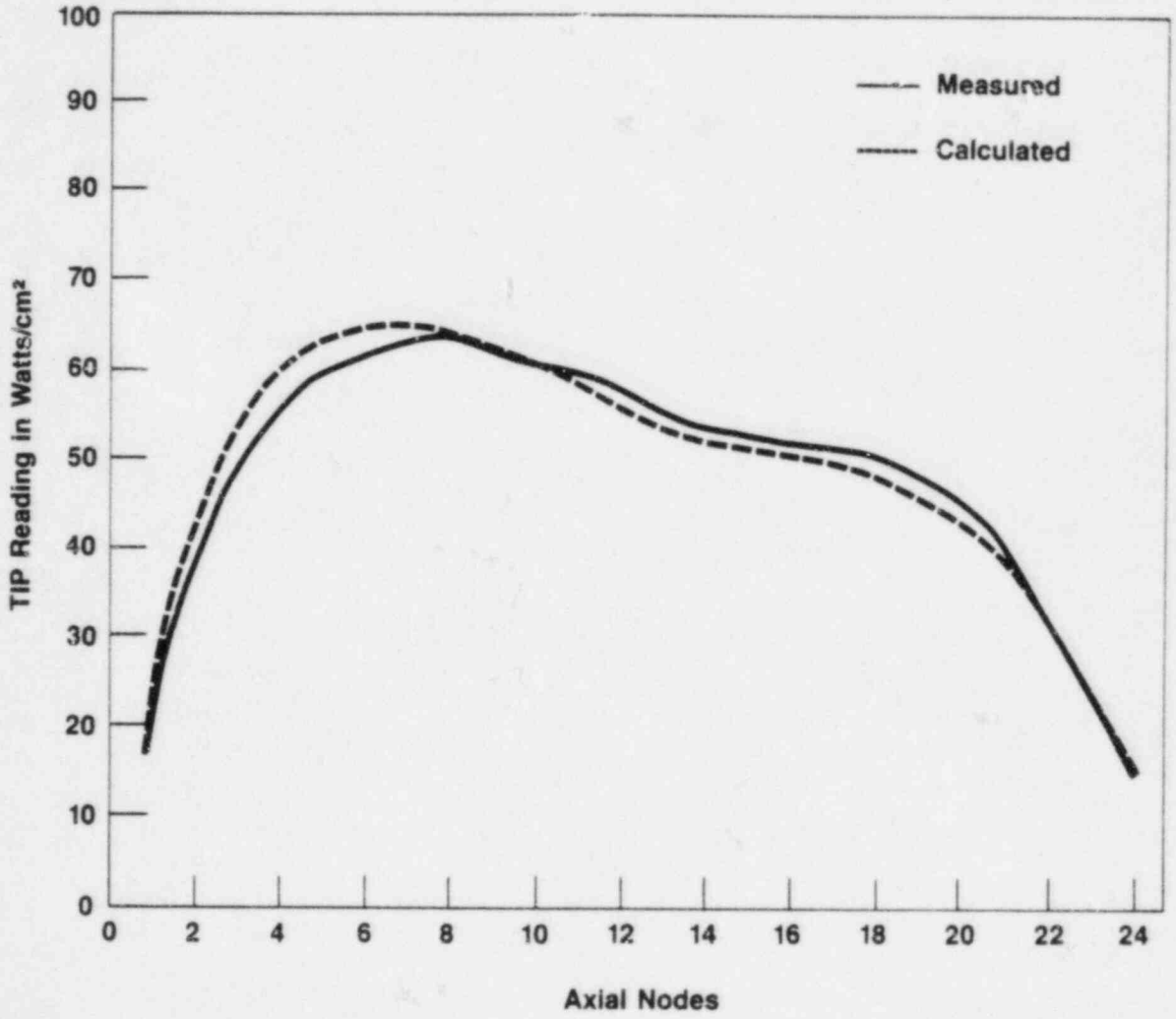

Figure 4.14
COMPARISON OF CORE AVERAGE AXIAL TIP READING FOR THE
OC CYCLE 9 STATEPOINT 08-29-80

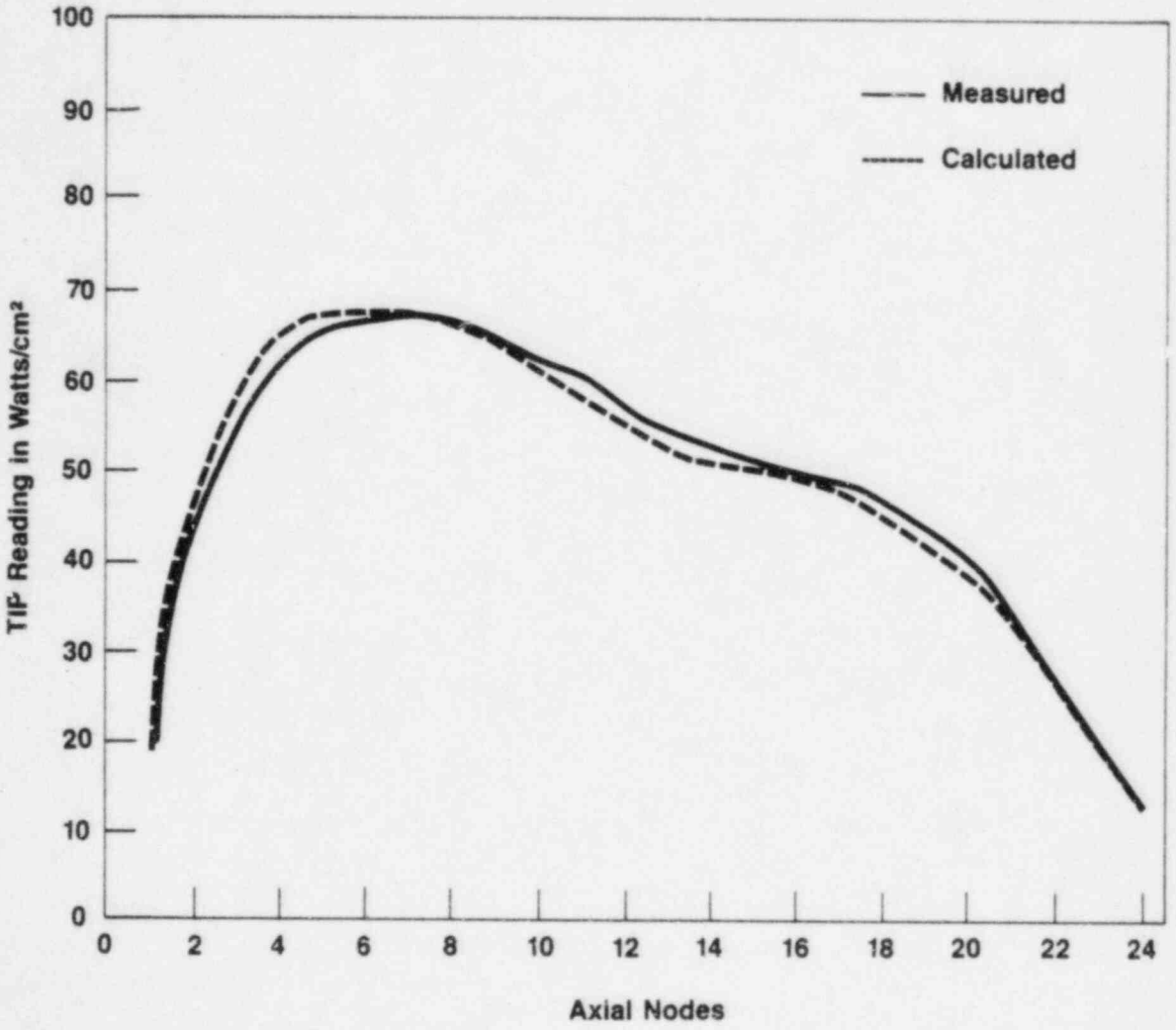

Figure 4.15
COMPARISON OF CORE AVERAGE AXIAL TIP READING FOR THE
OC CYCLE 9 STATEPOINT 09-29-80

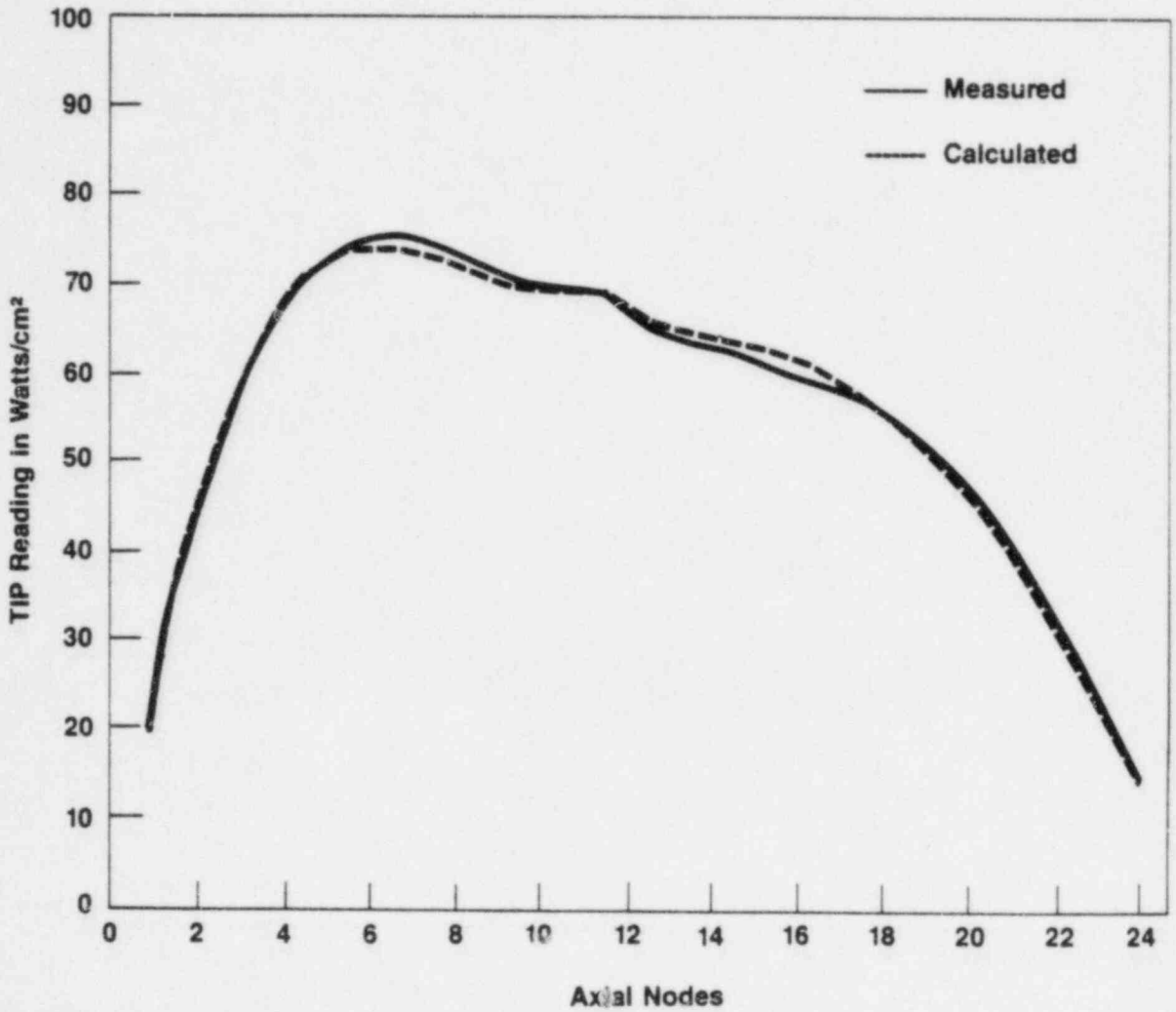

Figure 4.16
COMPARISON OF CORE AVERAGE AXIAL TIP READING FOR THE
OC CYCLE 9 STATEPOINT 11-11-80

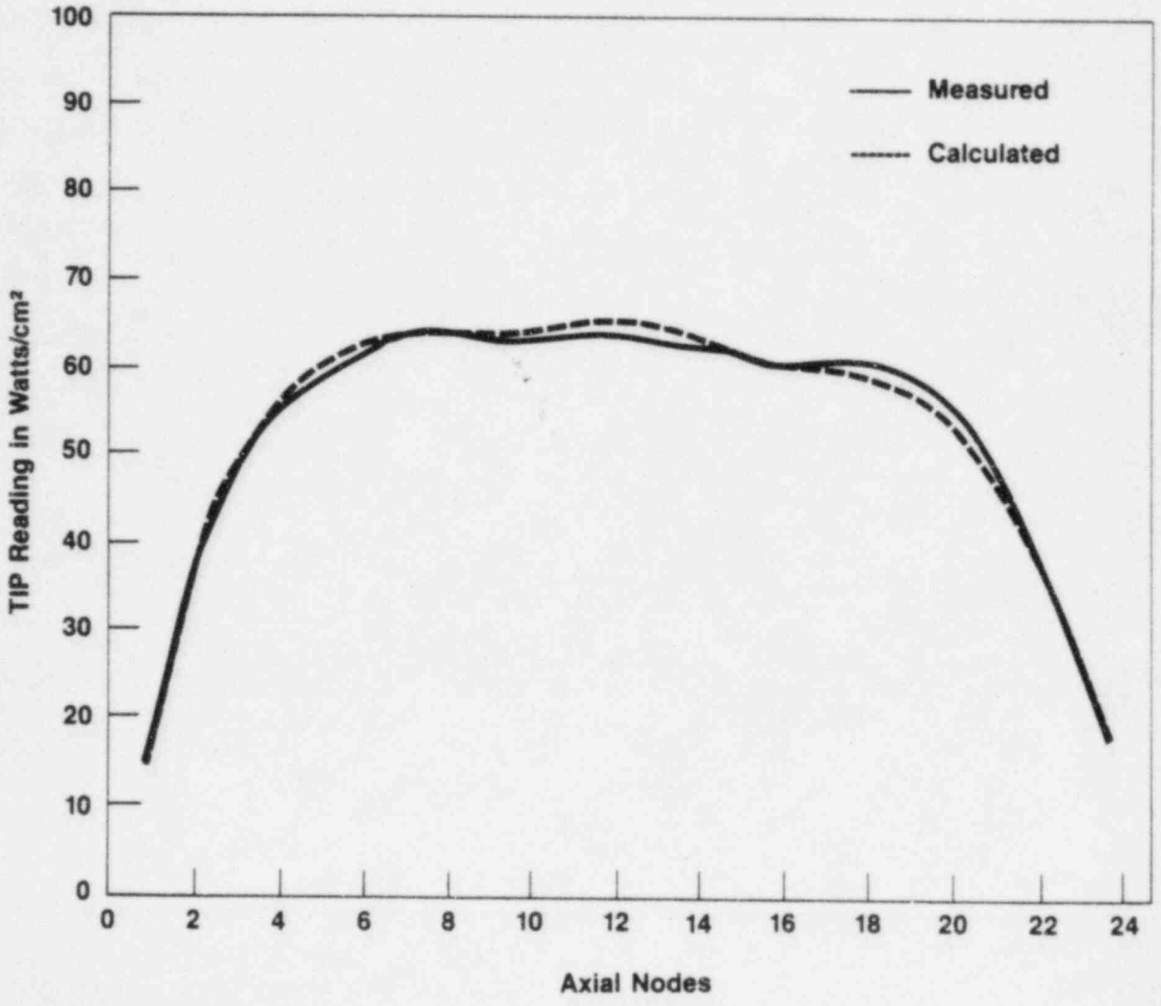

Figure 4.17
COMPARISON OF CORE AVERAGE AXIAL TIP READING FOR THE
OC CYCLE 9 STATEPOINT 12-16-80

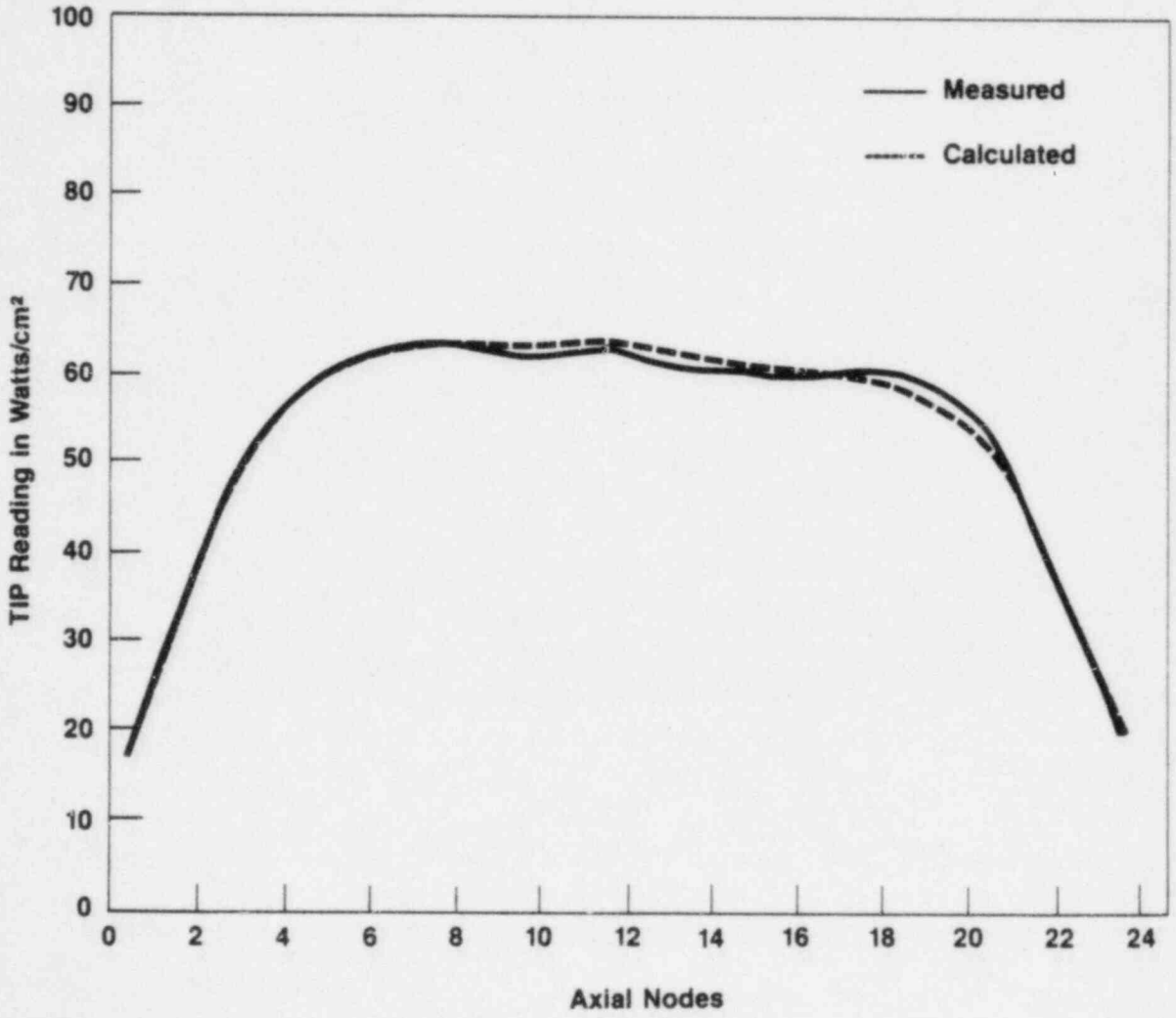

Figure 4.18
COMPARISON OF CORE AVERAGE AXIAL TIP READING FOR THE
OC CYCLE 9 STATEPOINT 02-27-81

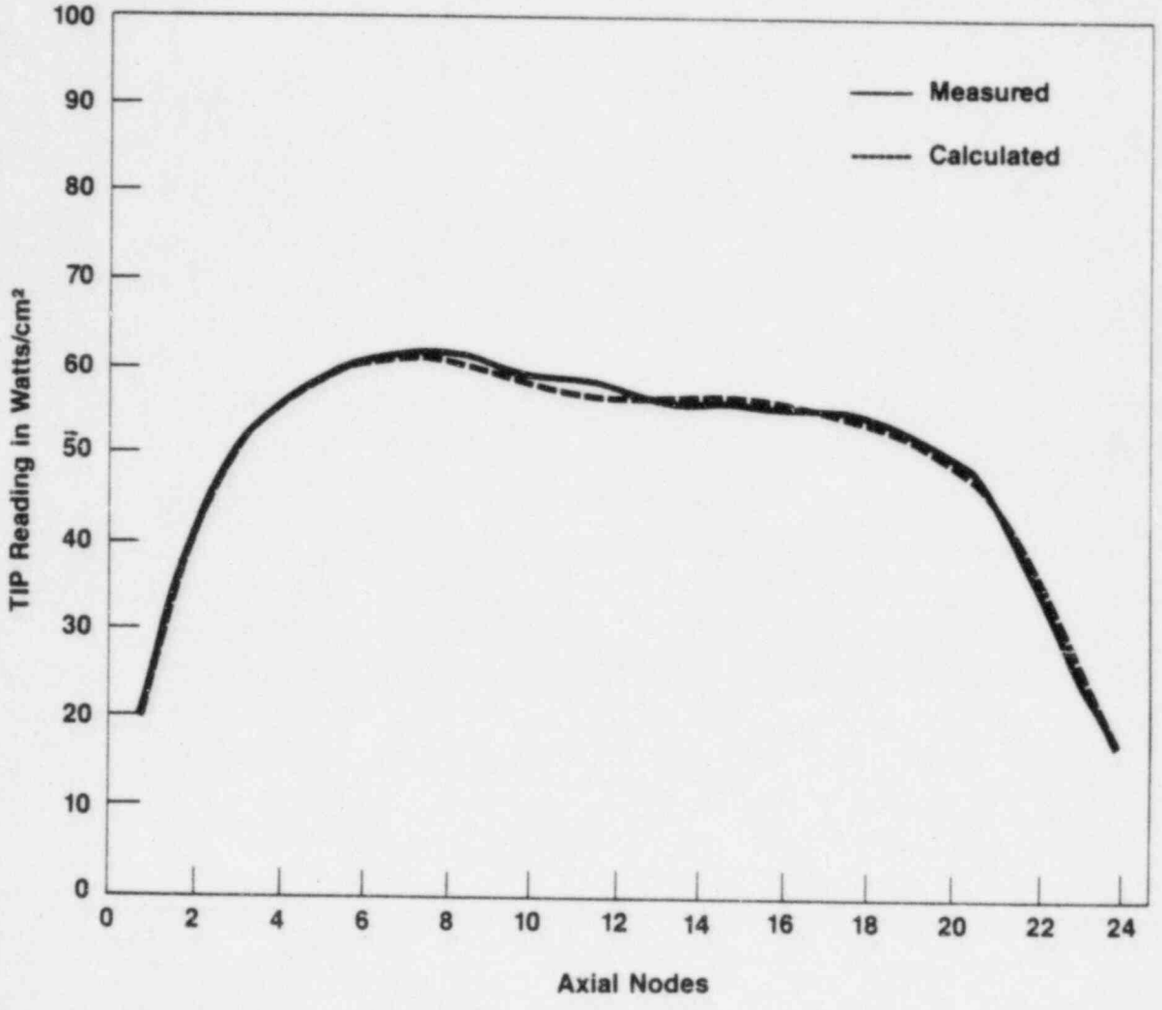

Figure 4.19
COMPARISON OF CORE AVERAGE AXIAL TIP READING FOR THE
OC CYCLE 9 STATEPOINT 03-24-81

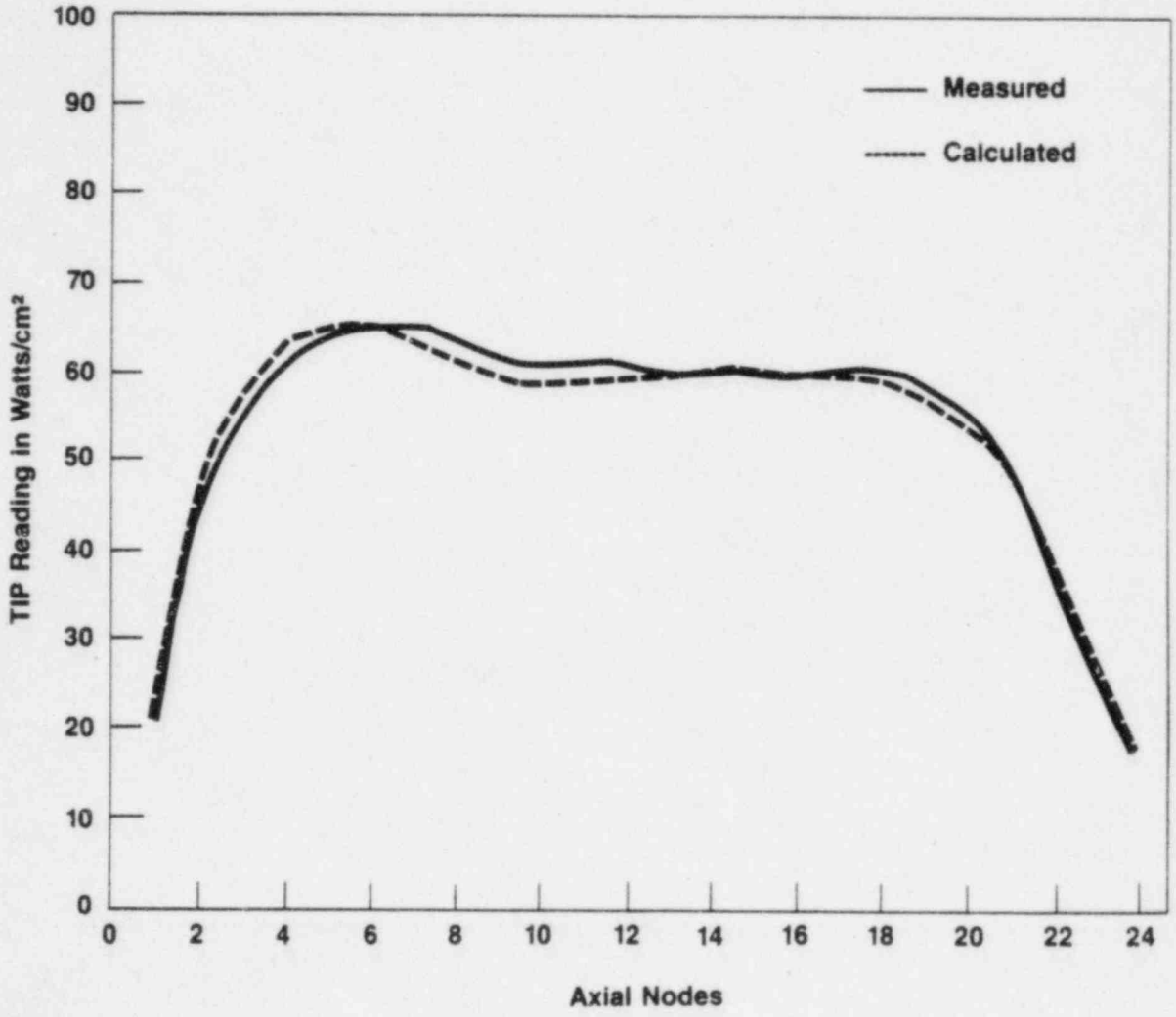

Figure 4.20
COMPARISON OF CORE AVERAGE AXIAL TIP READING FOR THE
OC CYCLE 9 STATEPOINT 06-16-81

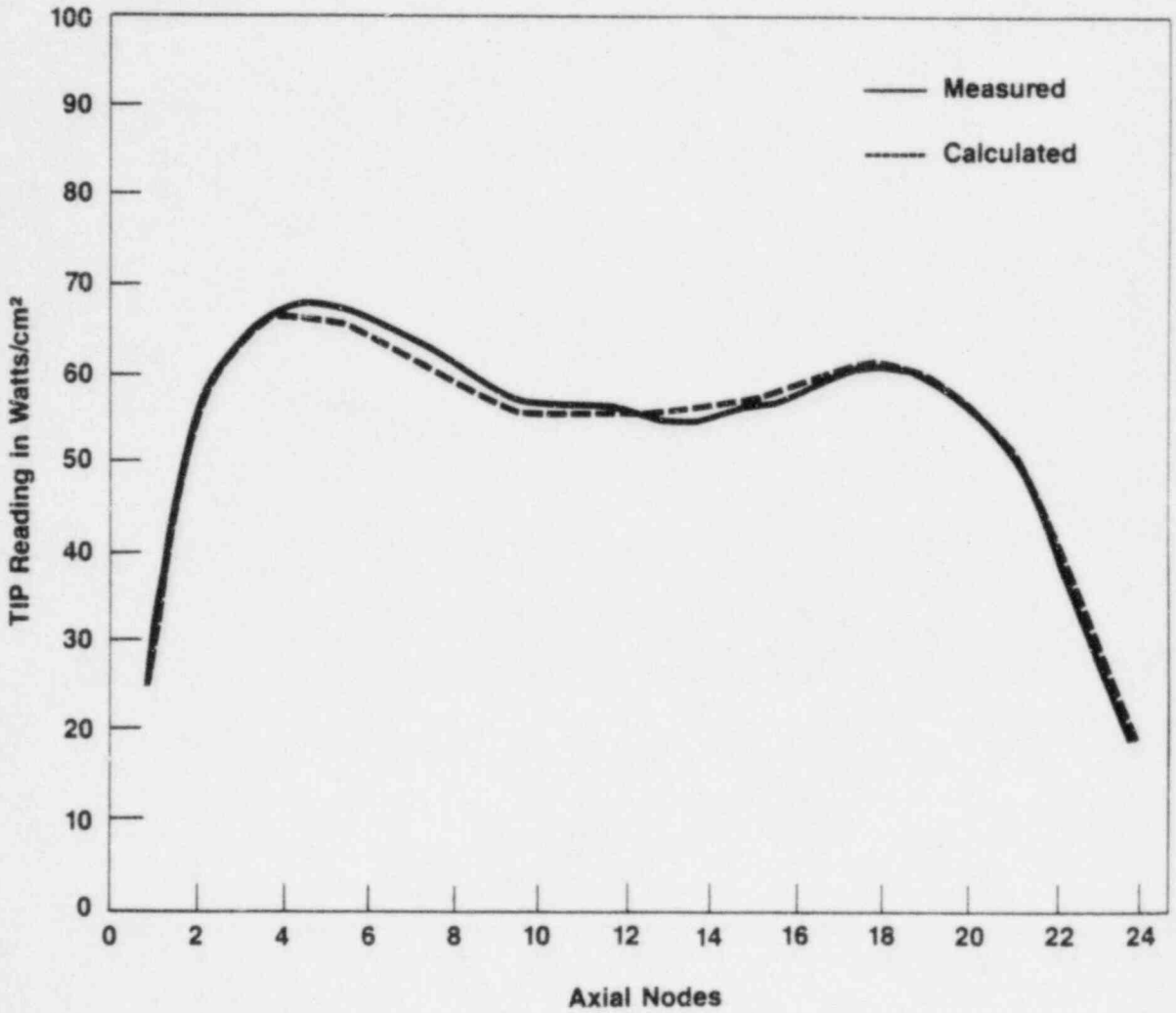

Figure 4.21
COMPARISON OF CORE AVERAGE AXIAL TIP READING FOR THE
OC CYCLE 9 STATEPOINT 07-09-81

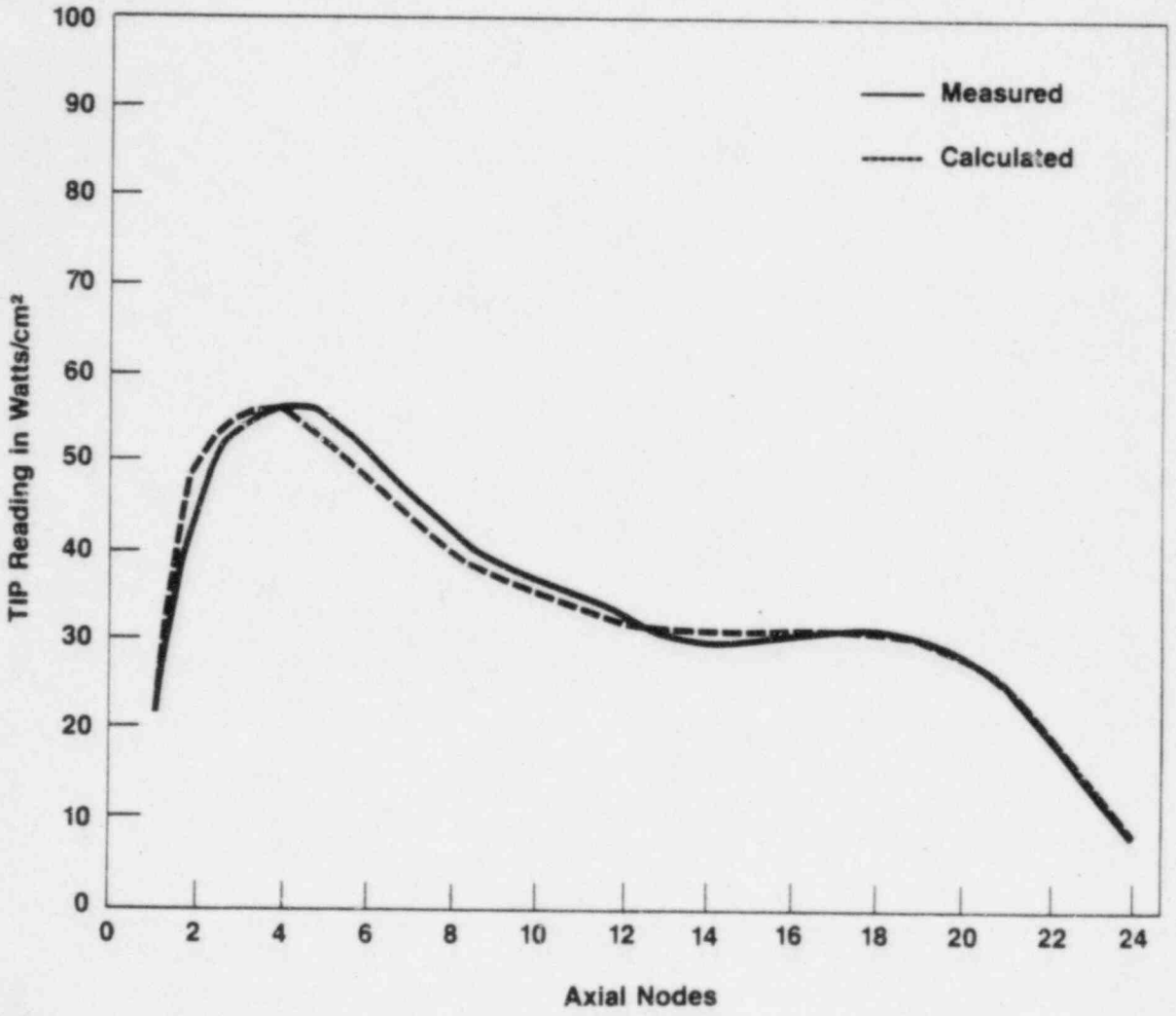

Figure 4.22
COMPARISON OF CORE AVERAGE AXIAL TIP READING FOR THE
OC CYCLE 9 STATEPOINT 08-11-81

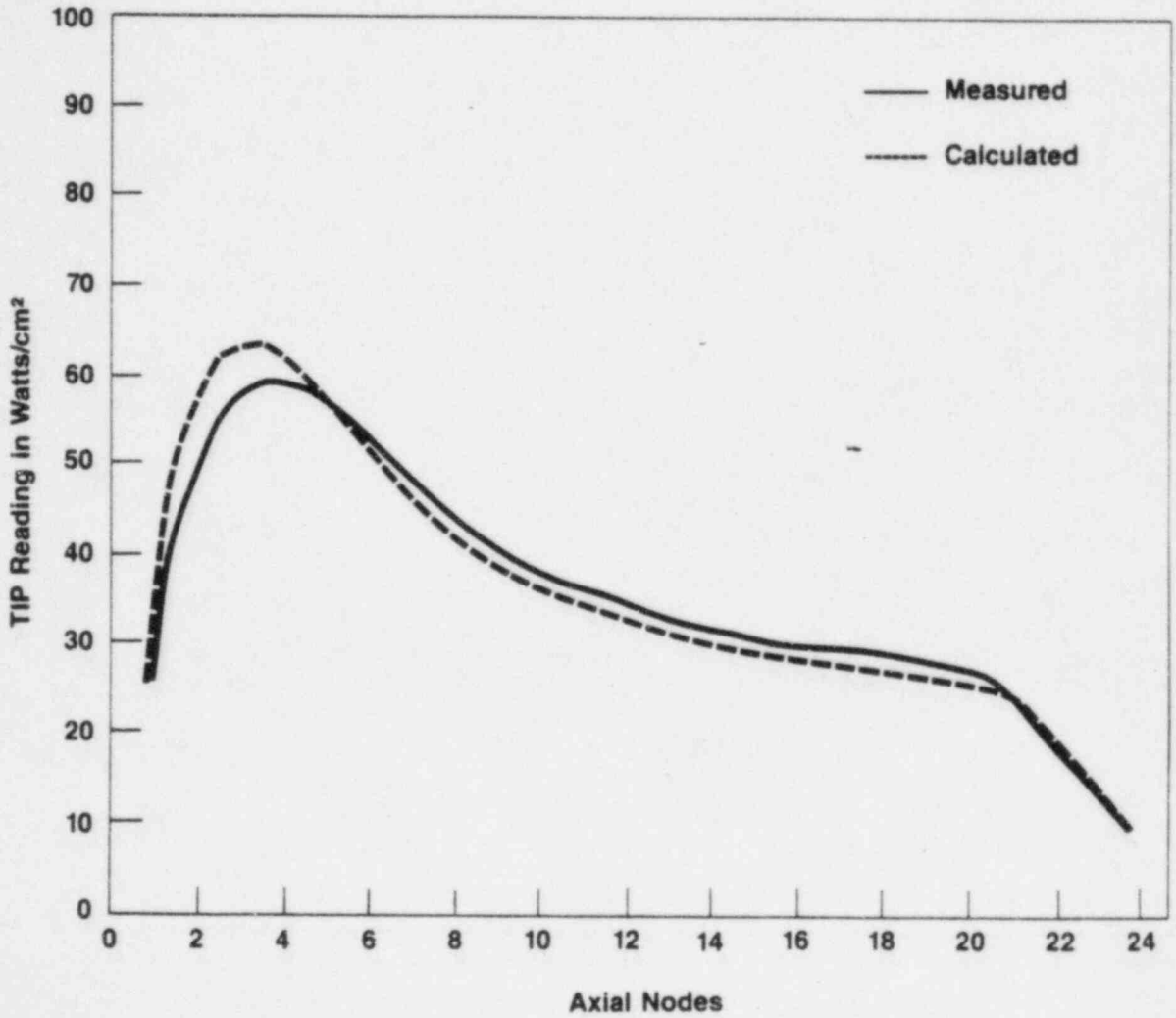

Figure 4.23
COMPARISON OF CORE AVERAGE AXIAL TIP READING FOR THE
OC CYCLE 9 STATEPOINT 11-25-81

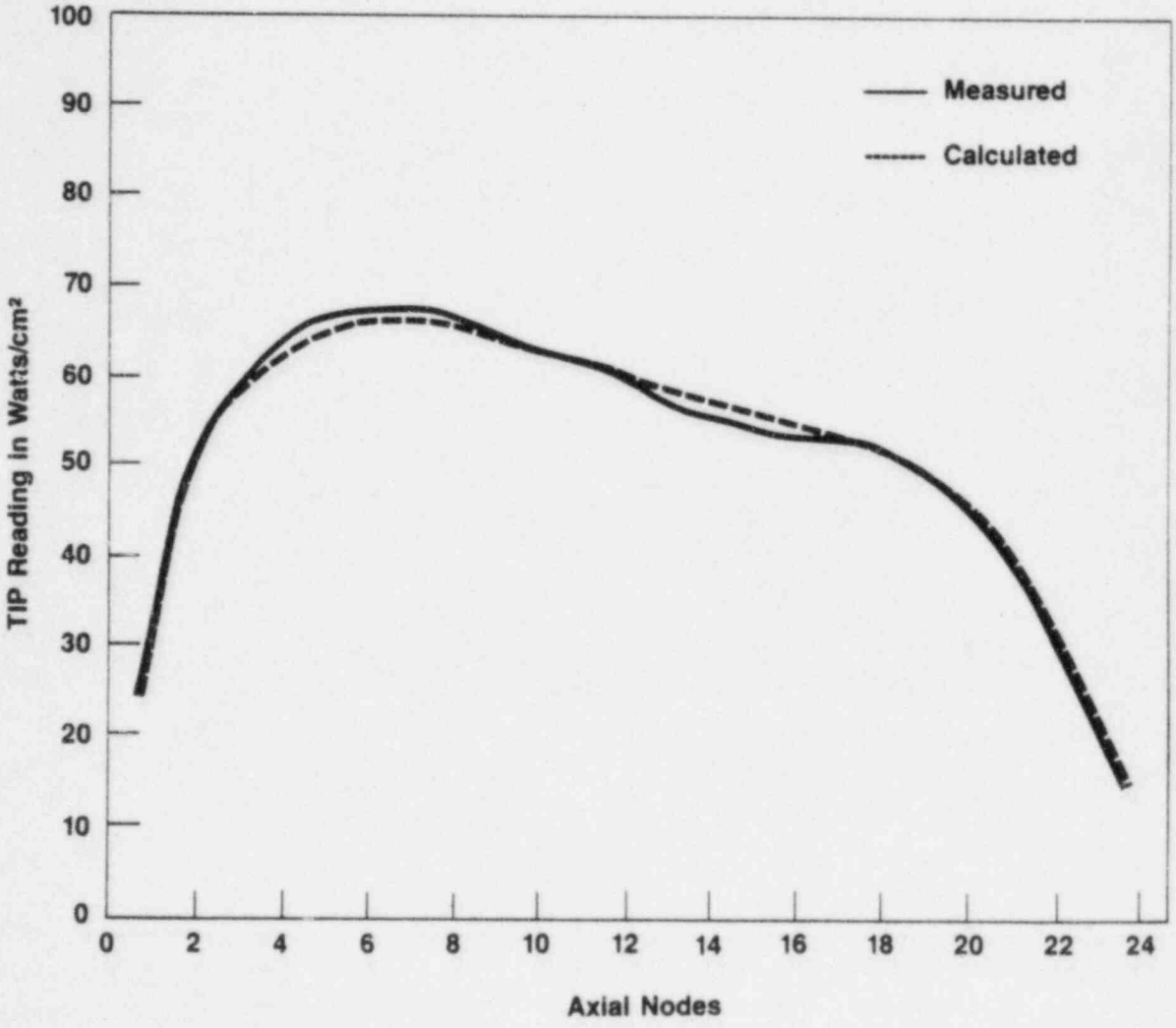

Figure 4.24
COMPARISON OF CORE AVERAGE AXIAL TIP READING FOR THE
OC CYCLE 9 STATEPOINT 12-09-81

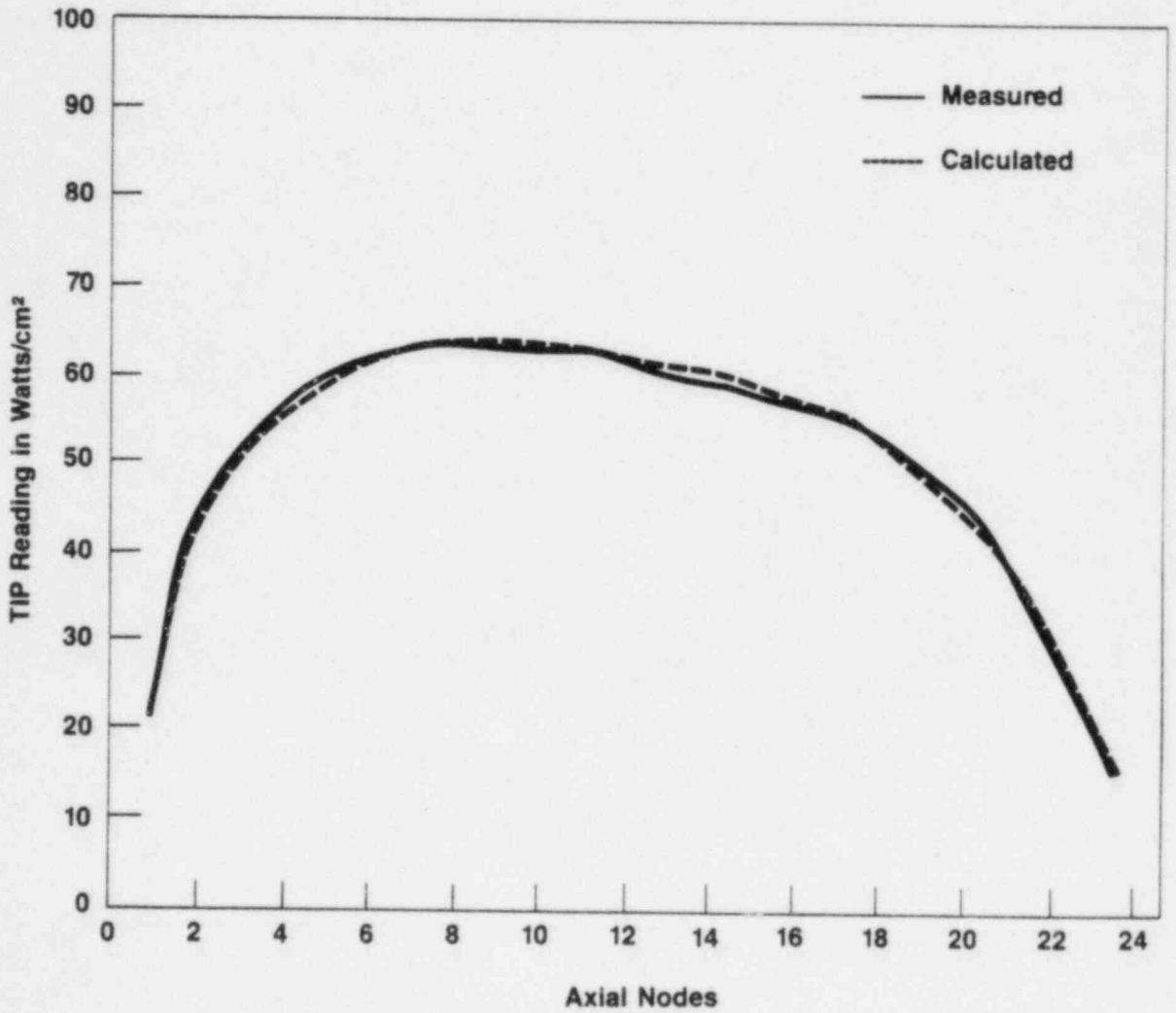

4.2 Comparison with Data Measured at Hatch 1

4.2.1 Hot Reactivity

NODE-B core follow calculations were performed for Hatch 1, cycle 1 operating history[10]. Seventeen statepoints (Table 4.8) were analyzed for the cycle with the core average k-effective shown in Table 4.9. The mean k-effective is 0.98498 with a standard deviation of 0.00537. The mean k-effective is similar to what was seen in Oyster Creek but with a larger standard deviation. This is due to the period following the 10-24-75 statepoint when the core k-effective decreased to less than 0.9800 and remained low through the 09-16-76 statepoint. After this statepoint, the core k-effective increased to 0.99 and remained there for the last six statepoints.

During an outage just prior to the 10-24-75 statepoint, holes in the lower grid plate (unused locations for instrument tubes) were plugged. The hole plugging decreased the bypass flow and created voiding in the bypass region of the core. NODE-B does not have a bypass void model. However, the lack of a bypass void model does not appear to be the cause of the decrease in core k-effective. The same behavior in k-effective was seen in similar studies[4] for the period following plugging where a bypass void model was used. In order to account for the change in core conditions during this period, the normalization parameters were re-evaluated at the beginning and end of the period. A

steam leak repaired during an outage in April 1976 indicates problems with the data as opposed to modeling deficiencies.

4.2.2 Power Distribution Comparison

The accuracy of the NODE-B model during the cycle was determined by comparing predicted and measured TIPs. The results for the 17 statepoints are summarized in Table 4.9. The overall nodal RMS is 9.14%. The cycle performance is generally in the 8 to 9% range except for the period following the bypass hole plugging where performance was in the 9 to 12% RMS range. The nodal asymmetry for Hatch cycle 1 is 4.02%. A comparison of the measured and predicted core average TIPs are shown in Figures 4.25 to 4.41.

4.2.3 Gamma Scan Comparisons

The end of cycle gamma scan measurements provide data to directly evaluate core power distribution predictions. The EOC 1, Hatch 1 gamma scan measurements[11] were made on 106 fuel assemblies; 75 comprising a complete octant of the core and 31 assemblies in octant symmetric locations. All 106 fuel assemblies were measured at a minimum of 12 axial positions.

The results of the gamma scan are summarized in Table 4.10. The core axial RMS is presented in

Table 4.11. The comparison of predicted and measured core average axial is shown in Figure 4.4.2. Individual bundle power distribution comparison are shown in Figures 4.43 to 4.47. Figure 4.48 shows the radial comparison (Bundle integrated RMS) for all 106 fuel assemblies. The definition of the residuals and statistics are provided in Appendix A.

The results were generally good. The overall nodal RMS of 7.95% is acceptable and falls below the 8.54% mean RMS of the TIP comparison for the last five statepoints. These were the power distributions used to generate the predicted end of cycle Ba-140 distribution used in the comparison. It demonstrates that the ability of the model to predict the TIPs is indicative of the models ability to predict power distribution.

TABLE 4.8

KEY INFORMATION FOR HATCH 1 CYCLE 1 STATEPOINTS

Date	Power (MWth)	Recirc. Flow (Mlbs/hr)	Core Avg. Exp. (GWD/MTU)	Rod Sequence	% Rod Density
03-28-75	1218	34.5	0.70	A	9.8
05-24-75	2189	68.0	1.28	A	7.5
08-26-75	2331	78.7	2.58	B	9.4
09-25-75	2098	66.7	3.12	B	10.8
10-24-75	2091	60.9	3.65	B	11.3
01-13-76	1947	64.3	4.16	B	14.2
01-25-76	1853	78.5	4.32	A	17.2
05-25-76	2104	73.5	5.79	B	17.5
07-22-76	2021	62.4	6.59	A	18.2
08-13-76	2269	75.3	6.98	A	18.2
09-16-76	2230	78.4	7.62	B	19.9
11-29-76	2037	78.5	8.94	B	19.9
12-29-76	2231	78.2	9.40	A	16.2
01-21-77	2131	78.7	9.83	A	16.2
01-25-77	2153	71.3	9.88	A	15.7
02-23-77	2208	78.6	10.12	A	15.7
03-07-77	2114	77.2	10.31	A	15.7

TABLE 4.9

CORE REACTIVITY AND POWER DISTRIBUTION COMPARISON
FOR HATCH 1 CYCLE 5

Statepoint	Calculated k_{eff}	TIP Nodal Uncertainty
03-28-75	0.98333	6.21
05-24-75	0.98425	6.26
08-26-75	0.98531	7.80
09-25-75	0.98435	8.90
10-24-75	0.98452	8.82
01-13-76	0.97938	10.70
01-25-76	0.97709	11.98
05-25-76	0.98093	9.75
07-22-76	0.97861	9.16
08-13-76	0.97937	9.23
09-16-76	0.97973	8.29
11-29-76	0.99319	9.23
12-29-76	0.99229	8.70
01-21-77	0.99124	8.09
01-25-77	0.99093	8.17
02-23-77	0.99005	8.92
03-07-77	0.99017	8.80
Mean	0.98498	9.14
1σ	0.00537	

TABLE 4.10

SUMMARY OF HATCH GAMMA SCAN POWER DISTRIBUTION COMPARISON

Comparison	% RMS
Nodal	7.95
Integral	2.82
Peak Node	6.07
Axial	5.81

TABLE 4.11

HATCH GAMMA SCAN AXIAL AVERAGE RESIDUAL
AND STANDARD DEVIATION

NODE	Residual	Standard Deviation
23	-1.46	3.99
21	-13.40	6.10
19	-1.77	6.36
17	1.28	7.79
15	7.60	9.47
13	7.36	5.71
11	3.10	3.83
9	-1.94	4.54
7	-7.10	4.34
5	-2.19	3.92
3	3.18	2.70
1	5.34	1.61

RMS = 5.81

Figure 4.25
COMPARISON OF CORE AVERAGE AXIAL TIP READING FOR
THE HATCH 1 CYCLE 1 STATEPOINT ON 03-28-75

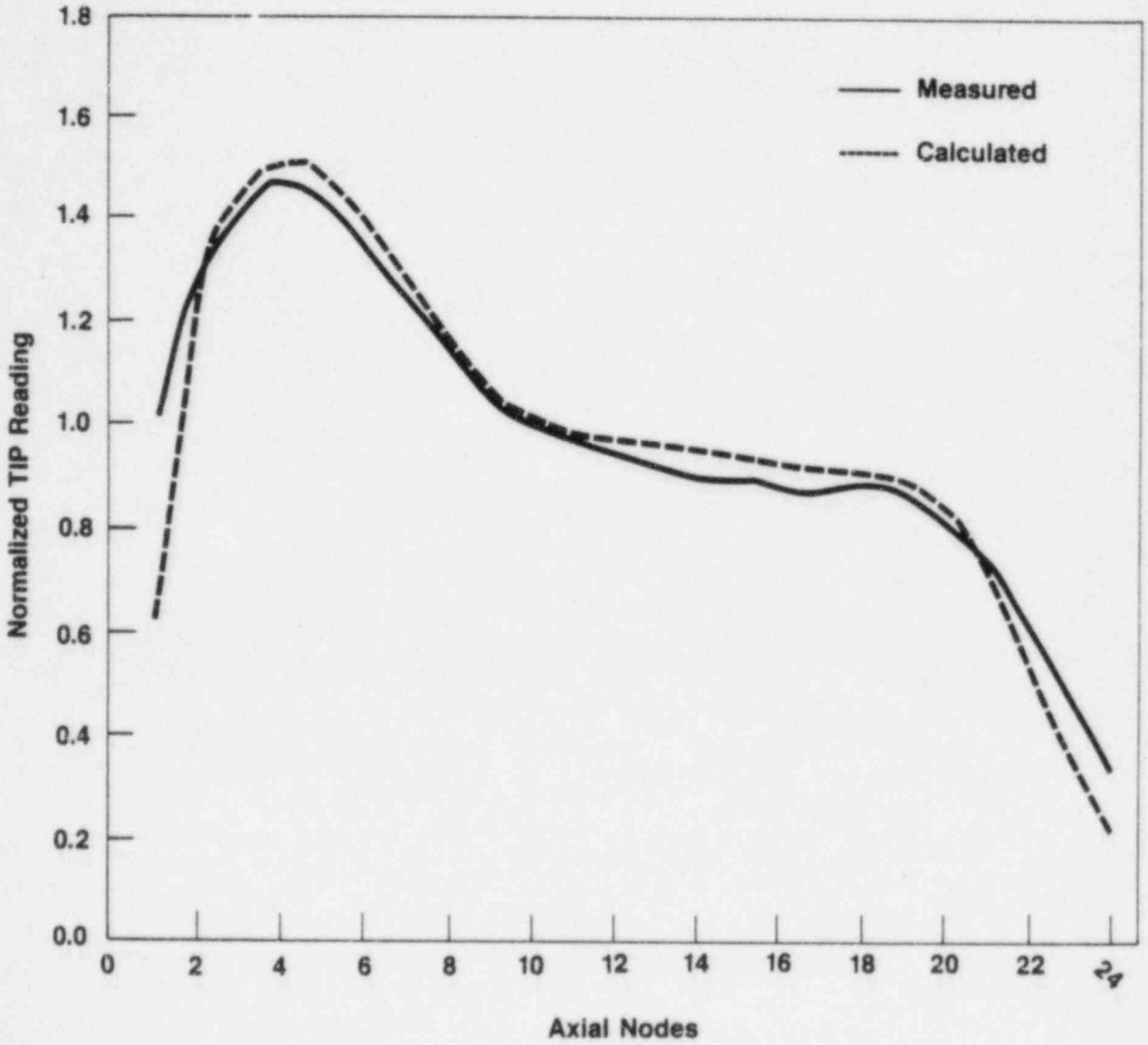

Figure 4.26
COMPARISON OF CORE AVERAGE AXIAL TIP READING FOR
THE HATCH 1 CYCLE 1 STATEPOINT ON 05-24-75

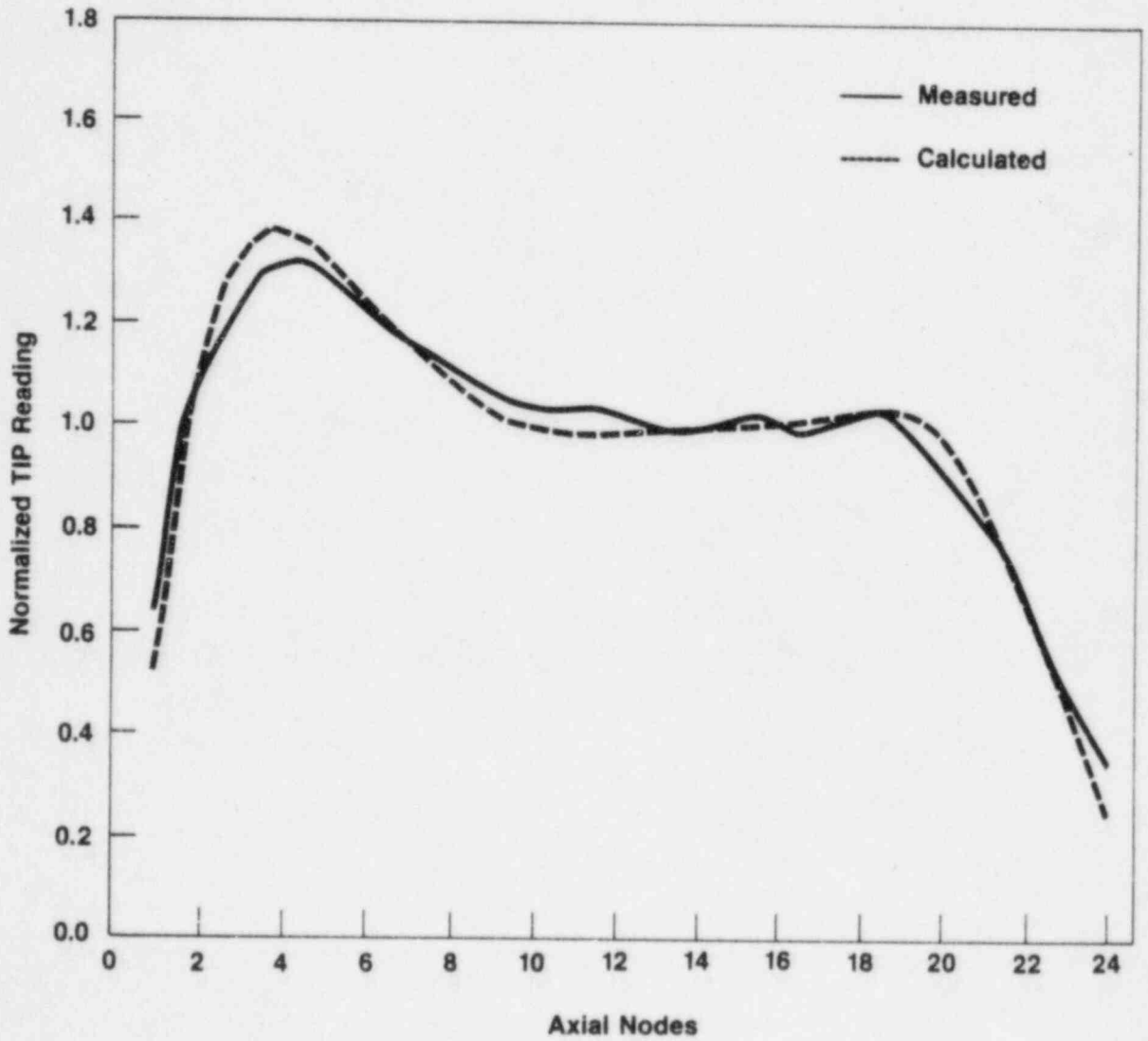

Figure 4.27
COMPARISON OF CORE AVERAGE AXIAL TIP READING FOR
THE HATCH 1 CYCLE 1 STATEPOINT ON 08-26-75

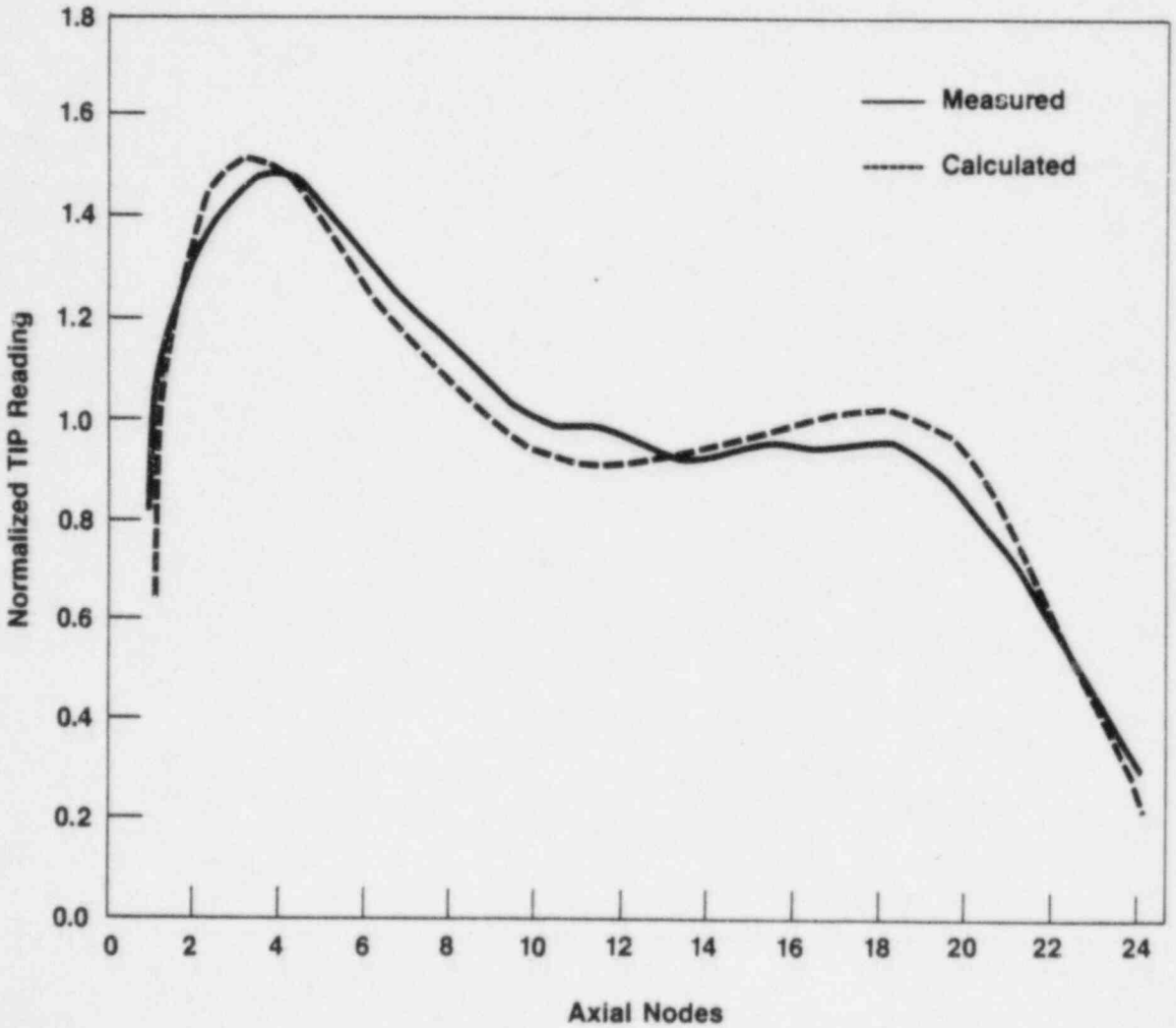

Figure 4.28
COMPARISON OF CORE AVERAGE AXIAL TIP READING FOR
THE HATCH 1 CYCLE 1 STATEPOINT ON 09-25-75

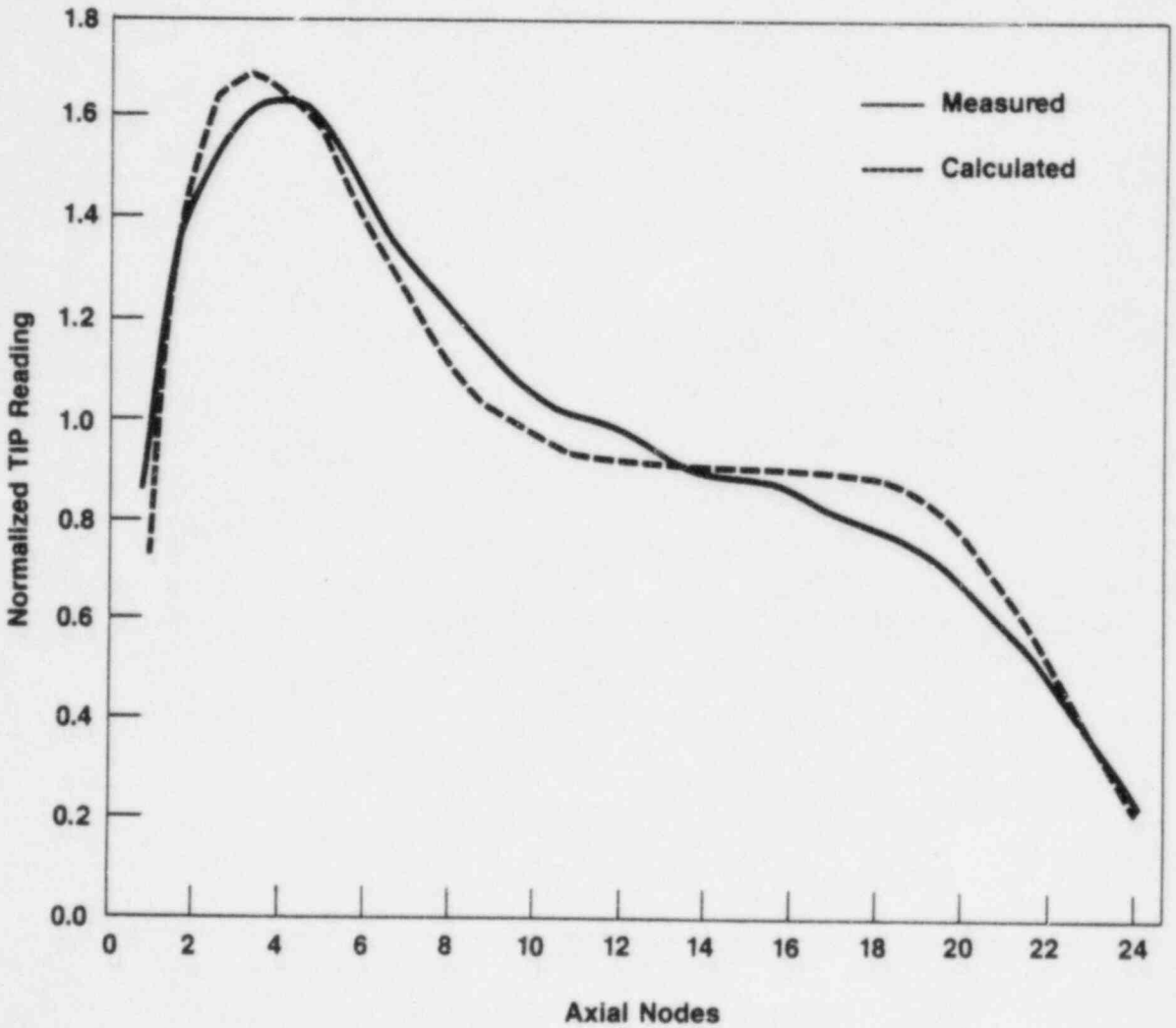

Figure 4.29
COMPARISON OF CORE AVERAGE AXIAL TIP READING FOR
THE HATCH 1 CYCLE 1 STATEPOINT ON 10-24-75

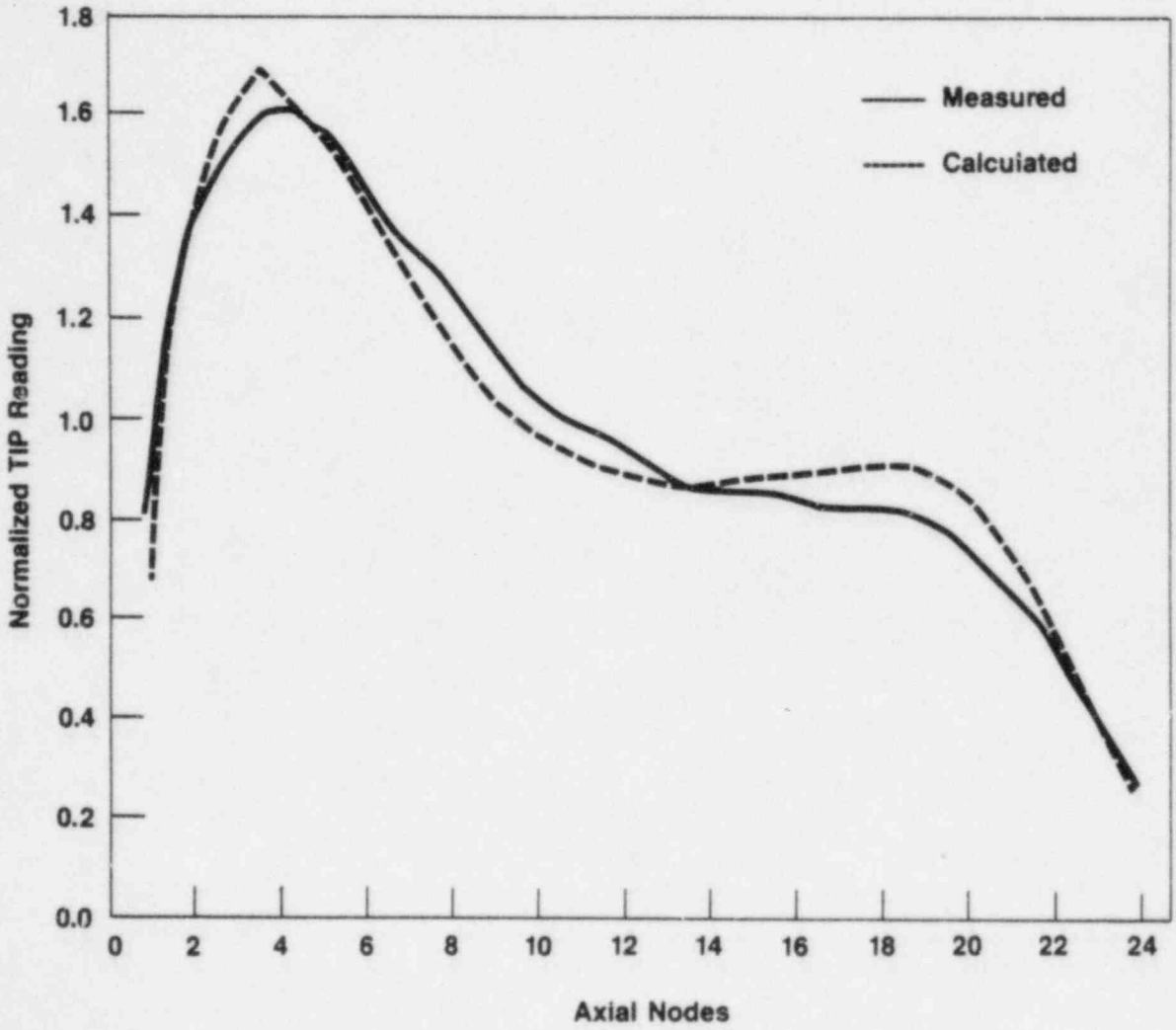

Figure 4.30
COMPARISON OF CORE AVERAGE AXIAL TIP READING FOR
THE HATCH 1 CYCLE 1 STATEPOINT ON 01-13-76

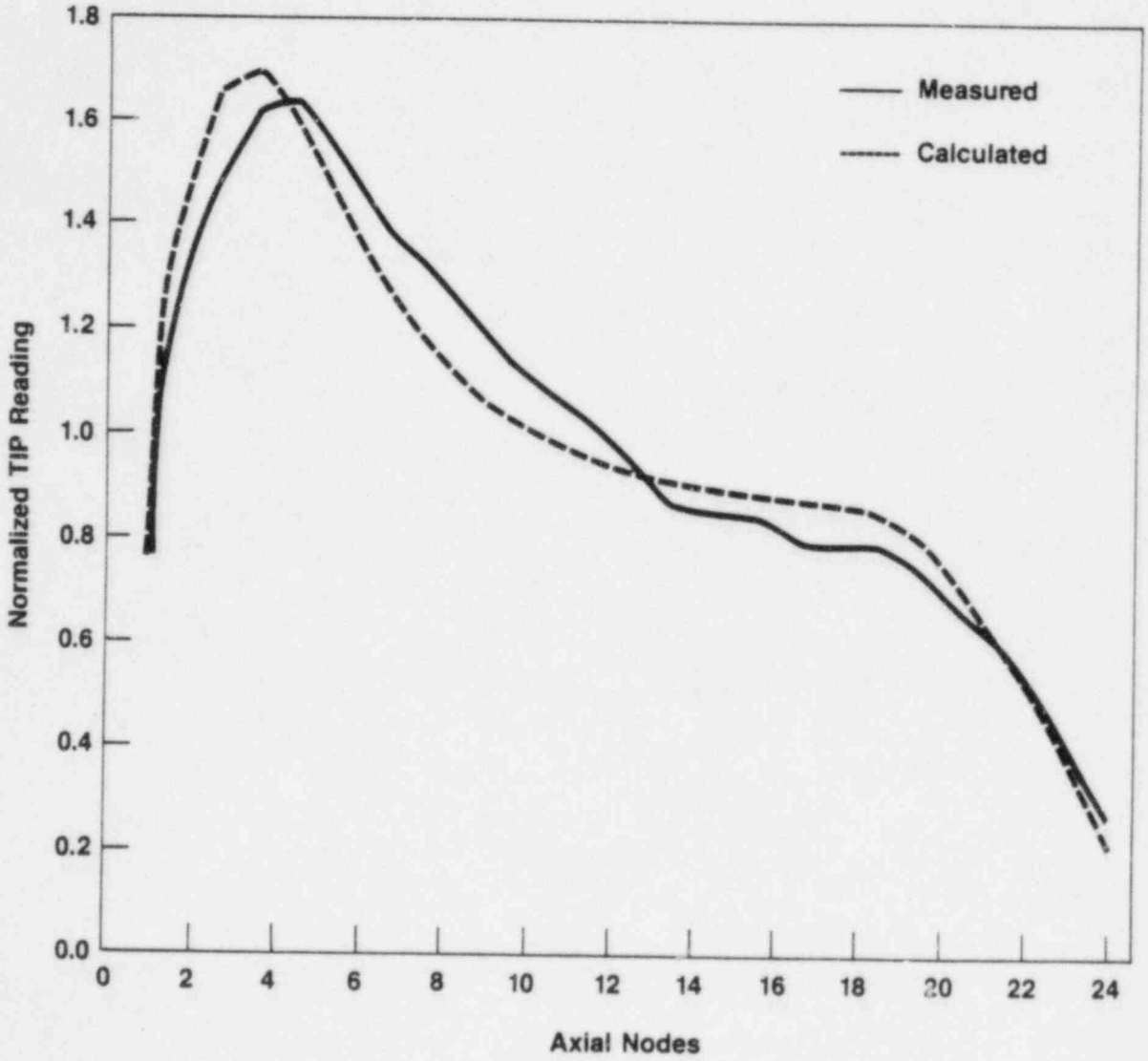

Figure 4.31
COMPARISON OF CORE AVERAGE AXIAL TIP READING FOR
THE HATCH 1 CYCLE 1 STATEPOINT ON 01-25-76

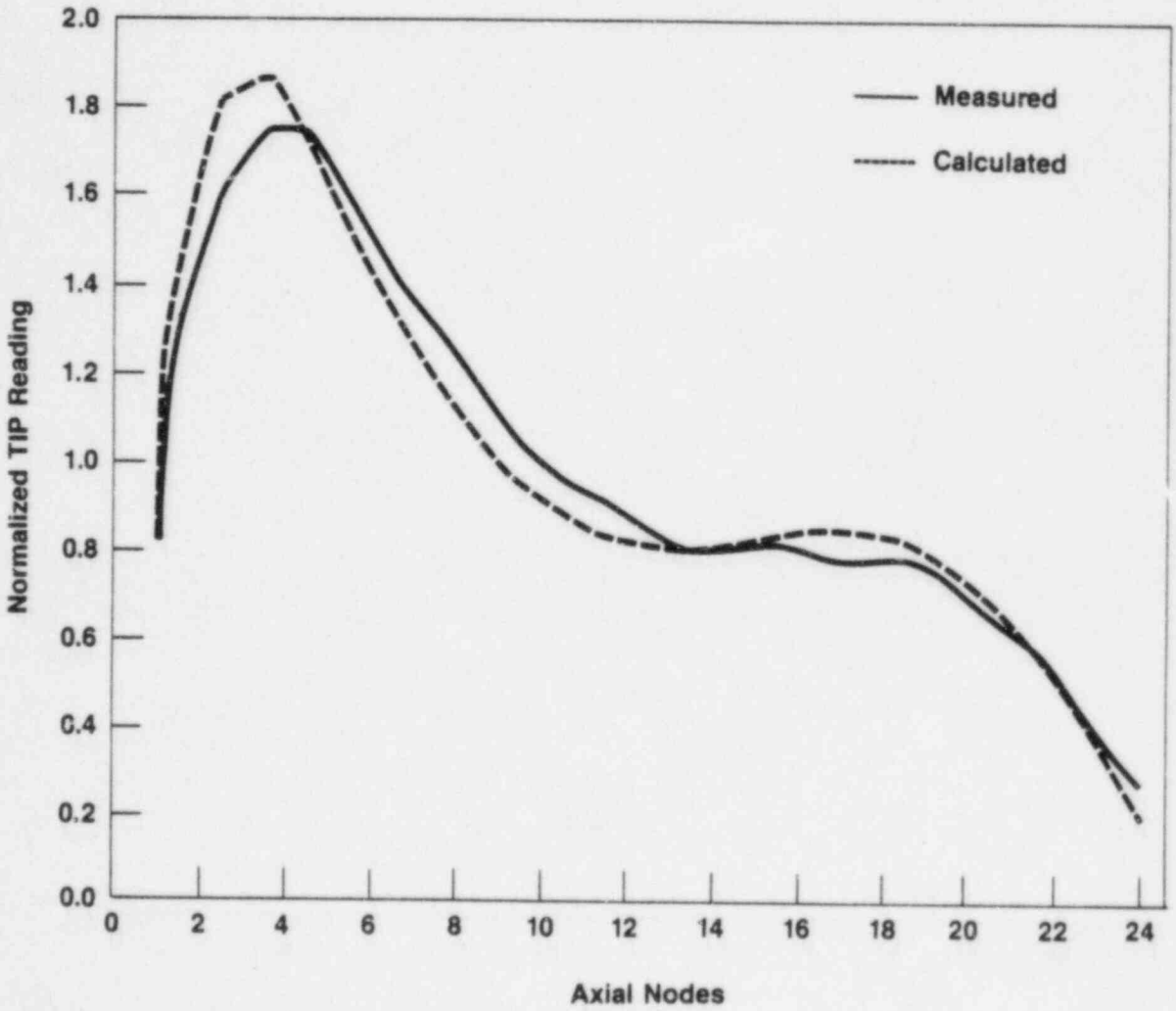

Figure 4.32
COMPARISON OF CORE AVERAGE AXIAL TIP READING FOR
THE HATCH 1 CYCLE 1 STATEPOINT ON 05-25-76

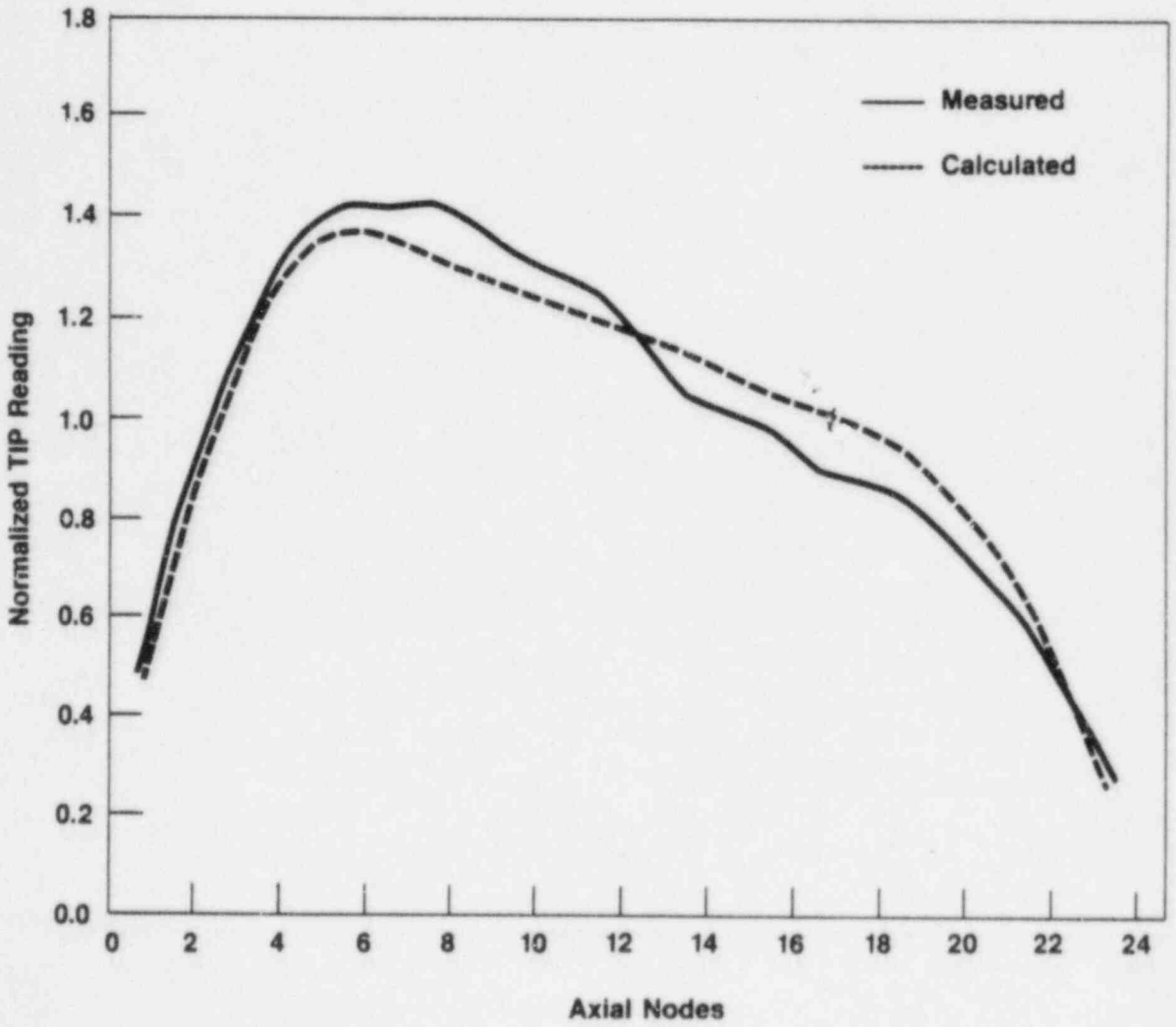

Figure 4.33
COMPARISON OF CORE AVERAGE AXIAL TIP READING FOR
THE HATCH 1 CYCLE 1 STATEPOINT ON 07-22-76

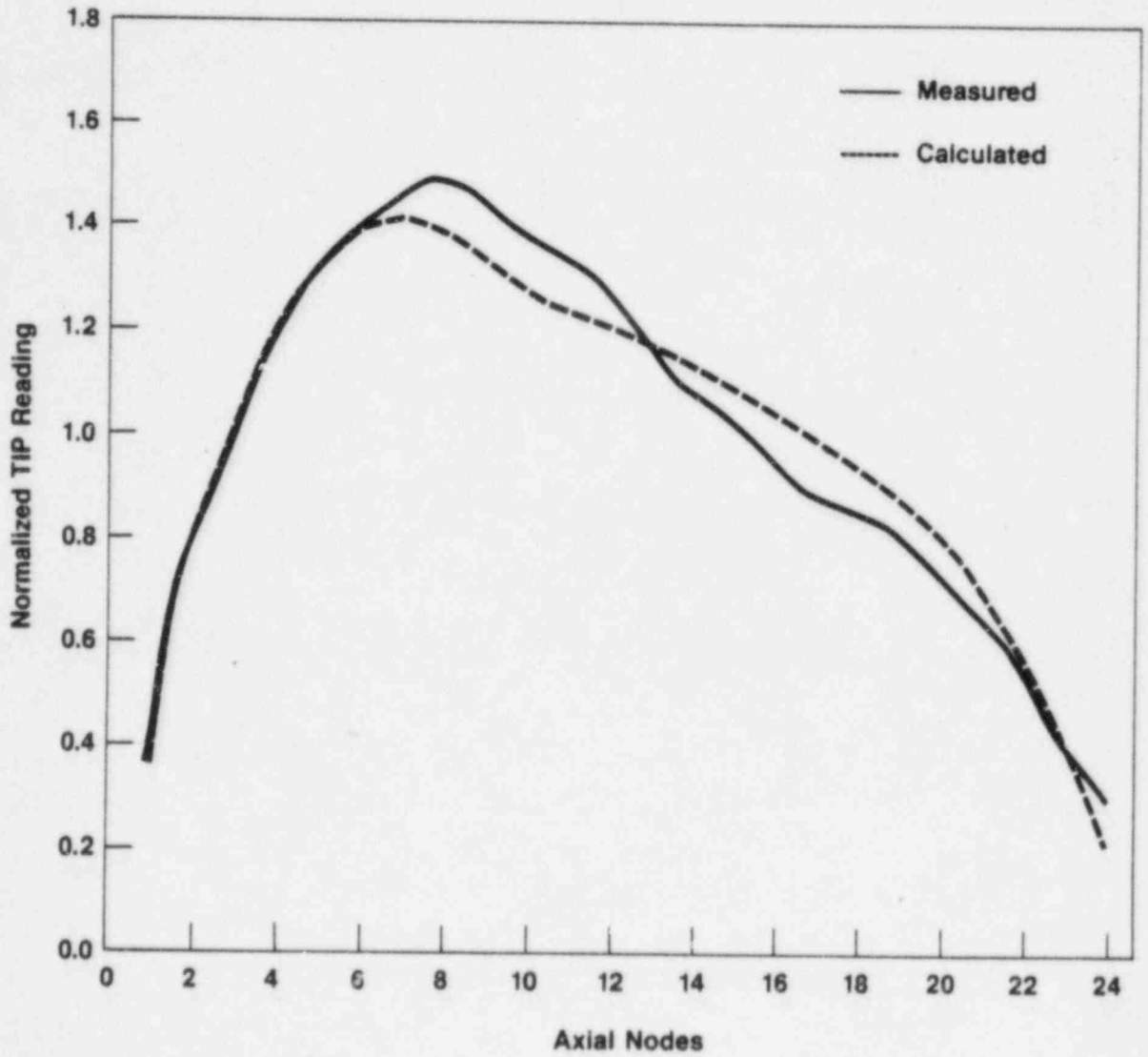

Figure 4.34
COMPARISON OF CORE AVERAGE AXIAL TIP READING FOR
THE HATCH 1 CYCLE 1 STATEPOINT ON 08-13-76

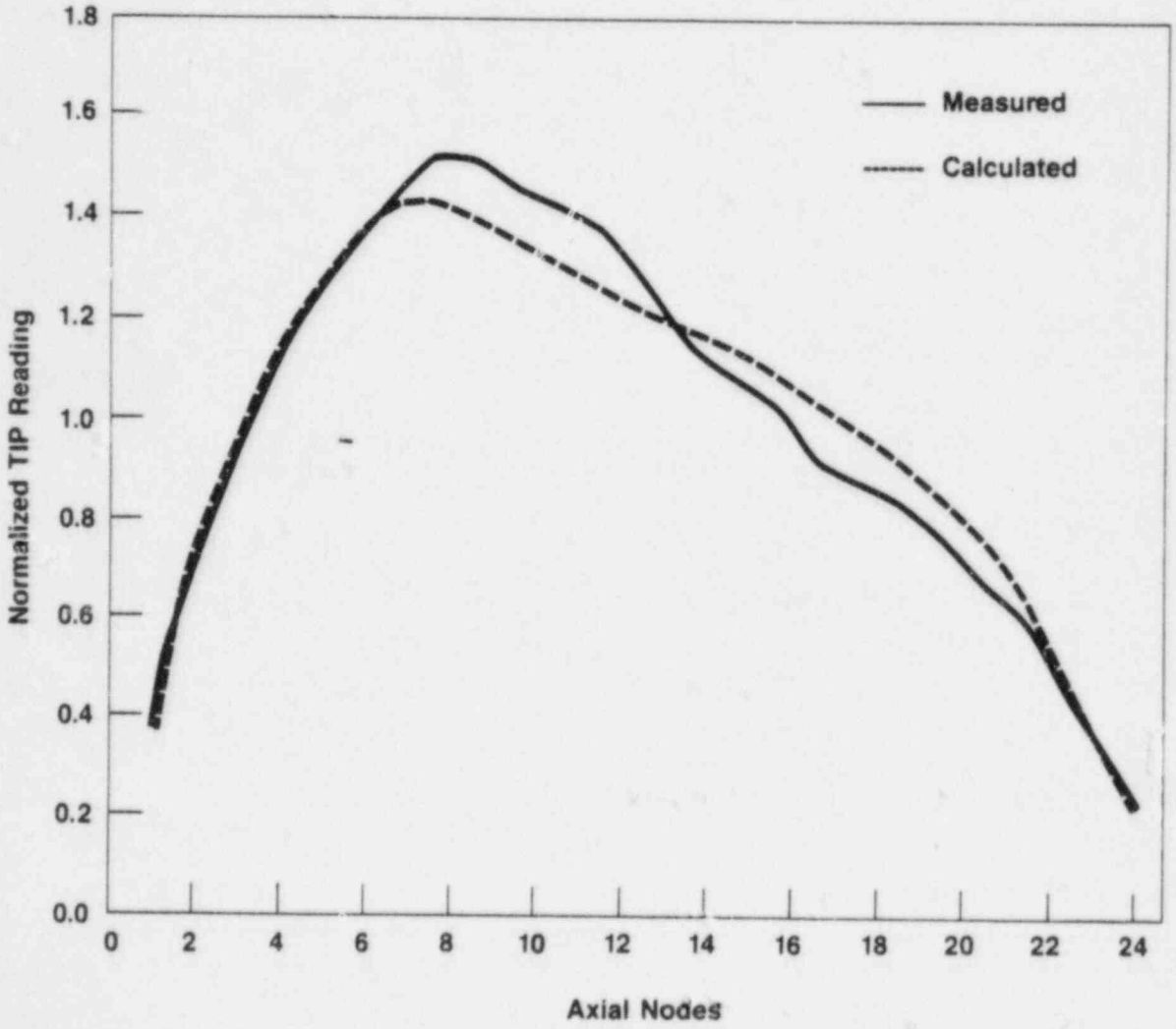

Figure 4.35
COMPARISON OF CORE AVERAGE AXIAL TIP READING FOR
THE HATCH 1 CYCLE 1 STATEPOINT ON 09-16-76

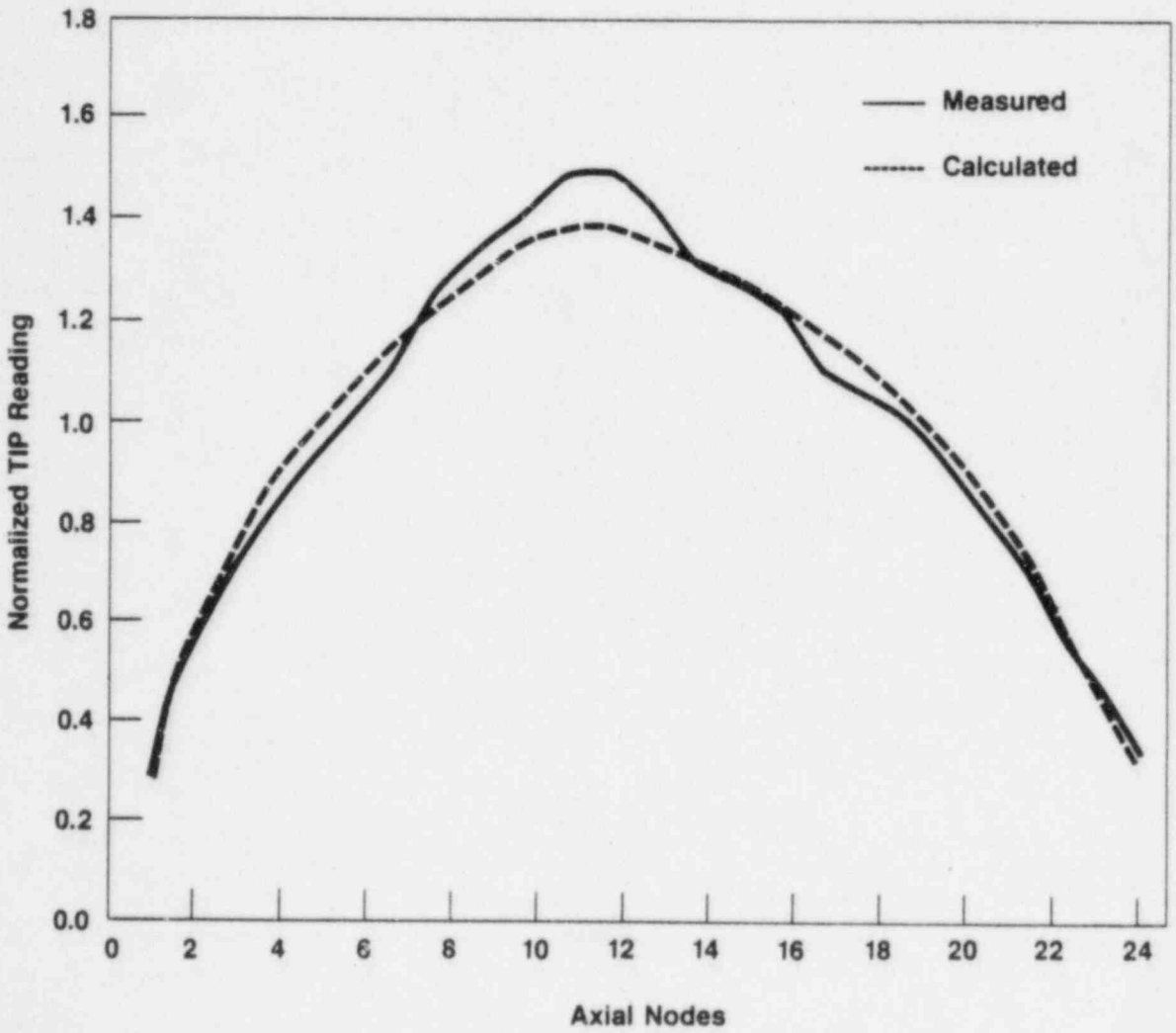

Figure 4.36
COMPARISON OF CORE AVERAGE AXIAL TIP READING FOR
THE HATCH 1 CYCLE 1 STATEPOINT ON 11-29-76

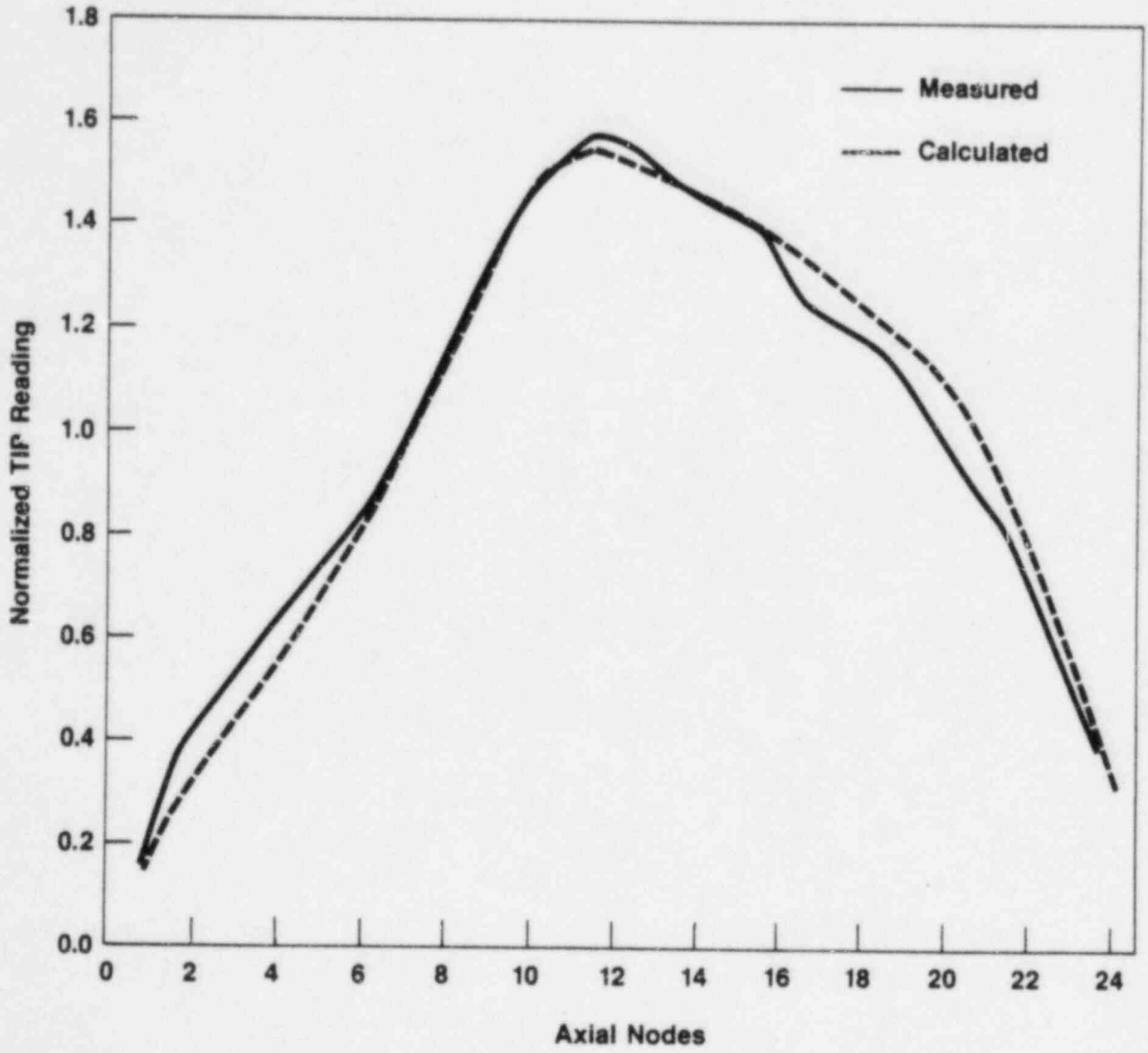

Figure 4.37
COMPARISON OF CORE AVERAGE AXIAL TIP READING FOR
THE HATCH 1 CYCLE 1 STATEPOINT ON 12-29-76

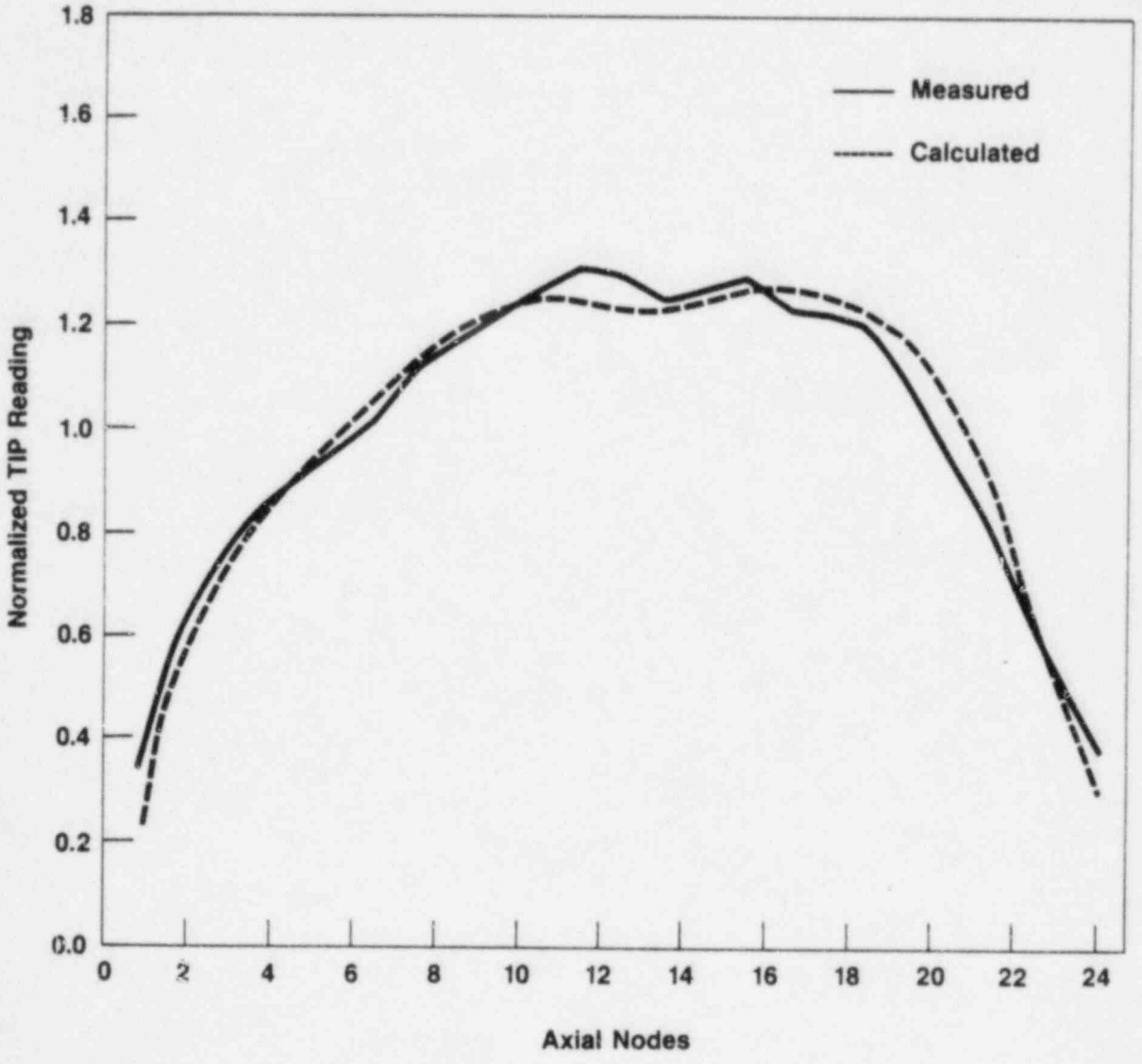

Figure 4.38
COMPARISON OF CORE AVERAGE AXIAL TIP READING FOR
THE HATCH 1 CYCLE 1 STATEPOINT ON 01-21-77

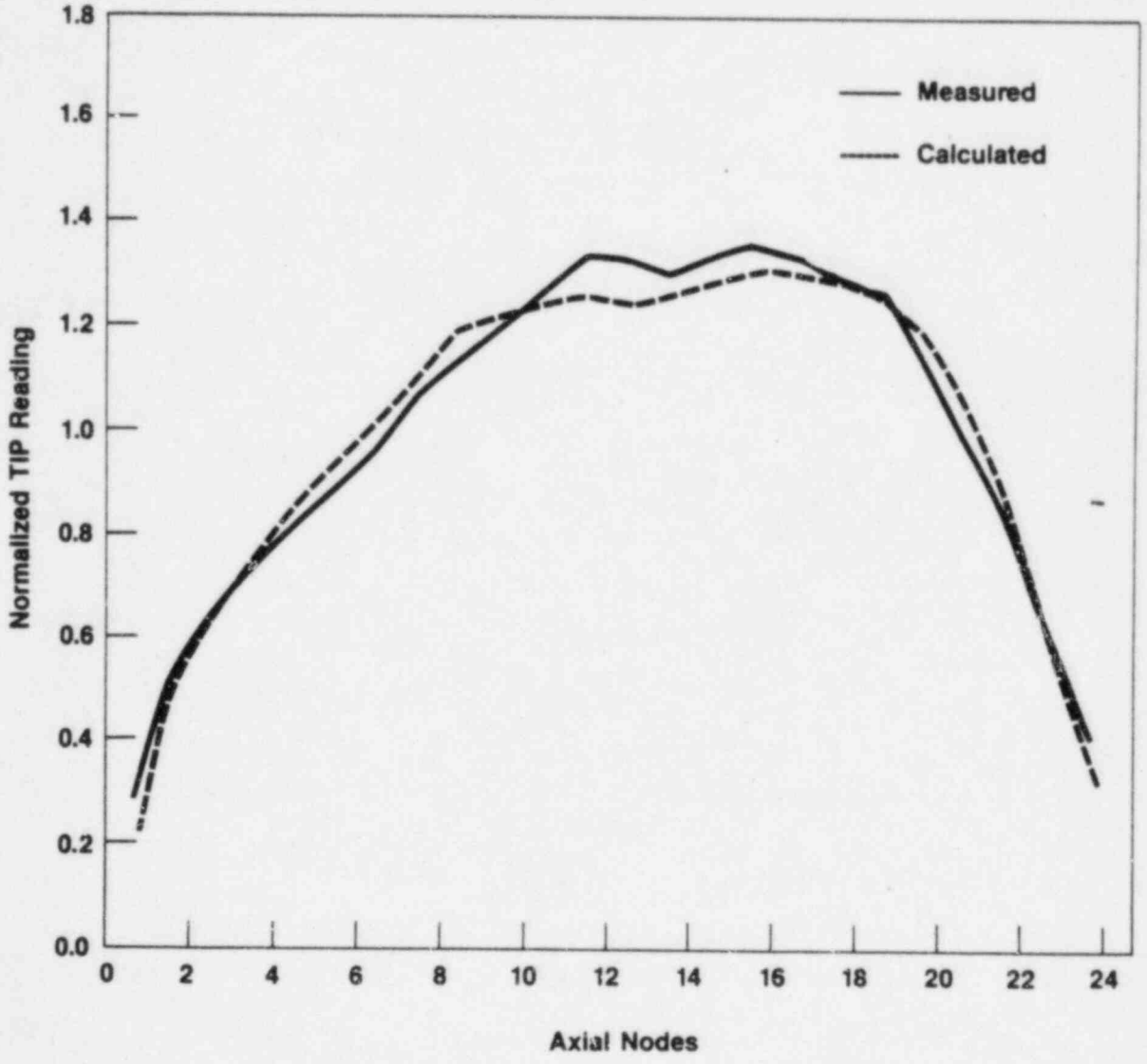

Figure 4.39
COMPARISON OF CORE AVERAGE AXIAL TIP READING FOR
THE HATCH 1 CYCLE 1 STATEPOINT ON 01-25-77

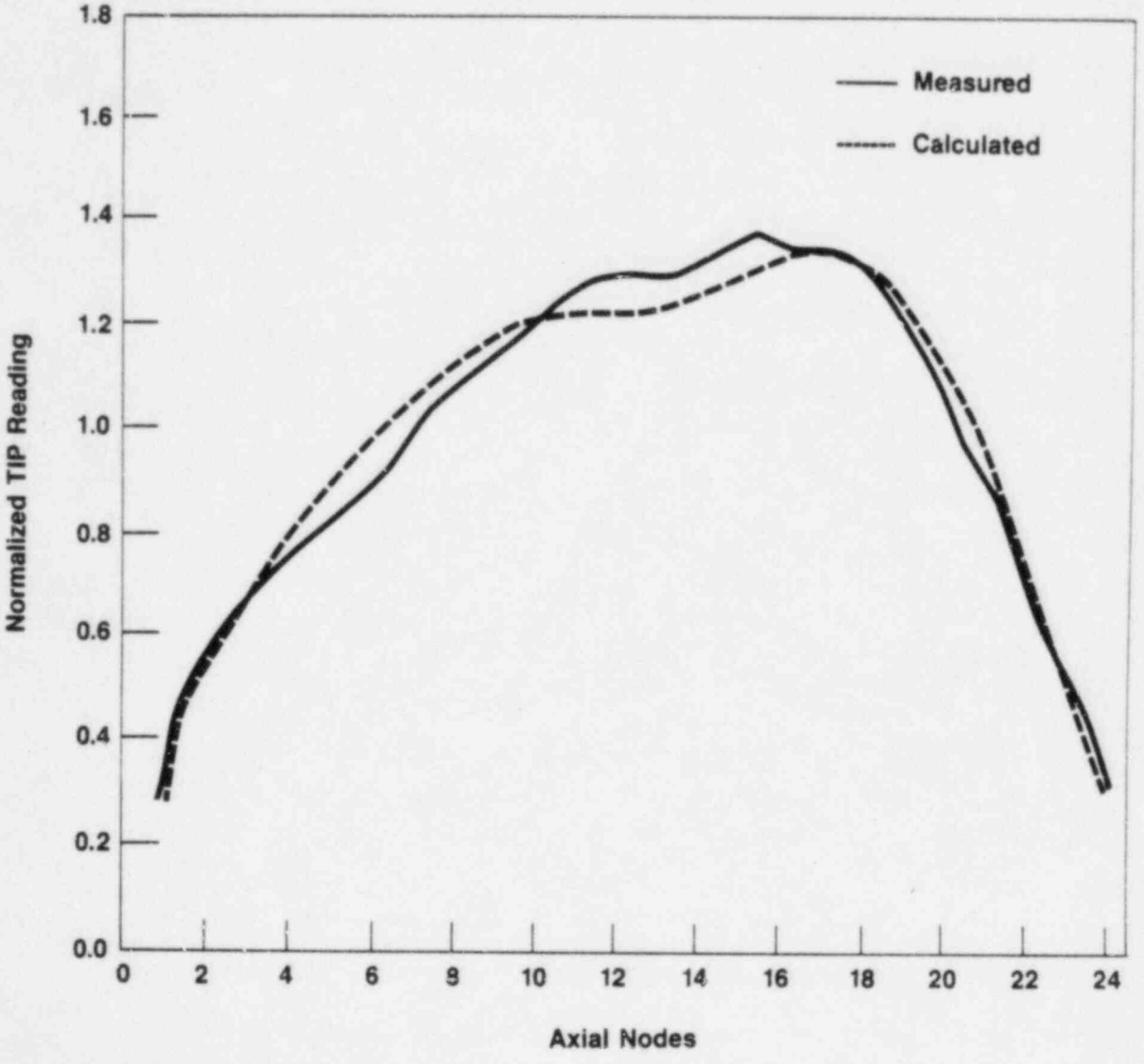

Figure 4.40
COMPARISON OF CORE AVERAGE AXIAL TIP READING FOR
THE HATCH 1 CYCLE 1 STATEPOINT ON 02-23-77

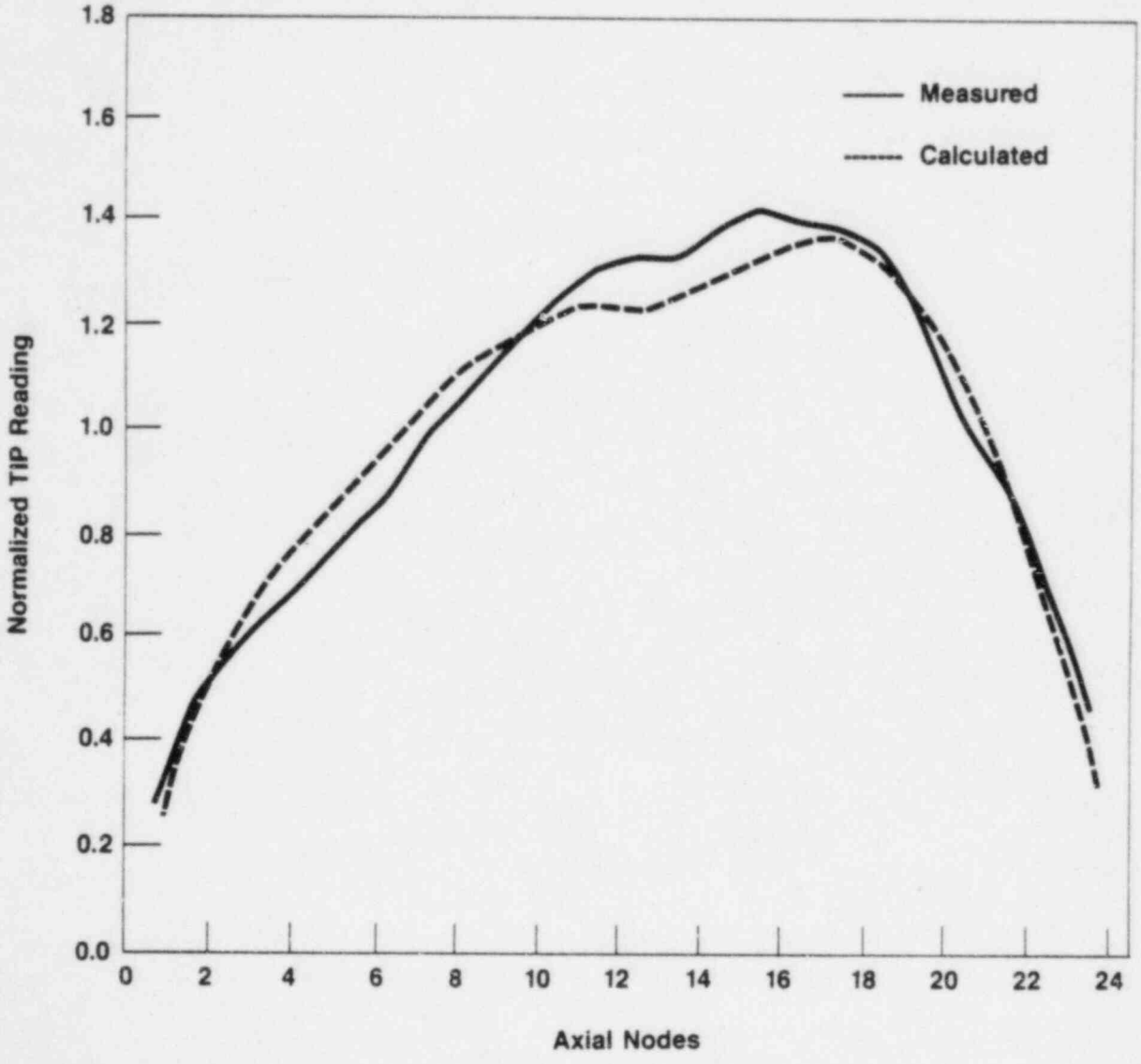

Figure 4.41
COMPARISON OF CORE AVERAGE AXIAL TIP READING FOR
THE HATCH 1 CYCLE 1 STATEPOINT ON 03-07-77

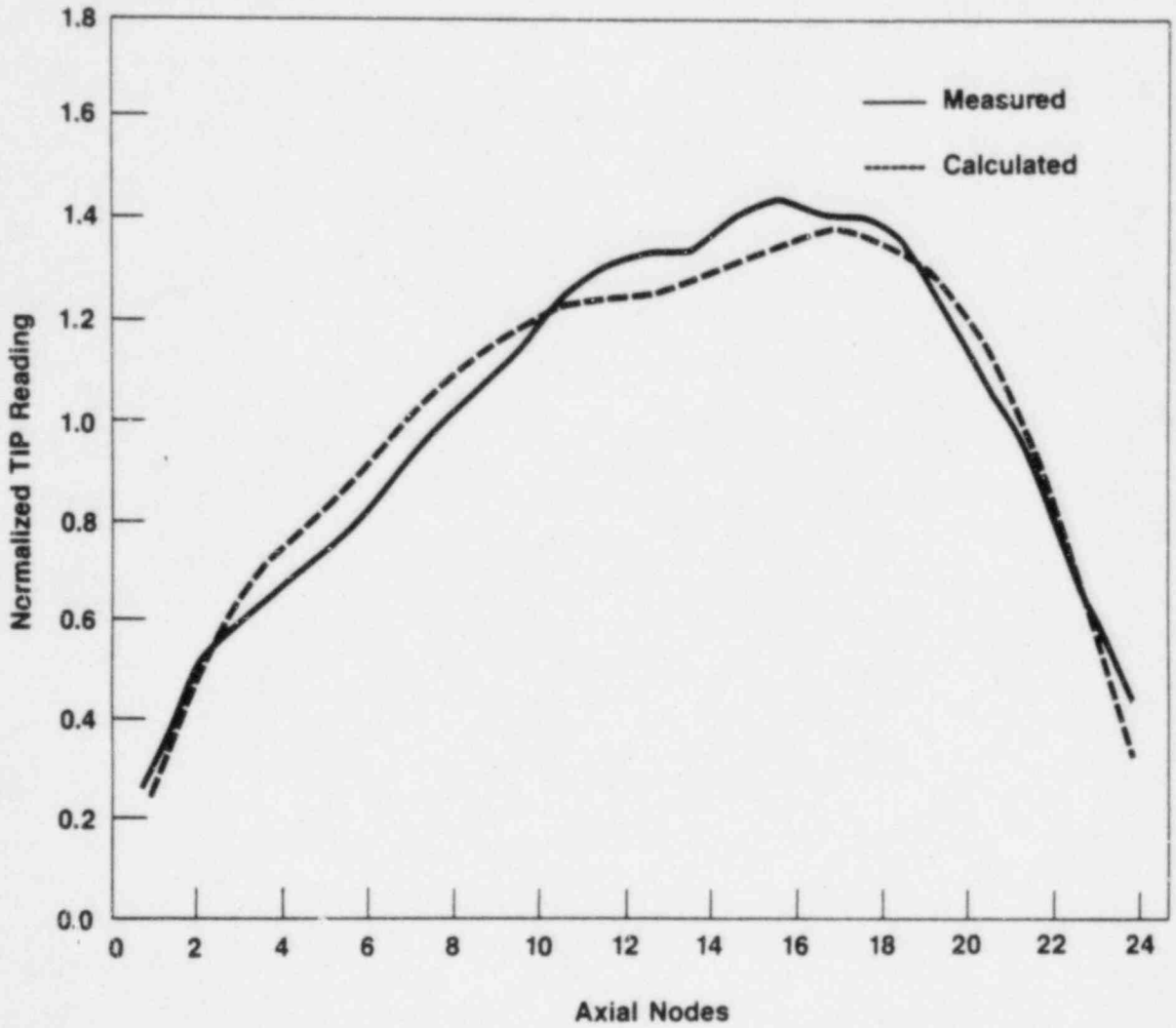

Figure 4.42
106 BUNDLE AVERAGE AXIAL Ba-140 DISTRIBUTION

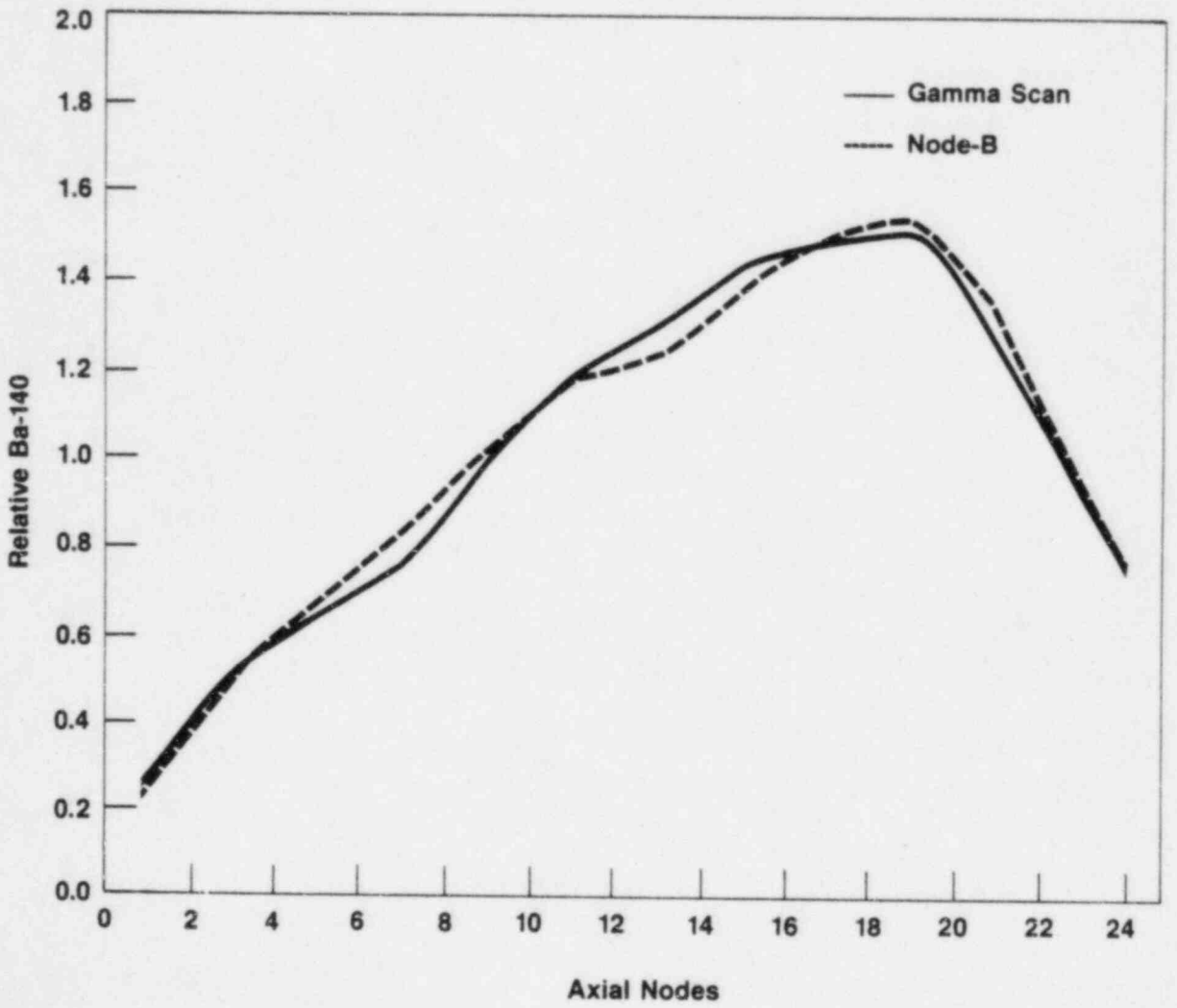

Figure 4.43
OCTANT NORMALIZED AXIAL Ba-140 DISTRIBUTION
FOR FUEL ASSEMBLY HX-169 (LOCATION 14,08)

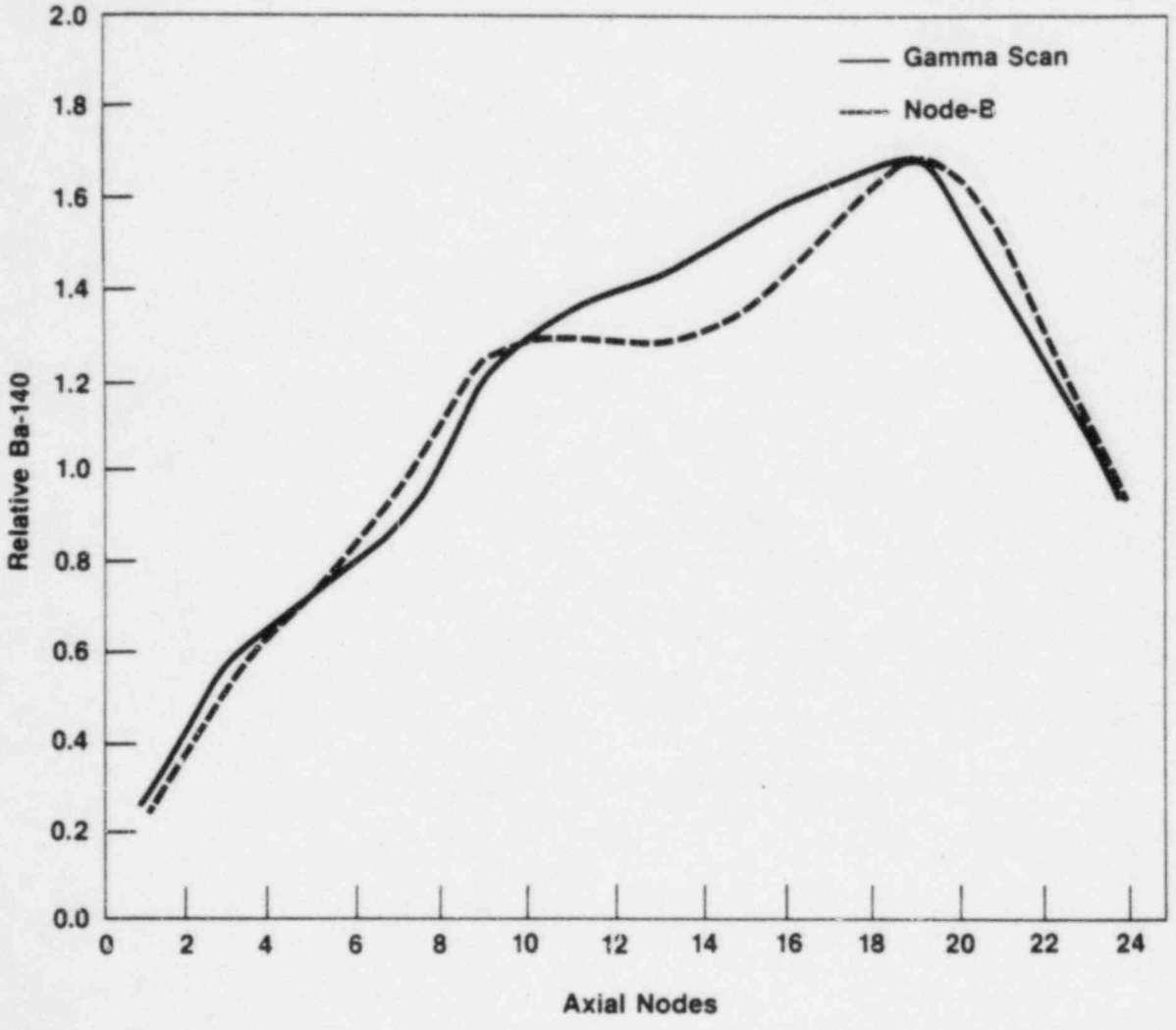

Figure 4.44
OCTANT NORMALIZED AXIAL Ba-140 DISTRIBUTION
.FOR FUEL ASSEMBLY HX-373 (LOCATION 15,08)

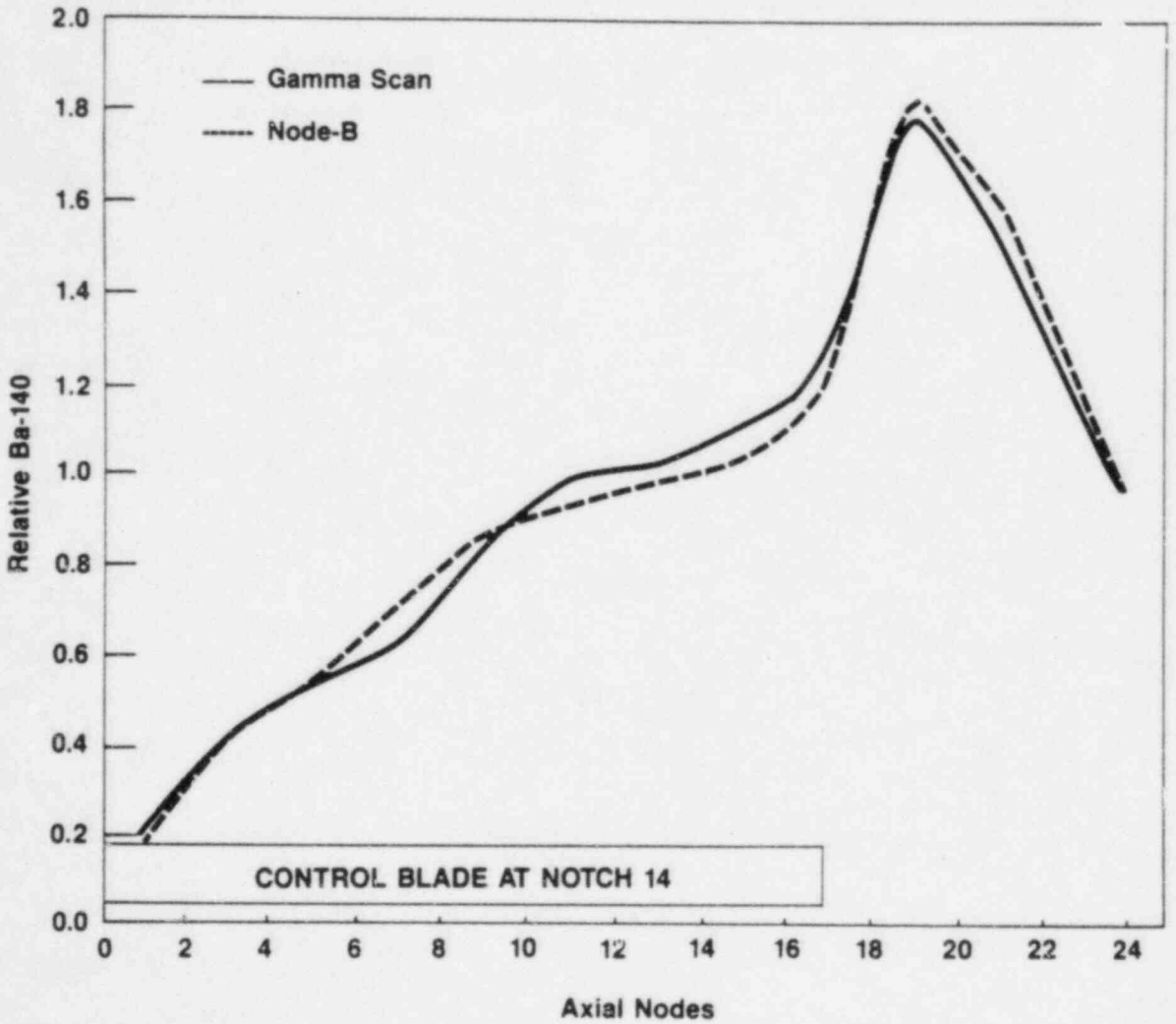

Figure 4.45
OCTANT NORMALIZED AXIAL Ba-140 DISTRIBUTION
FOR FUEL ASSEMBLY HX-393 (LOCATION 14,09)

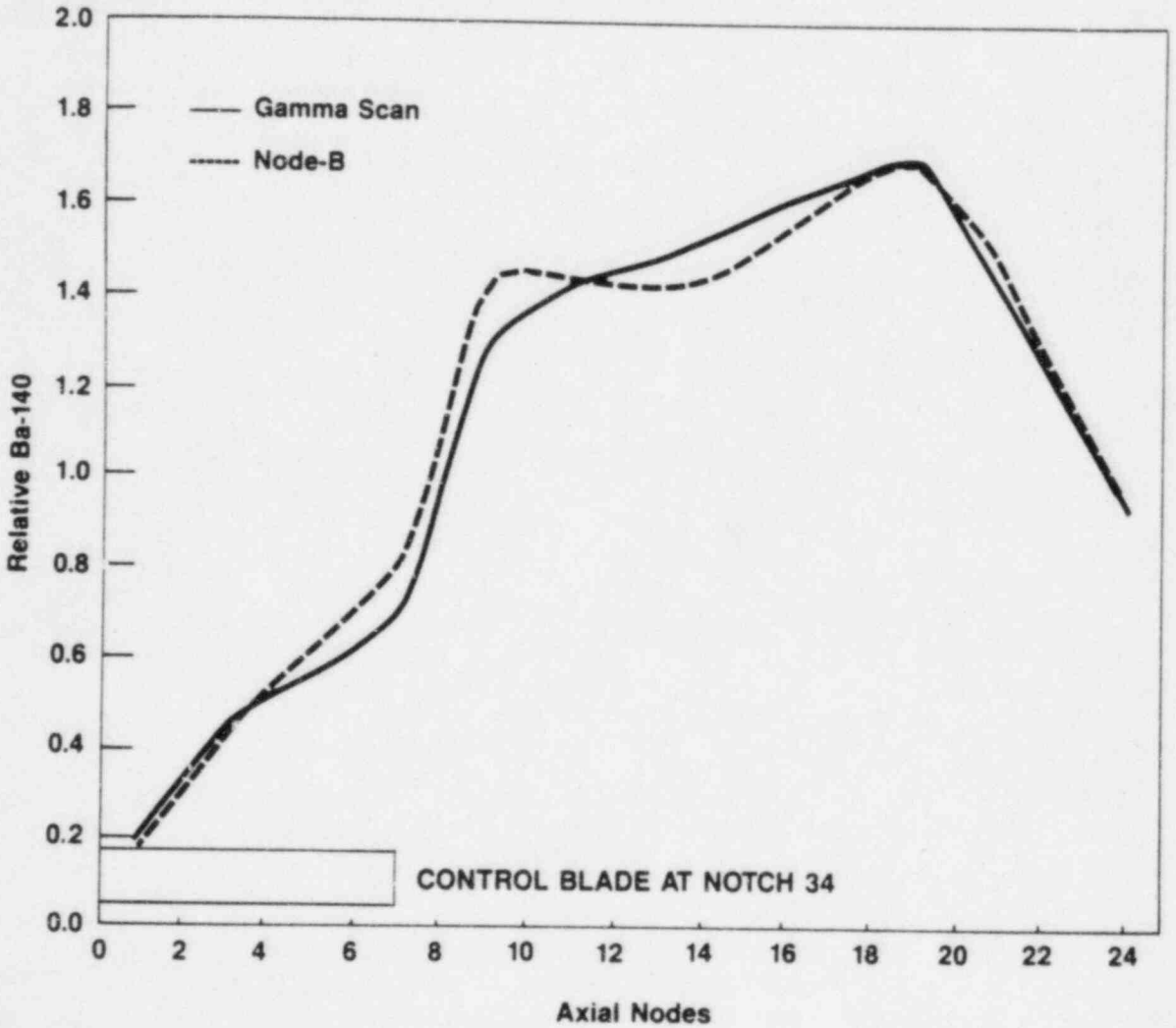

Figure 4.46
OCTANT NORMALIZED AXIAL Ba-140 DISTRIBUTION
FOR FUEL ASSEMBLY HX-141 (LOCATION 15,09)

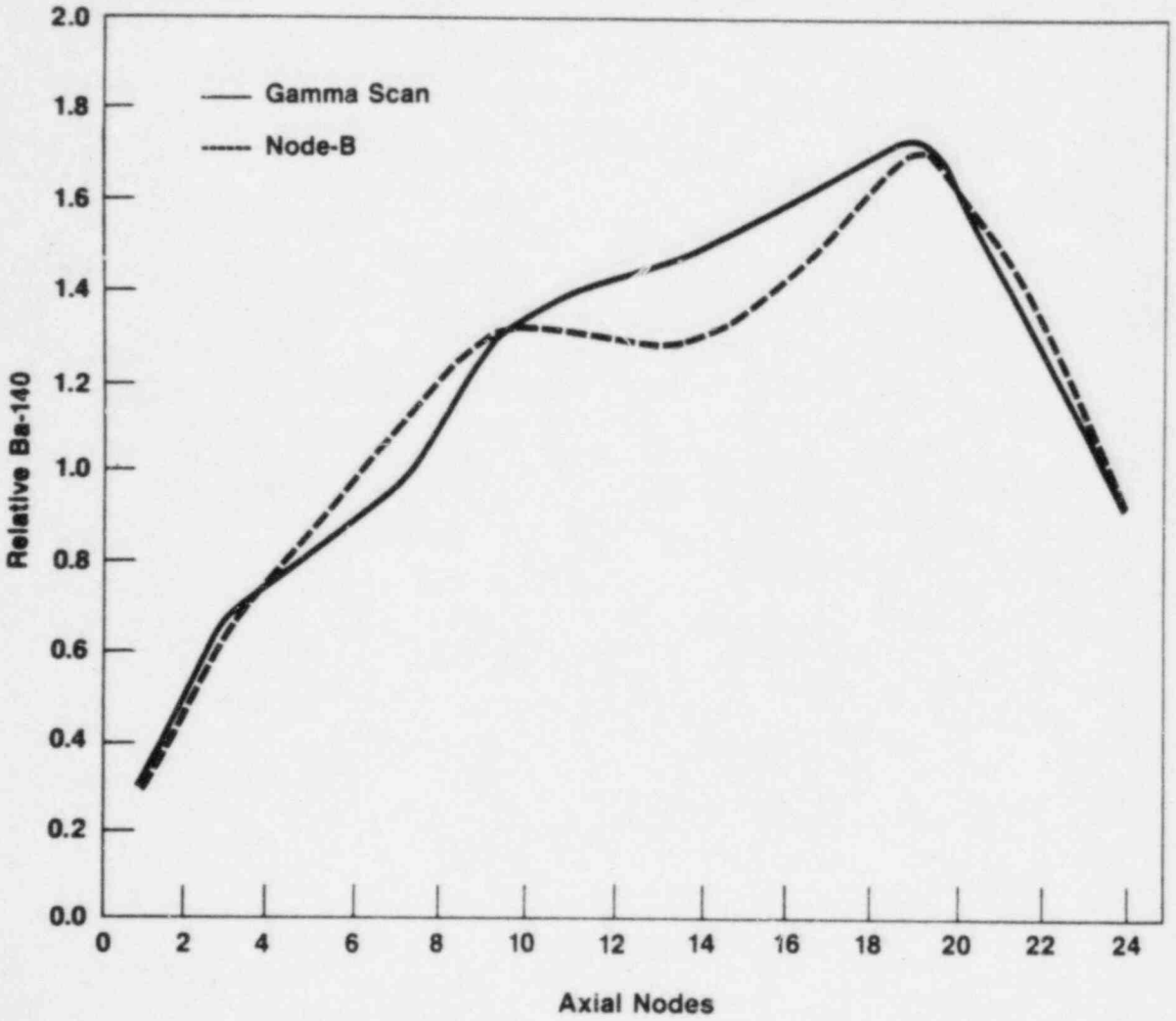

Figure 4.47
OCTANT NORMALIZED AXIAL Ba-140 DISTRIBUTION
FOR FUEL ASSEMBLY HX-413 (LOCATION 4,11)

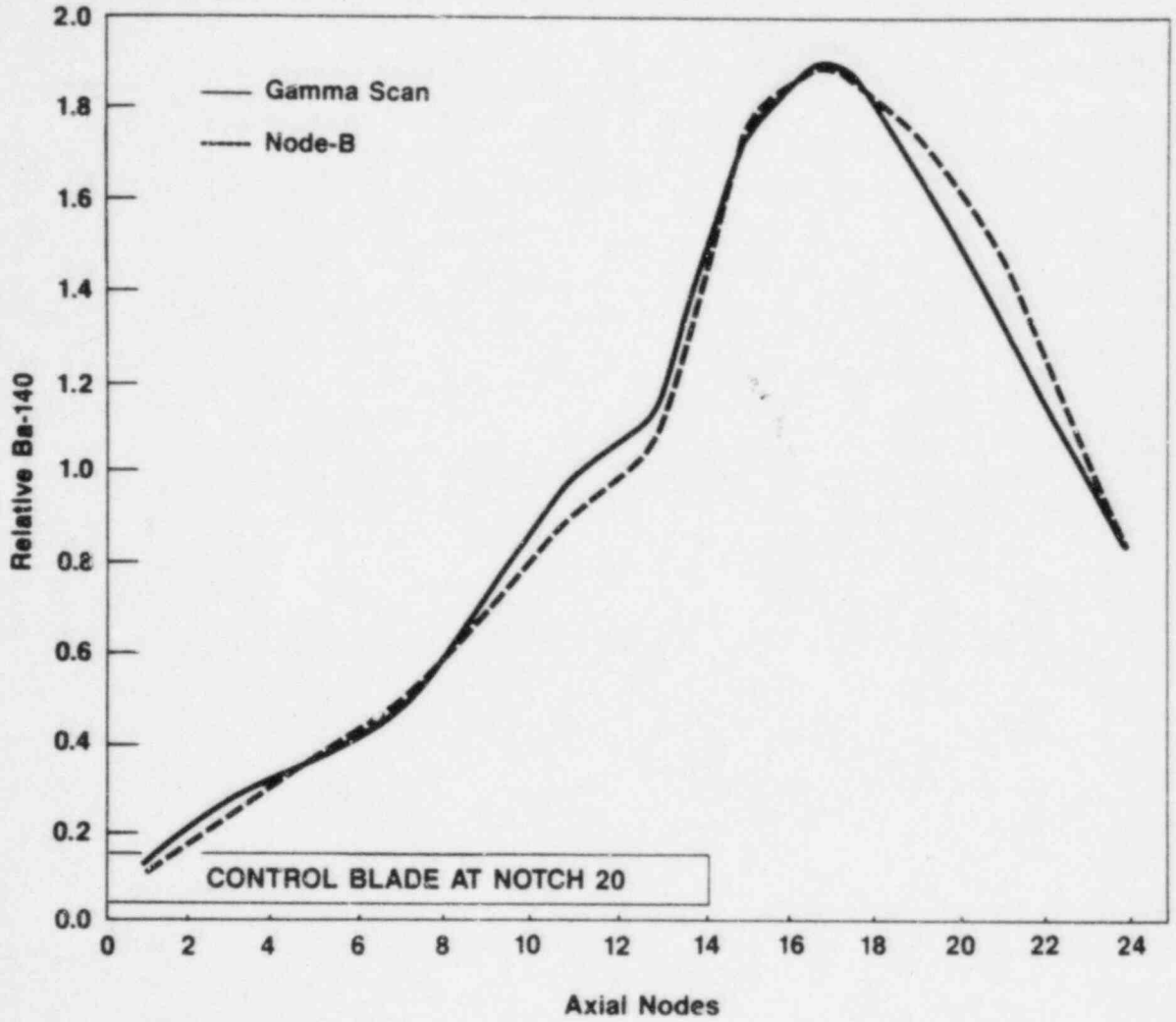

Figure 4.48
RELATIVE BUNDLE INTEGRATED Ba-140 DISTRIBUTION

I =	J = 10	11	12	13	14	15	16	17	18	19	20	21	22	23	24	25	26
1					0.699 0.773 -7.238	0.682 0.746 -6.284	0.663 0.718 -5.428	0.616 0.667 -5.047	0.572 0.524 4.746	GAMMA NODE-B % RMS							
2					0.904 0.953 -4.789	0.881 0.929 -4.694	0.843 0.902 -5.783	0.846 0.884 -3.715	0.790 0.802 -1.194	0.685 0.617 6.677							
3					1.038 1.043 -0.448	0.914 0.933 -1.893	0.893 0.925 -3.136	0.971 0.997 -2.539	0.966 0.984 -1.852	0.899 0.904 -0.452	0.795 0.823 -2.767	0.691 0.722 -3.062	0.590 0.546 4.369				
4	1.059 1.064 -0.569	0.970 0.976 -0.581			1.072 1.087 -1.483	0.957 0.992 -2.489	0.963 0.976 -1.232	1.063 1.064 -0.136	1.039 1.065 -2.541	1.010 1.054 -4.412	0.959 1.003 -4.333	0.904 0.933 2.888	0.776 0.809 -3.241	0.594 0.584 0.969			
5	1.075 1.064 0.999	1.118 1.105 1.249			1.110 1.117 -0.739	1.124 1.110 1.312	1.122 1.105 1.663	1.054 1.064 -0.983	1.040 1.070 -2.879	1.093 1.101 -0.788	1.070 1.094 -2.399	1.019 1.049 -2.980	0.939 0.972 -3.294	0.770 0.807 -3.632			
6					1.128 1.112 1.580	1.125 1.112 1.250	1.148 1.099 4.885	1.100 1.084 1.578	1.075 1.077 -0.156	1.118 1.107 1.079	1.096 1.097 -0.057	1.082 1.099 -1.642					
7					1.130 1.106 2.371	0.932 0.929 0.354	0.972 0.939 3.230	1.184 1.125 5.871	1.167 1.139 2.698	0.999 0.980 1.915	0.984 0.969 1.478	1.102 1.068 1.377					
8					1.134 1.111 2.300	0.941 0.946 -0.472	0.970 0.956 1.394	1.221 1.173 4.741	1.187 1.174 1.286	1.048 1.006 4.094	1.006 0.973 3.263		1.091 1.085 -0.438	1.008 1.043 -3.427			
9					1.113 1.133 -1.880	1.183 1.150 3.259	1.202 1.180 2.154	1.238 1.228 0.999	1.229 1.234 -0.487	1.191 1.167 2.343			1.036 1.046 -0.973	1.025 1.051 -2.516			
10					1.139 1.142 -0.269	1.193 1.167 2.628	1.232 1.179 5.184	1.255 1.237 1.770									
11					1.206 1.178 2.679	0.975 0.968 0.674	1.009 0.974 3.451	1.215 1.173 4.097									
12					1.198 1.200 -0.233	0.993 0.982 1.097	0.994 0.964 3.008		1.165 1.140 2.407	0.955 0.937 1.767			1.107 1.084 2.234	0.951 0.955 -0.350			
13					1.247 1.263 -1.559	1.200 1.193 0.662			1.115 1.127 -1.111	1.145 1.119 2.638			1.094 1.094 0.018	1.091 1.067 2.290			
14																	
15																	
16													1.086 1.077 0.896	0.938 0.939 -0.091			
17													1.042 1.034 0.777	1.043 1.044 -0.049			
18			1.169 1.150 1.880	1.135 1.133 0.230													
19			0.922 0.946 -2.422	1.143 1.111 3.158													

5.0 SUMMARY AND CONCLUSIONS

This report describes the code used at GPUN for steady state analysis of the Oyster Creek core. The code is an improved version of NODE-B which developed under the PSMS program sponsored by EPRI. It is a one group neutronic model integrated with a thermal hydraulic model (THERM-B).

The Oyster Creek core is modeled in nodes, one node radially and 24 axially for each fuel assembly. The neutron source, S, at each node is calculated in terms of k^{∞} and W_{mn}. W_{mn} is the probability of a neutron born in node m and is absorbed in node n and is a function of the migration area, M^2. The nodal k^{∞} is a function of fuel, exposure, coolant density, fuel temperature, control fraction and xenon concentration. The core k-effective is based upon a neutron balance summed over the entire core. The core flow distribution is calculated by equalizing the pressure drop across each channel. An EPRI developed mechanistic model is used to determine void fraction.

The nodal model was verified against measurements from Oyster Creek cycles 8 and 9 and Hatch 1 cycle 1. The verification data includes gamma scan measurements, TIP data and cold criticals. A variety of core conditions were covered and both 7x7 and 8x8 fuel designs were covered.

The verification work from Oyster Creek data showed:

- a hot reactivity of 0.986245 with a standard deviation of 0.00177;
- a cold Keffective of 1.00193 with a standard deviation of 0.00293;

- a nodal uncertainty of 7.65% based on comparison to TIP measurements.

The verification from Hatch 1 cycle 1 data showed:

- a hot reactivity of 0.98498 with a standard deviation of 0.00537;
- a nodal uncertainty of 9.14% based on comparison to TIP measurements;
- a nodal uncertainty of 7.95% based on comparison to gamma scan measurements.

The results of GPUN's off-line verification agree with the on-line benchmarking sponsered EPRI[4]. It demonstrates the adequacy of the off-line code.

6.0 REFERENCES

1. "Power Shape Monitoring System (PSMS), Technical Description," EPRI Report NP-1660, Vol. 2. Prepared by Quadrex Corp., February 1981.

2. "ARMP: Advanced Recycle Methodology Program," EPRI CCM-3, October 1976.

3. "BWR Hybrid Power Shape Monitoring System, Volume 1: Technical Description and Evaluation." EPRI Report NP-3195-CCM, prepared by Systems Control, Inc., Nuclear Associates International and Hitachi, Ltd., September 1983.

4. "BWR Hybrid Power Shape Monitoring System, Volume 5: Benchmark Report," EPRI Report NP-3195-CCM, prepared by Systems Control, Inc. and Utility Associates International, September 1983.

5. "Mechanistic Model for Predicting Two-Phase Void Fraction for Water in Vertical Tubes, Channels, and Rod Bundles," EPRI-NP-2246-SR, Prepared by G.S. Lelbouche and B.A. Zolotar, Special Report, February 1982.

6. McAdams, W.H., "Heat Transmission," 3rd ed., McGraw-Hill Book Company, Inc., New York (1954).

7. Lottes, P.A. and W.S. Flinn, "A Method of Analysis of Natural Circulation Boiling Systems," Nuclear Science and Engineering, 1. 461-476 (1956).

8. Martinelli, R.C., "Prediction of Pressure Drop During Forced Circulation Boiling of Water," Transactions of the ASME (August 1948).

9. Haling, R.K., "Operating Strategy for Maintaining an Optimum Power Distribution Throughout Life," ANS Topical Meeting on Nuclear Performance of Power-Reactor Cores, 1963 (TID-7672).

10. Larsen, N.H. and Goudey, J.L., "Core Design and Operating Data for Cycle 1 of Hatch 1," EPRI NP-562, 1979.

11. Shiraishi, L.M. and Parkos, G.R., "Gamma Scan Measurements at Edwin I. Hatch Nuclear Plant Unit 1 Following Cycle 1," EPRI-NP-511, 1978.

Appendix A

STATISTICAL DEFINITIONS

The following definitions are used for residuals and their statistics.

Residual

$$R = [M(\ell,k) - P(\ell,k)]/\bar{M}$$

where $M(\ell,k)$ - measured value for bundle ℓ at node k

$P(\ell,k)$ - predicted value for bundle ℓ at node k

$\bar{M}$ - average value of measured readings

L - number of bundles

K - number of nodes

Overall Nodal RMS error

$$RMS_N = \left[\sum_{\ell,k} R^2(\ell,k) \; / \ell * k \right]^{1/2}$$

Individual bundle

$$E_B(1) = \sum_{k} R(\ell,k)/K$$

$$RMS_B(1) = \left[\sum_{k} R^2(\ell,k)/K \right]^{1/2}$$

Integral

$$RMS_I = \left[\sum_B E^2(\ell)/L \right]^{1/2}$$

Axial Average

$$E_A(k) = \sum_\ell R(\ell,k)/L$$

$$SD_A(k) = \left[\sum_\ell (R(\ell,k) - E_A(k))^2/L-1 \right]^{1/2}$$

$$RMS_A = \left[\sum_\ell E^2(k)/K \right]^{1/2}$$

Peak Node

$$RMS_{peak} = \left[\sum_\ell R^2(\ell,k_{peak})/L \right]^{1/2}$$